19th
International Workshop on Inelastic Ion-Surface Collisions

Frauenchiemsee
Germany
16–21 September 2012

Book of Abstracts

edited by Ch. Linsmeier

The IISC-19 Workshop is supported by:

CANBERRA

HIGH VOLTAGE ENGINEERING

oerlikon
leybold vacuum

Omicron
An Oxford Instruments Company

PHYSICAL ELECTRONICS GMBH

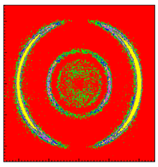

RoentDek
Handels GmbH

Supersonic Gas Jets
Detection Techniques
Data Acquisition Systems
Multifragment Imaging Systems

SPECS™

IPP Max-Planck-Institut
für Plasmaphysik
EURATOM Association

Christian Linsmeier
Max-Planck-Institut für Plasmaphysik
Boltzmannstr. 2
85748 Garching b. München, Germany

IPP Max-Planck-Institut
für Plasmaphysik
EURATOM Assoziation

2012-09-03

19th
International Workshop on Inelastic Ion-Surface Collisions

Frauenchiemsee
Germany
16–21 September 2012

Book of Abstracts

edited by Ch. Linsmeier

History of the IISC Workshop

IISC	Year	Location	Country	Organizer
1	1976	Bell Labs, Murray Hill, NJ	USA	N. Tolk
2	1978	McMaster University, Hamilton	Canada	R. Kelly
3	1980	Feldkirchen-Westerham	Germany	E. Taglauer, W. Heiland
4	1982	Hindsgavl Manor, Middelfart	Denmark	P. Sigmund
5	1984	Gold Canyon Ranch, AZ	USA	P. Williams
6	1986	Argonne National Laboratory, IL	USA	D. Gruen
7	1988	Jagellonian University, Krakow	Poland	M. Szymonski
8	1990	Wiener Neustadt	Austria	G. Betz, P. Varga
9	1992	Aussois	France	M. Bernheim, J.P. Gauyacq
10	1994	Grand Targhee, WY	USA	N. Tolk
11	1996	Island of Wangerooge	Germany	W. Heiland
12	1998	South Padre Island	USA	J.W. Rabalais, P. Nordlander
13	2000	San Carlos de Bariloche	Argentina	M.L. Martiarena
14	2002	Island of Ameland	The Netherlands	R. Hoekstra, P.A. Zeijlmans van Emmichoven
15	2004	Ise-Shima	Japan	K. Morita, T. Koshikawa
16	2006	Hernstein	Austria	F. Aumayr
17	2008	Porquerolles	France	H. Lebius, B. Ban d´Etat
18	2010	Gatlinburg, TN	USA	C.O. Reinhold, P.S. Krstić, F.W. Meyer
19	2012	Frauenchiemsee	Germany	Ch. Linsmeier

Committees

Conference Chair

Christian Linsmeier (IPP, Germany)

International Scientific Committee

F. Aumayr (Austria)
R. Hoekstra (The Netherlands)
I. Juaristi (Spain)
K. Kimura (Japan)
T. Koshikawa (Japan)
H. Lebius (France)
Ch. Linsmeier (Germany)
M.L. Martiarena (Argentina)
F. Meyer (USA)
J . Pomeroy (USA)
P. Roncin (France)
M. Schleberger (Germany)
H. Winter (Germany)
Y. Yamazaki (Japan)

Local Organizing Committee

J. Brinkmann
P. Douglas
Ch. Linsmeier
E. Neitzert
M. Oberkofler
R. Piechoczek
Th. Schwarz-Selinger


The Future.
Most exciting!
TURBOVAC MAG integra
TURBOVAC MAG integra
MAG.DRIVE iM
©BICOM_11619.02 0.01.2012

Time Schedule

P	Plenary Talk	(45 min)
R	Progress Report	(30 min)
O	Oral contribution	(20 min, all times incl. discussion)

Sunday, 16 September 2012

15:00	**Registration open**

Monday, 17 September 2012

9:00	**Ch. Linsmeier** Welcome and opening
	Session Chair: Ch. Linsmeier
9:10	**P. Bauer** (Austria) P On the information depth in LEIS
9:55	**K. Nakajima** (Japan) R Molecular composition and orientation at the surface of binary mixtures of ionic liquids
10:25	**Coffee break**
	Session Chair: H. Winter
10:40	**N. Stolterfoht** (Germany) R Experiments and simulations of ion guiding through nanocapillaries in insulating polymers
11:10	**E. Gruber** (Austria) O Temperature control of ion guiding through straight insulating macro-capillaries
10:30	**T. Suzuki** (Japan) R Scattering of spin-polarized ^{4}He^{+} ions at surfaces
12:00	**Lunch**

Monday, 17 September 2012, continued

Session Chair: H. Rothard

13:30 **M. Trassinelli** (France) O
Magnetic properties modifications of ferromagnetic films of MNAS irradiated with highly charged ions

13:50 **E. Artacho** (Spain) R
TDDFT and its application to energy deposition of slow projectiles in metals and insulators

14:20 **N.E. Koval** (Spain) O
Dynamic screening of a localized hole and a photoelectron emitted from a metal cluster

14:40 **R. Lake** (USA) R
Highly charged ion interactions with thin dielectric films

15:10 Coffee break

Session Chair: T. Koshikawa

15:30 **J.M. Pomeroy** (USA) O
Measurements of velocity dependent energy deposition from highly charged ions on solids

15:50 **J.E. Miraglia** (Argentina) O
A simple model to calculate exciton production in proton LiF grazing collisions

16:10 **D. Roth** (Austria) O
A procedure to determine electronic energy loss from relative measurements with TOF-LEIS

16:30 **P. Tiwald** (Austria) O
Neutralization probability of protons scattered off a lithium fluoride surface: A quantum chemistry approach

16:50 **P. Chakraborty** (India) O
MCs_n^+-SIMS: An approach for complete compensation of 'matrix effect' and exact composition analysis of MBE-grown Si/Ge superlattice and $Si_{1-x}Ge_x$ alloy structures

Tuesday, 18 September 2012

Session Chair: K. Kimura

9:00 **B. King** (Australia) P
High sensitivity SNMS surface analysis

9:45 **A. Wucher** (Germany) O
Secondary ion formation in sputtering of metals: Experiment and theory

10:05 **K. Wittmaack** (Germany) O
In need of a novel site specific model of ion formation at surfaces

10:25 Coffee break

Session Chair: K.D. Krantzman

10:40 **G. Wachter** (Austria) R
A microscopic model for track formation by swift heavy ions

11:10 **K. Kimura** (Japan) O
Ion tracks produced by sub-MeV C_{60} ions in amorphous Si_3N_4

11:30 **M. Karlušić** (Croatia) R
Thermal spike analysis of highly charged ion tracks

12:00 Lunch

Session Chair: R. Hoekstra

13:30 **J. Seifert** (Germany) R
Surface structure determination via fast atom diffraction

14:00 **A. Zugarramurdi** (France) O
Transition from fast to slow atom diffraction

14:20 **H. Winter** (Germany) O
Longitudinal coherence in fast diffraction at surfaces

Tuesday, 18 September 2012, continued

14:40 **M. Debiossac** (France) O
Grazing incidence fast atom diffraction applied to thin film growth

Session Chair: P. Bauer

15:00 Poster Introduction
Oral introductions for each poster. A time limit of 2 minutes for each poster is strictly enforced by the session chairperson!

16:00 Poster Session (incl. coffee break)

F. Aumayr (Austria)
Nano-holes milled in 1 nm thick carbon nanomembranes with slow-highly charged ions

J. Brinkmann (Germany)
Depth-resolved deuterium concentration of plasma-exposed tungsten alloys

L. Chen (China)
Formation of negative ions in grazing scattering of hydrogen atoms from insulator surfaces

K. Dobes (Austria)
Electron emission due to impact of highly charged ions on C_{60} covered gold surfaces and HOPG

A.S. El-Said (Germany)
Creation of surface nanostructures in Al_2O_3 by slow highly charged ions

R. Feder (Germany)
Systematic investigations of ion beam sputtering of Si: First experimental and simulation results

D. Göbl (Austria)
A quantitative investigation of quasi-resonant neutralization of He^+ ions at a germanium surface

M.S. Gravielle (Argentina)
Interaction potentials for multi-electronic atoms in front of a LiF(001) surface investigated via rainbow scattering

M.S. Gravielle (Argentina)
Grazing incidence fast atom diffraction for helium atoms impinging on a Ag(110) surface

E. Gruber (Austria)
Controlling ion guiding through tapered glass-capillaries with temperature

C. Heuser (Germany)
Energy and impact angle dependence of sub-threshold external electron emission

J. Hopster (Germany)
Highly charged ion irradiation of two-dimensional systems

A.E. John (Germany)
Energy distribution of sputtered atoms and ions from energetic ion bombardment of GaAs.

H. Jouin (France)
Calculations of neutral fractions and angular distributions for H(1s) and H^+ impinging on Al(111) at grazing incidences

G.A. Kachurin (Russia)
Synthesis of light-emitting Si nanocrystals in Si/SiO_2 multilayers stimulated by inelastic losses of swift heavy ions

D. Keerthisinghe (USA)
Energy and time dependence of guided electrons through PET nanocapillaries

E. Kolodney (Israel)
Formation and emission of gold and silver carbide cluster ions in a single C_{60}^- surface impact at keV energies: Characterization and echanisms

T. Koshikawa (Japan)
High depth analysis with ion beam and nano-area analysis with novel compact high brightness and high spin-polarized SPLEEM

M. Marpe (Germany)
Energy and angular resolved detection of sputtered ions and neutrals

R. Monreal (Spain)
Auger neutralization of He^+ on Cu surfaces: Simulation of azimuthal scans

K. Narumi (Japan)
Energy dependence of nonlinear effect on sputtering yields of Si bombarded with 10-540 keV C_{60} ions

O. Osmani (Spain)
Transient metal-like electrical conductivity in swift heavy ion irradiated SiO_2

P. Petersson (Sweden)
Heavy ion elastic recoil detection and nuclear reaction analysis in studies of nitrogen-15 transport marker in tokamaks

W. Rößler (Austria)
Analysis of Mo/Si multilayers by means of RBS

P. Salou (Austria)
New experimental setup to measure slow ion-induced sputter yields in graphite

D. Schrempf (Austria)
An ultra-compact setup for measuring ion-induced electron emission statistics

P. Singh (India)
(e, 2e) triple differential cross sections of Ar and Xe atoms

Y.Y. Wang (China)
Electron emission and surface etching by slow and medium highly charged ions on HOPG surface

Wednesday, 19 September 2012

	Session Chair: I. Juaristi
9:00	**A.W. Kleyn** (The Netherlands) P Nitrogen interactions at metal surfaces
9:45	**E. Kolodney** (Israel) O Multifragmentation modes in cluster-surface collisions: Experiment and simulations
10:05	**K.D. Krantzman** (USA) O Effects of chemistry in C_{60} bombardment of Si
10:25	**Coffee break**
	Session Chair: J. Pomeroy
10:40	**K. Dobes** (Austria) R Sputtering of fusion relevant surfaces by seeding impurities
11:10	**A. Keim** (Austria) O Collisions of seedings gas ions Ar^+ and N_2^+ with tungsten and beryllium surfaces
11:30	**S. Bielesch** (Germany) O Depth resolution of nuclear reaction analysis of buried hydrogen-containing layers
11:50	**H. Rothard** (France) R Radiolysis of astrophysical ices by energetic heavy ions (cosmic rays)
13:05	**Boat departure for excursion to Kampenwand** **Don‘t forget to pick up your lunch box!**

Thursday, 20 September 2012

Session Chair: F. Aumayr

9:00 **K. Krieger (**Germany) P
Ion-surface interaction processes and their implication for fusion devices

9:45 **G. de Temmerman** (The Netherlands) R
Synergistic effect during simultaneous steady-state and transient plasma loads

10:15 **Ł. Ciupiński** (Poland) O
TEM observations of radiation damage in self-irradiated tungsten

10:35 Coffee break

Session Chair: T. Schwarz-Selinger

10:55 **L. Chen** (China) R
Li^+ ion neutralization on metal surfaces and thin films

11:25 **D. Primetzhofer** (Sweden) R
Electronic stopping at low ion velocities: Going beyond bandstructure effects

12:00 Lunch

Session Chair: G. Andersson

13:30 **J.A. Yarmoff** (USA) R
Ion scattering investigations of the temperature dependence of charge exchange and surface composition

14:00 **K. Khalal-Kouache** (Algeria) O
Calculation of the scattering probability in LEIS: Effect of the screening function choice

Thursday, 20 September 2012, continued

14:20	**J. Gregory** (USA) O Coherent acoustic phonon spectroscopy of ion-implanted diamond
14:40	**N. Okabayashi** (Japan) R Povtential sputtering from F/Si(100) surface with extraction of the surface bond direction
15:10	**Coffee break**
	Session Chair: M.S. Gravielle
15:30	**G. Schiwietz** (Germany) R Local electronic short-time effects due to interactions of fast highly charged ions with insulators
16:00	**E. Bodewits** (The Netherlands) O Secondary electron yield from HCI on Au and thin films of C_{60}
16:20	**K. Narumi** (Japan) O Vicinage effect on secondary-electron emission from carbon foils penetrated by swift H_2^+ and C_2^+ ions
16:40	**M. El Kharrazi** (Germany) O Deep shell Auger recombination after highly charged ion impact: Electronic excitation and relaxation

Friday, 21 September 2012

Session Chair: D. Primetzhofer

9:00 **T. Michely (**Germany) P
Ions at surfaces: An atomistic view of defect and pattern formation

9:45 **R.M. Bradley** (USA) R
Self-assembled nanoscale patterns produced by ion bombardment of two-component materials

10:15 **S. Facsko** (Germany) R
Periodic nanoscale patterns induced by ion irradiation: ripples, dots, and holes

10:45 **Coffee break**

Session Chair: Ch. Linsmeier

11:00 **K.-H. Heinig** (Germany) O
Surface patterning of Ge and Si by heavy ion and cluster impacts: Experiments, atomistic simulations and theory

11:20 **M. Engler** (Germany) O
Silicide induced ion beam patterning of silicon(001)

11:40 **G. Andersson** (Australia) O
Determining the structure of dye layers adsorbed on nanoporous titania substrates

12:00 **Closing**

12:30 **Lunch**

Abstracts

Monday
16 September 2012

ON THE INFORMATION DEPTH IN LEIS

D.Goebl[1], *D.Primetzhofer*[1,2], *M.Spitz*[1],*S. Rund*[1], *D. Roth*[1], *E.Taglauer*[3], *and P. Bauer*[1,*]

[1] Institut für Experimentalphysik, Johannes Kepler Universität Linz, A-4040 Linz, Austria
[2] Institutionen för Fysik och Astronomi, Uppsala Universitet, Box 516, S-751 20 Uppsala, Sweden
[3] Max-Planck-Institut für Plasmaphysik, EURATOM Association, D-85748 Garching bei München, Germany

1. INTRODUCTION

In Low Energy Ion Scattering (LEIS) keV noble gas ions are used as projectiles and positive ions are registered when scattered into a detector at a scattering angle, typically > 90°. Amongst the noble gas ions, He^+ is the simplest projectile, for which only single excitations have to be considered and the relevant charge exchange processes are well known [1]. On this basis, a detailed physical understanding of the information depth in LEIS can be obtained for diverse scenarios of interest.

2. CHARGE EXCHANGE PROCESSES FOR HE

2.1. Auger- and quasi-resonant neutralization

Both mechanisms refer to "one-way" processes, which lead to neutralization only, without equivalent possibility to ionize neutral He. Thus, if only Auger neutralization (AN) and quasi-resonant neutralization (qRN) are possible, only so-called "survivals" are detected, i.e. projectiles in their original charge state. One can evaluate the efficiency of the neutralization by looking at the fraction of ions amongst the backscattered particles, or ion fraction, P^+.

For AN, the neutralization probability is governed by a characteristic rate, Γ_{AN}, and the interaction time, τ, via $P^+ = \exp(-\tau \cdot \Gamma)$. Since AN is a nonlocal process, the approximation $P^+_{AN} = \exp(-v_c/v_\perp)$ has been found useful, with $v_c = \int \Gamma(z)dz$. Typical values are $v_c \approx 10^5$ m/s, corresponding to rates of the order of 10^{15}/s active along a path length of about 1Å.

In contrast, qRN is an atomic process, for which P^+_{qRN} should be given by $\exp(-v_{qRN}/v)$, and $v_{qRN} = \int \Gamma(r)dr$. However, for qRN oscillations in the neutralization probability occur as a function of *1/v*, as a consequence of quantum-mechanical interference. These oscillations have been observed [2], but, apart from those, P^+ follows a single exponential as a function of 1/v [3]. For qRN, a higher neutralization efficiency is observed compared to AN. Since the process will not be active for larger distances than AN, $\Gamma_{qRN} > \Gamma_{AN}$ will hold true. Consequently, neutralization will take place within 2Å for both processes. This strongly favors contributions from the outer atomic layer, since for 2nd layer contributions the ions have to travel much longer, leading to much lower survival probability. A quantitative analysis for 2 keV He^+ and Cu(100) revealed that even for this open surface the 1st layer contributes 80% to the yield of detected ions, and only 20% originate from the 2nd layer. For He^+-Ge(100), where neutralization is also due to qRN, the 2nd layer should contribute even less than for He^+-Cu(100).

2.2. Reionization regime

Reionization and resonant neutralization in a close collision are due to a completely different process. They occur via electron promotion at ion-atom distances smaller than a critical distance, r_{min}. Electron promotion is due to electronic interaction between the projectile level and target atom states. Collisions with such a minimum distance lead to smaller scattering angles at higher ion energy. The efficiency of these processes is governed by probabilities P_{RI} and P_{RN}, respectively, which for fixed scattering angle depend on the projectile energy only. A study for He^+-Cu and He^+-Au determined these probabilities [4] and found that $P_{RN} > P_{RI}$, a finding which was confirmed for He^+-Al and is expected to hold true for many other systems as well.

In the reionization regime, the survivals' contribution to the ion fraction is $P^+_{in} \cdot (1 - P_{RN}) \cdot P^+_{out}$, while reionized projectiles contribute $(1 - P^+_{in}) \cdot P_{RI} \cdot P^+_{out}$. The contribution due to reionization has been found to increase with increasing energy, the increase of P_{RI} and P_{RN} with energy being the dominant factor [4]. At typical LEIS energies (3 keV) and for polycrystalline Cu, 2nd layer contributions are ~ 10%. For single crystals and appropriate scattering geometry, focusing collisions may lead to rather high scattering yields from deeper layers and to an information depth >> 1 monolayer [5].

3. REFERENCES

[1] HH. Brongersma, M. Draxler, M. De Ridder and P.Bauer, Surface Science Reports 62, 3, 63-109 (2007)
[2] R.L. Erickson, D.P. Smith, Phys.Rev.Lett.34 (1975) 297.
[3] D. Goebl, D. Valdés, E. Abad, R. C. Monreal, D. Primetzhofer, and P. Bauer, Phys. Rev. B 84 (2011) 165428
[4] D. Primetzhofer, M. Spitz, E. Taglauer, and P. Bauer; Surf. Sci. 605 (2011) 1913
[5] D. Primetzhofer, S.N. Markin, J.I.Juaristi, E. Taglauer, and P. Bauer, Phys. Rev. Lett. 100 (2008) 213201

---

[*] Corresponding author e-mail address: peter.bauer@jku.at

MOLECULAR COMPOSITION AND ORIENTATION AT THE SURFACE OF BINARY MIXTURES OF IONIC LIQUIDS

K. Nakajima[1,*], *S. Oshima*[1], *T. Miyashita*[1], *M. Suzuki*[1] *and K. Kimura*[1]

[1] Department of Micro Engineering, Kyoto University

1. INTRODUCTION

Ionic liquids (ILs) are salts molten at or below 100°C. Among them, room temperature ionic liquids (RTILs), which are liquid at room temperature (~25°C), have been intensively studied in the last decade because they have many favorable properties, such as wide liquid ranges, low volatilities (negligible vapor pressure), good thermal stabilities, electrolytic conductivity, nonflammability and so on. One important feature of ILs is that their properties are roughly tunable by varying the combination of constitutive cations and anions. Furthermore, mixing two or three ionic liquids is considered to be effective to tune the properties finely for an intended application. However, even surface composition of binary mixture is still controversial [1,2]. In this study, molecular composition and orientation at the surface of several equimolar binary mixtures of RTILs, which consist of a common cation and different anions, was investigated by high-resolution Rutherford backscattering spectroscopy (high-resolution RBS).

2. RESULTS

Figure 1 shows the elemental depth profiles for one of mixture of ionic liquids investigated in this study, equimolar mixture of 1-hexyl-3-methylimidazolium bis(trifluoromethylsulfonyl)imide ([C_6MIM][TFSI]) and 1-hexyl-3-methylimidazolium hexafluorophoshate ([C_6MIM][PF_6]).

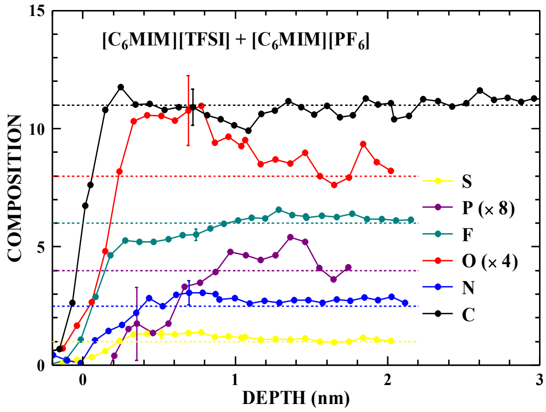

Figure 1: Elemental depth profiles of the equimolar mixture of [C_6MIM][TFSI] and [C_6MIM][PF_6] obtained by high-resolution RBS.

It is clearly seen that the composition of oxygen (phosphorus) in the surface region (< ~1 nm depth) is significantly higher (lower) than that expected from bulk composition. This indicates that [TFSI] anion is enriched relative to [PF_6] anion in the topmost molecular layer. Furthermore, the relative position of leading edge for each element in the profiles gives an insight into the orientation of cations and anions in the topmost molecular layer. In this mixture, for example, [C_6MIM] cation and [TFSI] anion in the topmost layer are oriented with their longer alkyl chain and either or both CF_3 group(s) pointing the vacuum side, respectively. In addition, the phosphorus atom of [PF_6] anion in the topmost layer is located somewhat deeper relative to the S-N-S part of [TFSI] anion and the imidazolium ring of [C_6MIM] cation.

Other mixtures, equimolar mixture of [C_6MIM][TFSI] and [C_6MIM][Cl] and that of [C_6MIM][PF_6] and [C_6MIM][Cl] were also investigated by high-resolution RBS. No enrichment of either anion is found for these mixtures, while there is also a similar orientation of cations/anions in their topmost molecular layer.

3. REFERENCES

[1] R. Souda, Surf. Sci. **604**, 1694 (2010).

[2] F. Maier, T. Cremer, C. Kolbeck, K. R. J. Lovelock, N. Paape, P. S. Schulz, P. Wasserscheid, H.-P. Steinrück, Phys. Chem. Chem. Phys. **12**, 1905 (2010).

---

[*] Corresponding author e-mail address: nakajima.kaoru.4a@kyoto-u.ac.jp

EXPERIMENTS AND SIMULATIONS OF ION GUIDING THROUGH NANOCAPILLARIES IN INSULATING POLYMERS.

*N. Stolterfoht**

Helmholtz-Zentrum Berlin für Materialien und Energie, D-14109 Berlin, Germany

1. INTRODUCTION

During the last decade the guided transmission of ions through insulating capillaries has received considerable attention [1, 2]. Studies of dynamic properties concerning the ion guiding through nanocapillaries [3] etched in polyethylene terephthalate (PET) and polycarbonate (PC) are reviewed. The temporal evolution of the intensity and the angular distribution of the transmitted ions are analyzed. The experiments are compared with recent simulations of the ion trajectories by solving Newton's equation of motion using a non-linear surface conductivity within the capillary.

2. EXPERIMENTS AND SIMULATIONS

Experimentally, the angular transmission profiles of ions guided through insulating capillaries were analyzed both for PET and PC polymers. Specific results are shown in figure 1 for 3 keV Ne^{7+} ions traversing PET capillaries of 12 μm length and 200 nm diameter. The mean emission angle of the transmission profiles exhibit pronounced oscillatory structures. One notes that the mean emission angle varies within $\pm 1.5^\circ$ around the center angle equal to the tilt angle. The oscillations increase in amplitude and decrease in frequency as the tilt angle increases. These observations are the results of the Coulombic ion repulsion by transient charge patches formed by the incident charge deposition [3].

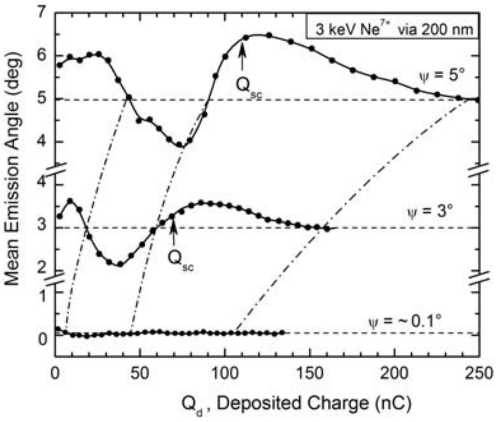

Figure 1: Mean emission angle of the transmitted Ne^{7+} ions for capillary tilt angles of 0°, 3°, and 5°. The dashed lines are drawn to guide the eye along the nodes of the mean angles. The results are discussed in detail in Ref. [3].

To interpret the experimental results, simulations of the ion trajectories guided in 3 dimensions by the electrostatic field within the capillaries are performed. This field was determined from the charges deposited at the walls of the capillaries taking into account the charge transport by means of the exponential conductivity law by Frenkel [4].

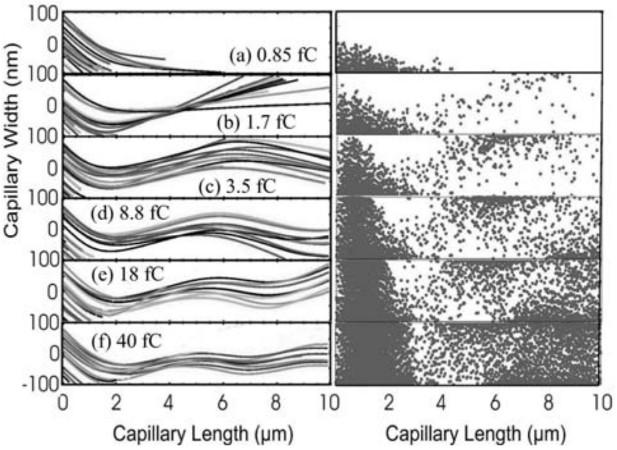

Figure 2: Trajectories of 3 keV Ne^{7+} (left-hand panels) and corresponding distributions for the deposited charges (right-hand panels). Tilt angle of the capillaries are 5°. The inserted charge Q_{in} is indicated in each panel.

Figure 2 shows results of the simulations for ions and capillaries as used in the experimental studies. The numbers in the panels refers to the charge deposition in a single capillary before 20 ion trajectories are inserted. The left-hand panels show the 20 ion trajectories and the right-hand panels represent the deposited charges. The latter panels clearly indicate the formation of the charge patches, while the trajectories perform oscillatory movements in accordance with the experimental results.

3. REFERENCES

[1] N. Stolterfoht *et al.*, Phys. Rev. Lett. **88**, 133201 (2002).

[2] K. Schiessl *et al.*, Phys. Rev. A **72**, 062902 (2005).

[3] N. Stolterfoht *et al.*, Phys. Rev. A **79**, 022901 (2009), ibid, A **83**, 062901 (2011).

[4] J. Frenkel, Phys. Rev. **54**, 647 (1938)

---

*Corresponding author e-mail address: nico@stolterfoht.com

TEMPERATURE CONTROL OF ION GUIDING THROUGH STRAIGHT INSULATING MACRO - CAPILLARIES

G. Kowarik[1], R. J. Bereczky[2], E. Gruber[1], F. Ladinig[1], D. Schrempf[1], P. Gunacker[3],
C. Lemell[3], J. Burgdörfer[3], K. Tökési[2], and F. Aumayr[1,*]

[1] Institute of Applied Physics, TU Wien - Vienna University of Technology, 1040 Vienna, Austria, EU
[2] Institute of Nuclear Research of the Hungarian Academy of Sciences, (ATOMKI), 4001 Debrecen, Hungary, EU
[3] Institute of Theoretical Physics, TU Wien - Vienna University of Technology, 1040 Vienna, Austria, EU

1. INTRODUCTION

First experiments on guiding of highly charged ions (HCI) through straight insulator nano-capillaries showed a remarkable effect: after an initial charge up phase, the ion beam could be steered by tilting the capillary axis while remaining in the initial charge state indicating that the transmitted ions never touched the inner walls [1]. Subsequent experiments confirmed this guiding effect also for macroscopic glass capillaries, both straight [2,3] and tapered ones [4]. The microscopic simulations revealed that a self-organized charge up of the capillary walls due to preceding HCI impacts leads to an electric guiding field, which steers the incoming projectile ions along the capillary axes [5]. Ion guiding ensues as soon as a dynamical equilibrium of charge-up by the ion beam and charge relaxation by bulk or surface conductivity is established. The simulations showed that a stable transmission regime required a delicate balance between incident ion flux and charge relaxation via surface and bulk conduction, conditions, which were obviously met in almost all cases studied experimentally so far. In this contribution we show that a key control parameter for guiding is the small residual electric conductivity of the highly insulating capillary material whose dependence of temperature σ(T) is nearly exponential.

2. EXPERIMENTS

We use a single straight macroscopic glass capillary (inner diameter: 160 µm; length: 11.4 mm) made of Borosilicate (Duran) for which the guiding effect has been previously established [2]. The current experimental set-up allows for a controlled and uniform temperature variation of the glass capillary between -30°C and +90°C [6]. Within such a moderate variation of the temperature the conductivity changes by almost five orders of magnitude. Beams of Ar^{7+} and Ar^{9+} ions with a kinetic energy of 4.5 keV are collimated to a divergence angle of less than 0.5° and eventually hit a metallic entrance aperture directly in front of the capillary (120 µm diameter). Transmitted ions are registered by a position sensitive micro-channel-plate detector with wedge-and-strip anode, located about 18 cm behind the sample. Transmission rates are recorded for each capillary tilt angle after steady-state conditions (i.e. a dynamical equilibrium) are reached.

3. RESULTS

Experimental transmission curves are normalized with respect to the transmission in forward direction (Fig.1).

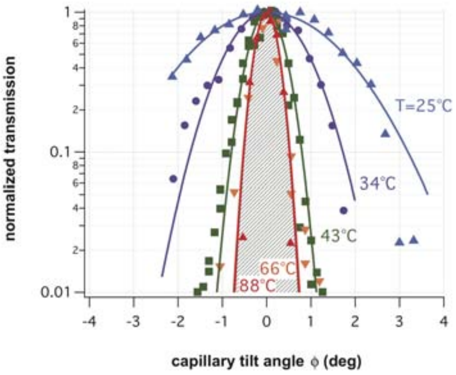

Figure 1: Normalized transmission curves for 4.5 keV Ar^{9+} ions guided through a glass capillary for different temperatures ranging from 24°C to 88°C. The flux of the incident 4.5 keV Ar^{9+} ions was kept constant at about 5000 ions entering the capillary per second. The shaded area indicates the geometric limit of transmission in the absence of guiding.

Our experiments [7] show that increasing the temperature of a glass capillary and therefore its conductivity leads to a reduction of guiding and, eventually, to a complete disappearance of the guiding effect. This strong temperature dependence can be employed to stabilize guiding against Coulomb blocking due to a high incident ion flux [8].

4. REFERENCES

[1] N. Stolterfoht et al. Phys.Rev.Lett. **88**, 133201 (2002).
[2] R. J. Bereczky et al. Nucl.Instr.Meth.B **267**, 317 (2009).
[3] G. Kowarik et al. Nucl.Instr. Meth.B **267**, 2277 (2009).
[4] T. Ikeda et al. Appl.Phys.Lett. **89**, 163502 (2006).
[5] K. Schiessl et al. Phys. Rev. A **72**, 62902 (2005).
[6] R. J. Bereczky et al. Nucl.Instr.Meth.B **279**, 182 (2012).
[7] G. Kowarik, et al. arXiv:1109.3953v1 [cond-mat.other] (2011).
[8] M. Kreller, et al. Nucl.Instr.Meth.B **269**, 1032 (2011).

---

[*] Corresponding author e-mail address: aumayr@iap.tuwien.ac.at

Scattering of spin-polarized $^4He^+$ ions at surfaces

*T. Suzuki**, *Y. Yamauchi, and S. Hishita*

National Institute for Materials Science

1. INTRODUCTION

The ionization energy of helium is so large (24.6 eV) that He^+ ions are neutralized on surfaces typically via the interatomic Auger process (Auger neutralization) with quite high probability in low energy ion scattering (LEIS). In Auger neutralization, the spin of a surface electron filling the He^+ 1*s* hole should be opposite to that of the He^+ 1*s* electron because of the Pauli exclusion principle. Thus, the survival probability P_S of the projectile He^+ ions on electron-spin-polarized surfaces, i.e., magnetic surfaces, varies with the electron spins of the projectiles. The spin dependence of P_S is estimated from the scattered He^+ ion yield I ($\propto P_S \cdot \sigma$, where σ is a scattering cross-section). If σ is spin independent, the surface spin polarization can be analyzed by using the spin dependence of I, that is, the spin asymmetry (spin-polarized ion scattering spectroscopy, SP-ISS). The spin independence of σ has been assumed for projectiles with kinetic energies of several keV or less.

2. EXPERIMENT

Electron-spin-polarized $^4He^+$ ions were generated by Penning ionization of spin-polarized metastable He atom 2^3S_1 (He*). We employed an optical pumping technique to spin polarize He* [1]. Spin polarization of the He^+ ion beam was about 0.2. The spin direction of the incident He^+ ion beam was defined by the guiding field (～0.3 Oe), which was perpendicular to both the scattering plane and the surface normal of the target as shown in Fig. 1.

3. RESULTS

Figure 1 shows the ISS spectra and spin asymmetry of gold surfaces. The ISS intensity I and the spin asymmetry A are defined as $I_\uparrow + I_\downarrow$ and $(I_\uparrow - I_\downarrow)/P_{He+} \cdot I$, where $I_\uparrow$ and $I_\downarrow$ are the scattered intensities of projectile ions whose magnetic moments are parallel and anti-parallel to the guiding magnetic field $\boldsymbol{B}$, respectively. In the ISS spectrum, the scattering peak of gold is observed at 1410 eV in addition to the secondary ions below 100 eV. Because gold is a non-magnetic material, the neutralization probability of the incident He^+ ions with up spins should be equal to that with down spins. Therefore, the gold surface is not expected to exhibit spin asymmetry. However, it is clearly observed at the elastic peak position of gold; it becomes maximum at the He^+-Au binary collision energy. We confirmed that the fluctuation in the beam current is much less than 1% from direct analysis by a picoammeter placed between the electrically floated target and ground. The agreement of the spin asymmetry in single crystalline and polycrystalline gold in Fig. 1 indicates that the target crystal structure has no effect; in other words, the fact that the target is solid has no effect. Moreover, the spin asymmetry of gold was independent of both the incident and the exit angles (not shown), i.e., the projectile trajectory near the surface. The neutralization of the projectile ion is sensitive to its trajectory because of neighboring atoms of the collision partners, so these results indicate that ion neutralization has no effect on the spin asymmetry on non-magnetic surfaces. Thus, it should be attributed to the scattering cross-section. We interpret this spin-dependent scattering in terms of the spin-orbit coupling that acts transiently on the He^+ 1*s* electron spin in the He^+-target binary collision. This interpretation qualitatively explains the relationship between the spin-dependent scattering and the scattering geometry, incident velocity, and magnetic field arrangement [2].

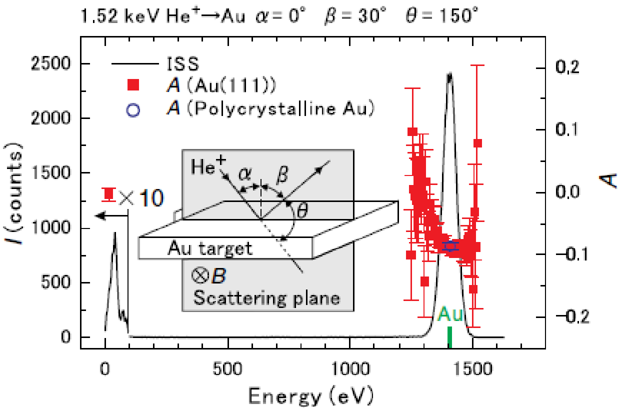

Figure 1: ISS spectrum of the Au(111) surface with the calculated He^+-Au binary collision energy. Filled squares represent the spin asymmetries of Au(111); an open circle indicates that of polycrystalline Au. The error of the spin asymmetry corresponds to statistics. The inset shows the scattering geometry. The scattering plane is perpendicular to both the Au surface and the magnetic field $\boldsymbol{B}$.

4. REFERENCES

[1] T. Suzuki, Y. Yamauchi, Nucl. Instr. Meth. Phys. Res. **A 575**, 343 (2007).

[2] T. Suzuki, Y. Yamauchi, S. Hishita, Phys. Rev. Lett. **107**, 176101 (2011).

---

* Corresponding author e-mail address: suzuki.taku@nims.go.jp

MAGNETIC PROPERTIES MODIFICATIONS OF FERROMAGNETIC FILMS OF MNAS IRRADIATED WITH HIGHLY CHARGED IONS

*M. Trassinelli**, *V.E. Gafton, M. Eddrief, V.H. Etgens, E. Lamour, X. Luo, M. Marangolo, C. Prigent,*
R. Reuschl[†]*, J.-P. Rozet, S. Steydli and D. Vernhet*

CNRS and Université Pierre et Marie Curie, INSP, UMR7588, 4 Place Jussieu, F-75005 Paris, France

1. INTRODUCTION

In the last decade, many investigations on the modification of magnetic properties of thin film by ion collision have been performed. So far, experiments were mainly dedicated to studies of transition ferromagnetic metals and some of their corresponding alloys (see [1] as example). Here we present recent studies on ion bombardment on more peculiar magnetic material, namely the manganese arsenide. MnAs is a metallic compound that is ferromagnetic below $T_C = 313$ K where the first-order phase transition from hexagonal (α phase) to orthorhombic (β phase, MnP type) is accompanied by a ferromagnetic-paramagnetic transition. The possibility of epitaxial growth of MnAs thin films on standard semiconductors such as GaAs has renewed interest in MnAs for spintronic research and their properties have been widely studied in the last years [2]. The epitaxial strain disturbs the phase transition that leads to the $\alpha-\beta$ phase coexistence and to an alternating ridges (α phase) and grooves (β phase) pattern (see fig. 1 left). Very recently, we discovered that these peculiar characteristics can be modified by the implantation of highly charged ions in the MnAs epilayers with a consequent change of its magnetic property. Such changes open new perspectives and provide important information about the robustness of this material in hostile environment. We present here the result of the first experiment on modifications of MnAs induced by ion impact that have been precisely characterized through different techniques.

2. PRODUCTION AND BOMBARDMENT OF THE SAMPLES

The 150-200 nm thick MnAs films are grown by molecular beam epitaxy on GaAs(001) substrate after a GaAs buffer layer [3]. At the end, an amorphous arsenic capping is used for oxidation prevention. Subsequently the samples are irradiated at the INSP ion facility SIMPA (French acronym for “source of highly charged ions of Paris”) under ultrahigh vacuum conditions, once the capping has been removed. The SIMPA facility is composed by an electron-cyclotron resonance ion source coupled to a dedicated beam line [4]. The ion source can produce intense beams of highly charged ions such as Ne^{9+}, Ar^{16+}, $\mathrm{Xe}^{26+}\ldots$ The ions are extracted, transported and selected trough the beam line to the collision chamber. For the present experiment Ne^{9+} beam were impinging the samples with an incidence angle of 60° and a kinetic energy of $E_{kin} = 4.5$ KeV/u, corresponding to a mean penetration depth of 74 nm. The maximum beam intensity was about 1 eμA and it was monitored by a standard Faraday cup. Visible and X-ray radiations, emitted during the collision, were recorded by a CCD camera and a solid-state detector, respectively.

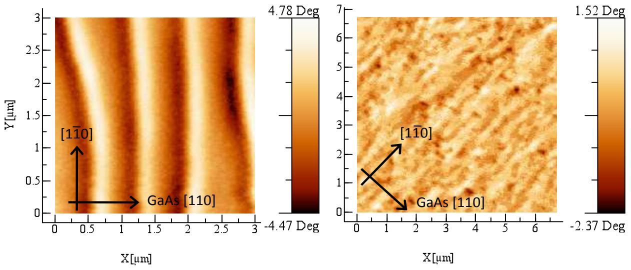

Figure 1: MFM images of 180 nm MnAs on GaAs before (left) and after ion bombardment (right) with a dose of about $5 \cdot 10^{13}$ ions/cm^2.

3. CHARACTERIZATION OF THE MAGNETIC AND STRUCTURAL PROPERTIES

After irradiation, several diagnostics have been applied to the samples and their results are compared to a non-irradiated reference sample. Structural changes of the film are investigated using an X-ray diffractometer and the surface topography is analyzed with an atomic force microscope (AFM). Changes on the magnetic properties are studied using the magneto-optical Kerr effect (MOKE) and magnetic force microscope imaging (MFM). Preliminary analysis shows a particular fragility of the magnetic properties of MnAs. Already with a bombardment of a few 10^{12} ions/cm^2, surface ferromagnetic signatures disappear. In correspondence, a strong disturbance of the characteristic $\alpha-\beta$ phase ridges and grooves of epitaxial MnAs is observed in the AFM and MFM images (See fig. 1), as well as a change of the crystal d-spacing. For comparison, MOKE measurements of bombarded thin iron films have been performed, which confirmed the uniqueness of MnAs behaviour.

4. REFERENCES

[1] W.M. Kaminsky *et al.*, Appl. Phys. Lett., **78**, 1589-1591 (2001); P.J. Cook *et al.*, J. Appl. Phys., **109**, 063917-5 (2011).

[2] L. Dweritz, Rep. Prog. Phys., **69**, 2581 (2006).

[3] F. Vidal, V. H. Etgens, V. Fernandes, B. Rache Salles and M. Eddrief, Phys. Rev. B **83**, 121305(R) (2011).

[4] A. Gumberidze, M. Trassinelli, N. Adrouche *et al.*, Rev. Sci. Instum., **81**, 033303-10 (2010)

[†] Present address: EMMI, GSI, Darmstadt, Germany.

*Corresponding author e-mail address: martino.trassinelli@insp.jussieu.fr

TDDFT AND ITS APPLICATION TO ENERGY DEPOSITION OF SLOW PROJECTILES IN METALS AND INSULATORS

M. Ahsan Zeb[1], *J. M. Pruneda*[2], *J. Kohanoff*[3], *D. Sánchez-Portal*[4,5], *A. Arnau*[4,5,6], *J. I. Juarisiti*[4,5,6], *and Emilio Artacho*[1,5,7,8,*]

[1] Cavendish Laboratory, Uinversity of Cambridge, J J Thomson Avenue, Cambridge CB3 0HE, United Kingdom
[2] Centre d'Investigación en Nanociéncia i Nanotecnologia (CSIC-ICN), Campus UAB, 08193 Bellaterra, Spain
[3] Atomistic Simulation Centre, Queen's University, Belfast BT7 1NN, United Kingdom
[4] Centro de Física de Materiales CFM/MPC (CSIC-UPV/EHU), 20018 San Sebastián, Spain
[5] Donostia International Physics Center DIPC, Paseo Manuel de Lardizábal 4, 20018 San Sebastián, Spain
[6] Departamento de Física de Materiales, Facultad de Químicas, UPV/EHU, 20018 San Sebastián, Spain
[7] Nanogune, Tolosa Hiribidea 76, 20018 San Sebastián, Spain
[8] Basque Foundation for Science, Ikerbasque, 48011 Bilbao, Spain

1. INTRODUCTION

When an ion shoots through a solid at a speed not too dissimilar from average electronic velocities, there is a transfer of energy from the ion to the host electrons which is measured by the electronic stopping power, $\mathcal{S}_e = dE/dx$, the energy loss rate per unit length along the path. The behaviour of $\mathcal{S}_e$ versus projectile velocity at low velocities is well understood for simple metals, which show typical dissipative force opposing the projectile, and thus a stopping power proportional to velocity. The situation is not so clear for other systems and recent experimental results have shown different behaviour for insulators (see e.g. [1]) and noble metals (see e.g. [2, 3]). The former show a threshold for the onset of stopping for $v \sim 0.1$ a.u., while the latter starts linear but changes slope in a similar velocity scale.

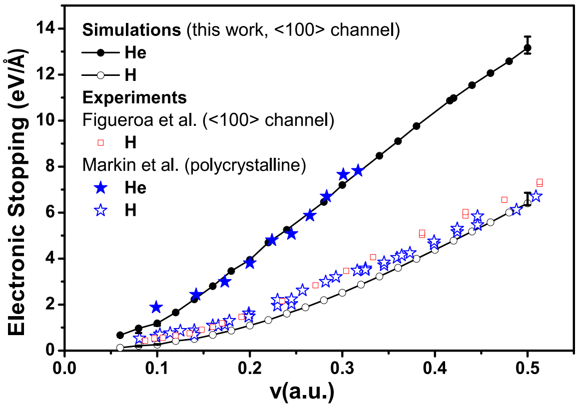

Figure 1: Electronic stopping power of H and He in Au versus velocity v. The simulation results are from [6], and the experiments from [2, 3].

2. RESULTS

Results will be reviewed on the application of time-evolving time-dependent density functional theory (t-TDDFT) for the calculation of electronic stopping power in different materials. Starting from insulators, simulations of the low-velocity threshold behaviour in LiF will be shown [4], as well as for ice [5]. The threshold behaviour was then reproduced semiquantitatively, while the Barkas effect between protons and antiprotons came out with significant accuracy. Very recently the electronic stopping power for H and He in gold was simulated [6], the results being displayed in the figure. The change in slope is a consequence of the involvement of d electrons in the electron-hole excitations of the stopping process, but it is a gradual process with increased velocity. At low velocities, when only s electrons are excited, it was expected that $\mathcal{S}_e^{\mathrm{H}} > \mathcal{S}_e^{\mathrm{He}}$, which was contradicted by experiments. Our results show how, although only s electrons are excited at low v, the d electrons are significantly involved in the mechanism of the excitation and the stopping, thus explaining the discrepancy. The latest results will be presented in the first-principles calculations of electronic stopping power in insulators and in non-jellium metals.

3. REFERENCES

[1] M. Draxler, S. P. Chenakin, S. N. Markin, and P. Bauer, Phys. Rev. Lett. **95**, 113201 (2005).

[2] E. A. Figueroa, E. D. Cantero, J. C. Eckardt, G. H. Lantschner, J. E. Valdés, and N. R. Arista, Phys. Rev. A **75**, 010901 (2007).

[3] S. N. Markin,D. Primetzhofer, M. Spitz, and P. Bauer, Phys. Rev. B **80**, 205105 (2009).

[4] J. M. Pruneda, D. Sanchez-Portal, A. Arnau, J. I. Juaristi, and E. Artacho, Phys. Rev. Lett. **99**, 235501 (2007).

[5] J. Kohanoff and E. Artacho, Radiation Damage in Biomolecular Systems Book Series, AIP Conference Proceedings **1080**, 78-87 (2008).

[6] M. A. Zeb, J. Kohanoff, D. Sanchez-Portal, A. Arnau, J. I. Juaristi, and E. Artacho, Phys. Rev. Lett. **108**, 225504 (2012).

---

*Corresponding author e-mail address: e.artacho@nanogune.eu

DYNAMIC SCREENING OF A LOCALIZED HOLE AND A PHOTOELECTRON EMITTED FROM A METAL CLUSTER

N. E. Koval[1,*], *D. Sánchez-Portal*[1,2], *A. G. Borisov*[3] *and R. Díez Muiño*[1,2]

[1] Centro de Física de Materiales CFM/MPC (CSIC-UPV/EHU), San Sebastián, Spain
[2] Donostia International Physics Center DIPC, San Sebastián, Spain
[3] Institut des Sciences Moléculaires d'Orsay, ISMO,
Unité de Recherches CNRS-Université Paris-Sud UMR 8214, Orsay Cedex, France

1. INTRODUCTION

Recent advances in attosecond spectroscopy techniques have fueled the interest in the theoretical description of electronic processes taking place in the subfemtosecond time scale. We study the coupled dynamic screening of a localized hole and a photoelectron emitted from a metal cluster using a semi-classical model [1]. Electron density dynamics in the cluster is calculated with Time-Dependent Density Functional Theory and the motion of the photoemitted electron is described classically. We show that the dynamic screening of the hole by the cluster electrons affects the motion of the photoemitted electron. At the very beginning of the photoemission process, the emitted electron is accelerated by the cluster electrons that pile up to screen the hole. This is a velocity dependent effect that needs to be accounted for when calculating the energy lost by the electron due to inelastic processes.

2. MODEL AND RESULTS

In our model metallic clusters are described using a spherical jellium model, in which the core ions are substituted by an homogeneous background of positive charge with a density defined by

$$n_0^+(\mathbf{r}) = n_0(r_s)\Theta(R_{cl} - r), \tag{1}$$

where R_{cl} is the radius of the cluster, $\Theta(x)$ is the Heaviside step-function and $n_0(r_s)$ is the constant bulk density, which depends only on the Wigner-Seitz radius r_s: $(1/n_0 = 4\pi r_s^3/3)$. The number of electrons in a neutral cluster is $N = (R_{cl}/r_s)^3$. The ground state density of the cluster $n(\mathbf{r})$ is defined using the spin-restricted density functional theory (DFT) within the Kohn-Sham (KS) formalism. Valence electron dynamics in the cluster is investigated by means of TDDFT. The detailed description of the numerical procedure can be found in Refs. [2, 3, 4].

The electron moves with a constant velocity along the z-axis (cylindrical coordinates (ρ, z) are used) and do not interact directly with the hole. The force created by the cluster on the emitted electron is defined by

$$F_z^{cls}(t) = 2\pi \int d\rho dz\, \rho \frac{n(\rho, z, t) - n_0^+(\rho, z)}{[(z_{el}(t) - z)^2 + \rho^2]^{3/2}} [z_{el}(t) - z] \tag{2}$$

To study the effect of the hole presence on the movement of the photoemitted electron we consider the cases without and with a localized hole at the center of the cluster.

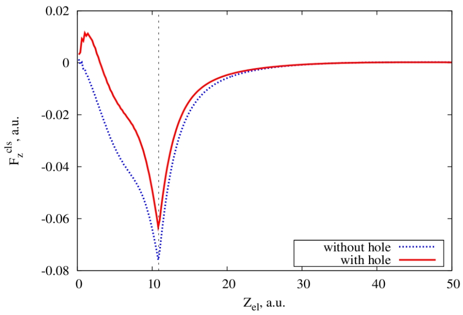

Figure 1: Cluster induced force [Eq. (2)] acting on the electron moving away from the center of the cluster (N=20, r_s=4) as a function of the electron position. The electron moves with a constant velocity $v = 1$ a.u.

From Figure 1 one can see that, in the case of the presence of the hole, the cluster induced force on the photoelectron has positive value at short times. This indicates that the cluster response tends to accelerate the electron at the very beginning of its movement. Although results on Figure 1 are obtained for an electron moving with constant velocity, this result is confirmed by using a more realistic approximation in which the velocity and coordinate of the electron are dependent on time and the hole and the electron interact via a regularized Coulomb potential [1].

3. REFERENCES

[1] N. E. Koval, D. Sánchez-Portal, A. G. Borisov and R. Díez Muiño, Submitted to Nanoscale Res. Lett.

[2] A. G. Borisov, J. I. Juaristi, R. Díez Muiño, D. Sánchez-Portal D, P. M. Echenique, Phys. Rev. A **73**, 012901 (2006).

[3] A. G. Borisov, J. P. Gauyacq, S. V. Shabanov, Surf. Sci. **487**, 243–257 (2001).

[4] M. Quijada, A. G. Borisov, I. Nagy, R. Díez Muiño, and P. M. Echenique, Phys. Rev. A **75**, 042902 (2007).

---

*Corresponding author e-mail address: natalia_koval@ehu.es

Highly charged ion interactions with thin dielectric films

R. E. Lake[1,2*], *J. M. Pomeroy*[1], *and C. E. Sosolik*[2]

[1]Quantum Measurement Division, National Institute of Standards and Technology, Gaithersburg, MD USA
[2]Department of Physics & Astronomy, Clemson University, Clemson, SC USA

1. INTRODUCTION

We present a progress report on experimental and modeling work to understand highly charged ion (HCI) interactions with thin dielectric films. HCI-induced modifications formed in thin films record potential and pre-equilibrium kinetic energy deposited by the projectiles. Additionally, growth of a thin film on a target changes the electronic properties of only the surface, which permits investigations on the role of surface versus bulk electrons in HCI neutralization and surface modification.

2. HCI MODIFIED TUNNEL JUNCTIONS

Tunnel junctions with HCI irradiated barriers were fabricated and measured in order to detect charge-dependent surface modifications formed by the ions [1]. We extract the depth of "crater" defects formed by the HCIs and deduce crater formation energies using a heated spike model (Fig. 1). Estimating an upper bound on the charge dependent pre-equilibrium kinetic energy deposition [2], we determine a lower bound of (27 ± 2) % of the available potential energy for each charge state is required to form of the craters.

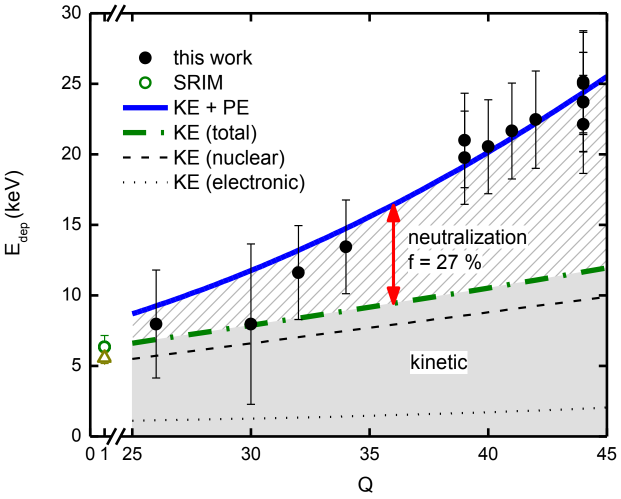

Figure 1: Crater formation energies obtained with a heated spike model. The devices were Co/Al_2O_3/Co tunnel junctions where the Al_2O_3 barriers were irradiated with charge selected beams of Xe^{Q+} (Q = 26 to 44) extracted at kinetic energies (8 x Q) keV.

3. CLASSICAL OVER-THE-BARRIER MODEL FOR THIN FILMS

We apply the classical over-the-barrier (COB) model to HCI neutralization above dielectric films on metals. We model the onset of neutralization as a function of film thickness, permittivity, electron binding energies and charge state. The model describes the crossover between COB for clean metal and bulk insulator targets as film thickness increases. We consider Al_2O_3/Co, LiF/Au and C_{60}/Au targets from recent experiments. The model predicts that for ultrathin C_{60} layers on Au the capture distance increases with respect to a clean metal (Fig. 2). This result is consistent with an observed film thickness-dependent increase in relative electron emission yield [3]. As film thickness grows we identify three regimes for the onset of neutralization: i) electron capture from the metal limited by the vacuum barrier (Fig. 2), ii) electron capture from the metal limited by the dielectric thin film and iii) electron capture from the valence band of the dielectric film.

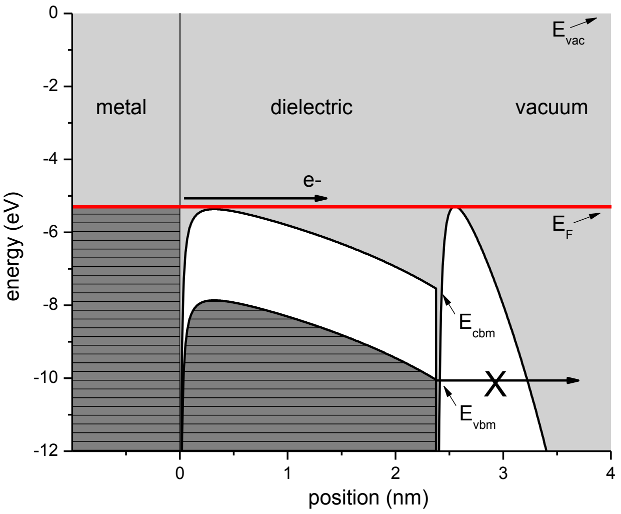

Figure 2: Potential energy near a Q = 24 ion at the critical distance R'_c =5.2 nm (from metal). The film thickness is s = 2.4 nm and the metal work function is W = 5.3 eV. Film parameters are from C_{60} in [3]. The first captured electron originates from the metal. The film increases the critical distance ($R'_c > [2Q]^{1/2}/W$ in a.u.).

[1] R. E. Lake *et al.*, Phys. Rev. Lett. **107**, 063202 (2011)
[2] J. P. Biersack, Nucl. Instrum. Methods Phys. Res., Sect. B **80–81**, 12 (1993)
[3] E. Bodewits *et al.*, Phys. Rev. A 84, 042901 (2011)

---

[*] Corresponding author e-mail address: rlake@g.clemson.edu

MEASUREMENTS OF VELOCITY DEPENDENT ENERGY DEPOSITION FROM HIGHLY CHARGED IONS ON SOLIDS

J.M. Pomeroy[1,2,*] *and R.E. Lake*[1,2]

[1]Quantum Metrology Division, NIST, 100 Bureau Dr., MS 8423, Gaithersburg, MD 20899-8423 USA
[2]Dept. of Physics and Astronomy, Clemson University, Clemson, SC 29634 USA

1. ABSTRACT

Preliminary data from ongoing experimental efforts indicate that total energy deposited by highly charged ions (HCIs) in a thin insulating film *decreases* as the kinetic energy *increases*. For singly charged ions, the kinetic energy deposition per length (stopping power) increases monotonically with kinetic energy up to the nuclear stopping power peak, where the crossover from nuclear to electronic stopping regimes may result in a shallow minima before strong electronic stopping leads to much higher stopping powers. However, for HCIs, the Coulombic interactions enhanced by the high charge state are predicted to dramatically increase the stopping power at low kinetic energies where interaction times are long, as calculated by Biersack[1] in Fig. 1. This is solely kinetic energy loss enhanced by charge state, separate from the deposition of the HCI's neutralization energy (electronic energy released by HCI during electron capture). Further, the uncertainty in the charge-enhanced kinetic stopping hampers accurate determination of neutralization energy absorption, e.g., [2].

In a few cases, the stopping power of HCIs has been measured, e.g., Ref. [3], but kinetic energy dependence in the "slow" regime requires further investigation. Following the experimental strategy used in Ref. [2], we are using tunnel junction devices to probe stopping powers as a function of kinetic energy, by way of measuring the change in the tunnel conductance due to HCI cratering. An example of initial results are shown in Fig. 2, where for Xe^{41+}, increasing the kinetic energy a factor of two led to an decrease of more than a factor of two in change in the tunnel conductance. A similar result has been obtained for Xe^{36+}.

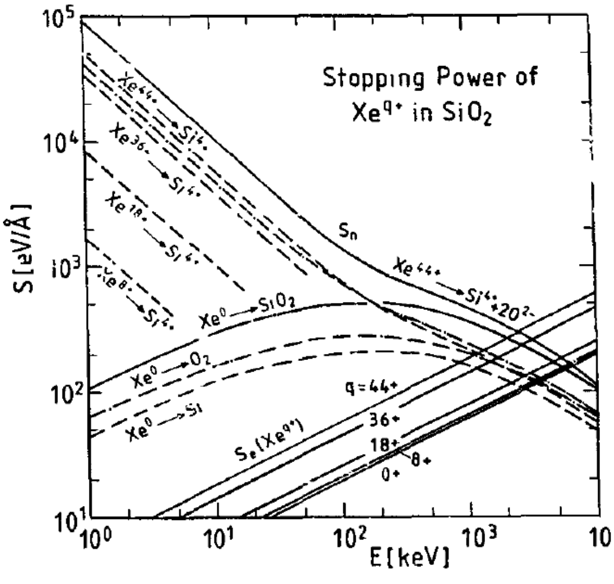

Figure 1: Theroretical prediction of increased nuclear and electronic stopping power as a function kinetic energy (reproduced from Ref. [1]).

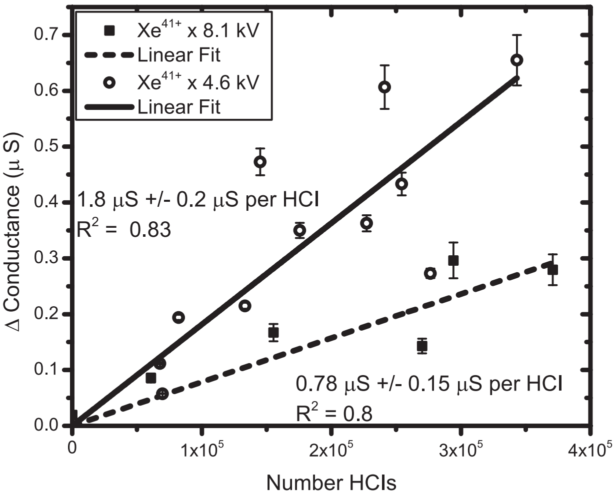

Figure 2: Recent experimental data indicating increasing crater depths (conductance) for HCIs incident on thin insulating films with decreased kinetic energy.

2. REFERENCES

[1] J. P. Biersack, Nucl. Instrum. Methods Phys. Res., Sect. B **80-81**, 12 (1993).

[2] R. E. Lake, J. M. Pomeroy, H. Grube, and C. E. Sosolik, Phys. Rev. Lett. **107**, 063202 (2011).

[3] D. Schneider, J. Steiger, T. Schenkel, and J. C. Lopez-Urrutia, in *Atomic physics with heavy ions*, edited by H. F. Beyer and V. P. Shevelko (Springer, Berlin; New York, 1999), Chap. 2, pp. 30–62.

---

[*] Corresponding author e-mail address: joshua.pomeroy@nist.gov

A SIMPLE MODEL TO CALCULATE EXCITON PRODUCTION IN PROTON LiF GRAZING COLLISIONS

J. E. Miraglia[1,*],and M. S. Gravielle[1]

[1] Instituto de Astronomía y Física del Espacio, CONICET –UBA, Buenos Aires, Argentina

In this work the production of excitons in a Lithium Fluoride crystal induced by proton impact is studied in the intermediate and high energy regime (from 50 keV to 1 MeV). To represent this process we propose a simple model that accounts for the influence of the Coulomb grid of the target by dressing the crystal ions with 44 concentric Coulomb cages, like an onion [1]. Due to the binding Madelung potential created by the Coulomb cages, the Fluor ions present excited states, which are much alike the hydrogen atomic states as the principal quantum number increases. These excited states are interpretated as Frenkel-type excitons [2], associated with a hole and an electron both placed in the same crystal ion. Therefore, the exciton formation is reduced to a local process of ion-onion excitation (H^+-F@ and H^+-Li@).

In the framework of the onion model, stopping power and total cross section are calculated by using the first Born and the Continuum Distorted Wave - Eikonal Initial State (CDW-EIS) approximations. Results for protons moving inside the crystal are compared with available experiments in Figure 1. Our model predicts quite well stopping power experiments at high energies [3],.and also in the intermediate energy range when the Born model is used. The contribution of the exciton production was found to be significant for the inelastic cross sections, which are associated with the projectile mean-free path. In particular, at low impact energies (less than 25 keV/amu) the exciton cross section seems to be more important than ionization.

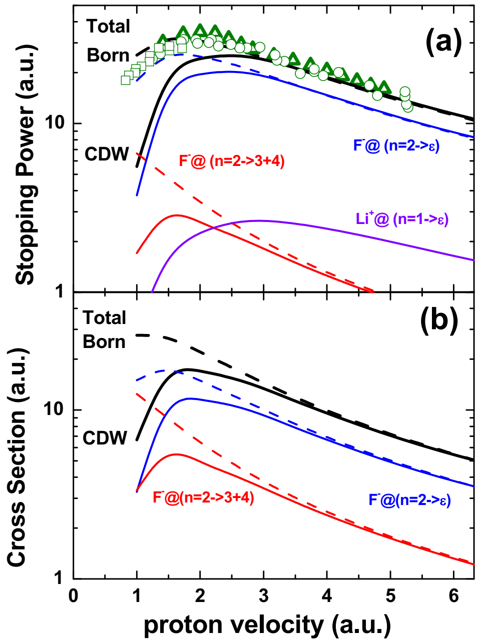

Figure 1: Stopping power (a) and total cross sections (b) for protons moving in a LiF crystal.

We also investigate the exciton production when heavy ions collide with LiF surfaces under grazing incidence conditions. In this case, we found that between 7 to 15 excitons per incident proton are produced (see Figure 2), becoming the exciton formation a relevant mechanism of inelastic transitions. After the exciton is created, it moves inside the crystal. Its movement can be interpreted as an excitation transfer mechanism [4] between different sites. We estimate the exciton velocity to be up to 0.02 a.u., which is smaller than the velocity of the hole. In our model the hole movement can be described as hole transfer between two neighbor onions, to give a velocity around 0.2, in agreement with Ref.[5]

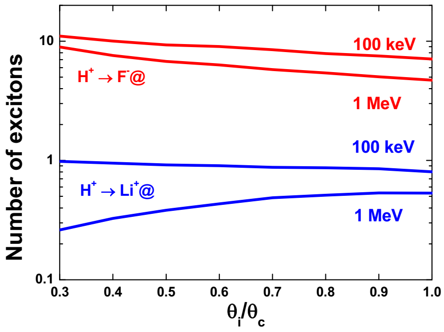

Figure 2: Number of excitons produced by grazing proton collisions on LiF surfaces, as a function of the incident angle (θ_i) divided the critical one (θ_c).

1. REFERENCES

[1] J. E. Miraglia and M. S. Gravielle Phys Rev A **84**, 62901 (2011).

[2] D. L. Dexter and R. S, Knox, Excitons (John Wiley & Sons N.Y. 1965).

[3] M. Draxler, Phys. Rev. Lett. **95** (2005) 113201, M. Bader, Phys. Rev. **103**, 32 (1956).

[4] R. A. Buckingham and A. Dalgarno, Proc. of the R. Soc. A **213**, 506 (1952).

[5] L. Wirtz, *et al*, Nucl.Inst. and Meth. B ***182***,36 (2001).

---

[*] miraglia@iafe.uba.ar

A PROCEDURE TO DETERMINE ELECTRONIC ENERGY LOSS FROM RELATIVE MEASUREMENTS WITH TOF-LEIS

D. Roth[1,*], *D. Goebl*[1], *D. Primetzhofer*[1,2], *and P. Bauer*[1]

[1] Institut für Experimentalphysik, Johannes Kepler Universität Linz, Altenbergerstraße 69, A-4040 Linz, Austria
[2] Institutionen för Fysik och Astronomi, Uppsala Universitet, Box 516, S-751 20 Uppsala, Sweden

1. INTRODUCTION

Low-energy ion scattering (LEIS) is a well established tool for composition analysis of the outermost atomic layers [1]. By use of a time-of-flight spectrometer (TOF-LEIS), it is possible to detect both species of backscattered particles, ions and neutral atoms. The energy loss of a projectile along its path in a solid is due to interaction with either the atoms (nuclear stopping) or the electrons (electronic stopping). For electronic interactions, the mean energy loss per monolayer is given by the electronic stopping cross section (SCS)

$$\varepsilon = \frac{1}{n}\frac{dE}{dx} \tag{1}$$

where n is the atomic density of the target material. The energy spectrum of backscattered projectiles contains information on electronic stopping in a twofold way: for nanometer films, the spectrum width is governed by ε, whereas the spectrum height at the high energy onset is – at least to first order – inversely proportional to ε. Whenever nanometer films of good quality cannot be produced, it is convenient to determine ε relative to a reference material, for which ε is known: spectra of two thick samples (reference and new material) are recorded under identical experimental conditions. Based on the single scattering model for backscattering, the ratio of the spectrum heights is given by the ratios of scattering cross sections and of stopping cross sections [2]:

$$\frac{H_{ref}}{H} = \frac{d\sigma_{ref}/d\Omega}{d\sigma/d\Omega}\frac{[\varepsilon]}{[\varepsilon_{ref}]} \tag{2}$$

However, in view of the increased probability of multiple scattering at low projectile energies, the question arises if this model still holds true in the regime of LEIS.

2. PROCEDURE OF DATA EVALUATION

In this contribution, we present a procedure for extracting information regarding the SCS from relative measurements. It is based on comparison of the height ratios obtained from both, experiment and simulation. In Fig. 1, the ratio of spectrum heights for 4 keV protons backscattered from amorphous Cu (reference) and Ge is compared to the corresponding ratio obtained from Monte Carlo simulations (using the TRBS code [3]). In the simulations, electronic stopping was varied systematically by multiplying the tabulated SCS for Ge by a correction factor, $c_{\varepsilon,Ge}$. The SCS for Cu was set in accordance with earlier measurements [4]. As shown in Fig. 1, different electronic stopping for Ge leads to different spectrum heights and, consequently, to different height ratios, H_{Cu}/H_{Ge}. Thus, from the comparison of the simulated height ratio to that deduced from experiment ε for Ge can be extracted.

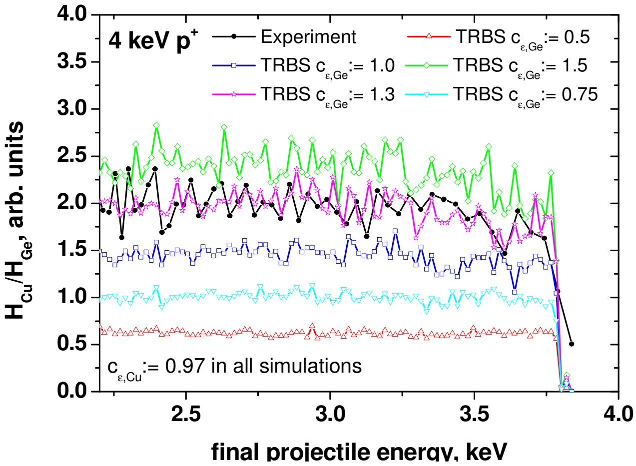

Figure 1: Comparison of experimental H_{Cu}/H_{Ge} with corresponding ratios obtained from MC simulations with varied ε_{Ge} and constant ε_{Cu}.

3. REFERENCES

[1] H.H. Brongersma, M. Draxler, M. de Ridder, and P. Bauer, Surf. Sci. Rep. **62**, 3: 63-109 (2007).
[2] W.K. Chu, J.W. Mayer, and M.A. Nicolet, Backscattering Spectrometry, Ch. 3, New York: Academic Press (1978).
[3] J.P. Biersack, E. Steinbauer, and P. Bauer, Nucl. Instr. Meth. B **61**: 77-82 (1991).
[4] S.N. Markin, D. Primetzhofer, M. Spitz, and P. Bauer, Phys. Rev. B **80**, 205105 (2009).

---

[*] Corresponding author e-mail address: dietmar.roth@jku.at

NEUTRALIZATION PROBABILITY OF PROTONS SCATTERED OFF A LITHIUM FLUORIDE SURFACE: A QUANTUM CHEMISTRY APPROACH

P. Tiwald[1,*], *S. Gräfe*[1], *J. Burgdörfer*[1], *and L. Wirtz*[2]

[1] Institute for Theoretical Physics, Vienna University of Technology, A-1040 Vienna, Austria, EU
[2] Physics and Materials Science Research Unit, University of Luxembourg, L-1511 Luxembourg, Luxembourg, EU

Many effects in heavy particle-surface scattering can be described within the adiabatic (or Born-Oppenheimer) approximation when the projectile velocity v_p is much smaller than the characteristic speed of the target electronic motion v_e (see e.g. [1, 2]). In this case a single potential energy surface (PES) corresponding to the electronic ground state of the system governs the interaction dynamics. Standard approaches to calculate the ground state PES are the Hartree-Fock approximation and density functional theory. Applying high level quantum chemistry methods, we go beyond the Born-Oppenheimer regime when v_p becomes comparable to v_e and non-adiabatic effects are no longer negligible. This makes the description of many interesting physical effects such as charge transfer between projectile and surface feasible.

Configuration interaction methods have proven to be a powerful tool to describe the transient quasi-molecule during ion-atom collisions and to accurately calculate charge transfer cross sections including correlation and polarization effects (see e.g. [3]). We use these methods within the framework of the embedded cluster approach to determine the charge transfer cross sections of a projectile scattered at a surface. In this approach a small active cluster is embedded into a surrounding matrix representing the infinite system. We incorporated non-adiabatic effects, the interaction of ground and excited states, correlation, and polarization in the description of particle surface scattering.

To benchmark the approach we study the charge exchange between a proton and a lithium fluoride (LiF) surface. LiF is a wide band gap insulator with low hole mobility for which a small active cluster should suffice to describe the interaction dynamics. At large distances between projectile and surface the capture level of the proton ($E_{cap} = -13.6$ eV) lies within the valence band of LiF (-12.3 eV $> E_{val} > -15.8$ eV) which implies that resonant charge transfer is likely to occur.

We use active clusters of varying sizes which are embedded into a large matrix of point charges to account for the infinitely large surface. By scanning the irreducible surface unit cell with the proton in x, y and z direction we calculate 3D potential energy surfaces of four electronic states including the non-adiabatic couplings between them.

This information serves as input for the determination of the neutralization probability of a proton beam (perpendicular incidence, 20 eV $\lesssim E_{kin} \lesssim$ 300 eV) scattered off a LiF surface using Tully's semiclassical surface hopping algorithm [4]. With this approach a detailed analysis of the scattering event is possible. As shown in Fig. 1 the neutralization probability of the backscattered projectile as a function of the initial projectile momentum p_p shows a maximum due to the interplay of increasing penetration of projectiles into the surface and increasing neutralization with increasing p_p. Furthermore, the neutralization probability exhibits traces of Stückelberg oscillations stemming from trajectories which are initiated within a narrow region above a surface fluoride ion.

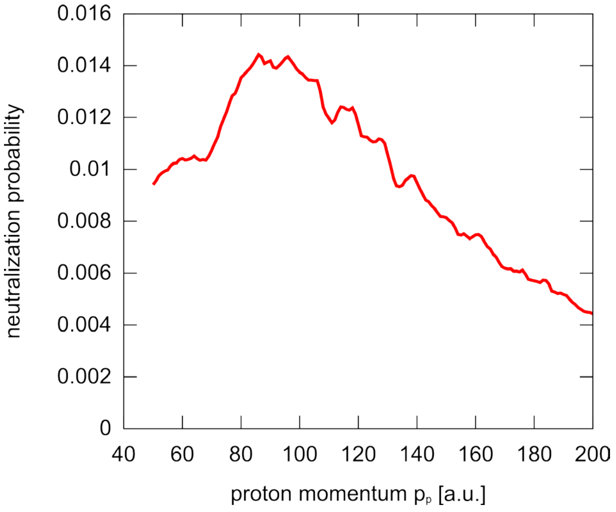

Figure 1: Neutralization probability of a proton beam backscattered from a LiF surface. Modulations in the neutralization probability in the range from $100 < p_p < 160$ are traces of Stückelberg oscillations.

REFERENCES

[1] F. Aigner et al., Phys. Rev. Lett. **101**, 253201 (2008).

[2] P. Tiwald et al., Phys. Rev. B. **82**, 125453 (2010).

[3] N. Vaeck et al., J. Phys. B: At. Mol. Opt. Phys. 32 409 (1999)

[4] J. C. Tully, J. Chem. Phys. **93**, 1061 (1990).

ACKNOWLEDGMENTS

This work was supported by the Austrian Science Fund (SFB F41, "ViCoM").

---

*Corresponding author e-mail address: paul@dollywood.itp.tuwien.ac.at

MCs_n^+-SIMS: AN APPROACH FOR COMPLETE COMPENSATION OF ‘MATRIX EFFECT’ AND EXACT COMPOSITION ANALYSIS OF MBE-GROWN Si/Ge SUPERLATTICE AND $Si_{1-x}Ge_x$ ALLOY STRUCTURES

P. Chakraborty*

[1] Surface Physics Division, Saha Institute of Nuclear Physics, Kolkata, INDIA

SiGe alloy, owing to its high electron and hole mobility, has potential applications in high-speed microelectronic device technology. The optimization of such technology requires the precise determination of Ge concentration in the full range of composition and the understanding and control of the Ge–Si interdiffusion phenomenon. The most appropriate analytical technique with highest detection sensitivity (~subparts per billion) for measuring elemental concentration is secondary ion mass spectrometry (SIMS). However, strong compositional dependence of secondary ion yield, i.e. “matrix effect,” has always made SIMS quantification extremely difficult. When the concentration of the analyzed element becomes too high with respect to the reference material, matrix effects may be even more dominant, thereby degrading the reliability of the measured SIMS profiles strongly. This is particularly the case with $Si_{1-x}Ge_x$ layers, in which matrix effects are systematically observed under conventional SIMS and these effects increase monotonically with Ge atomic fraction. Many solutions have been proposed to reduce and/or suppress the matrix effects, provided the impact energy is lower than 2 keV. A procedure based on MCs_n^+ ($n = 1, 2, 3, \ldots$)-SIMS approach for the accurate quantification of Ge concentration in molecular beam epitaxy (MBE)-grown $Si_{1-x}Ge_x$ ($0<x<0.72$) alloys has been proposed. The “matrix effect” is shown to be completely suppressed for all Ge concentrations irrespective of impact Cs^+ ion energies. Quantification of germanium content has essentially been achieved through precise estimation of “relative sensitivity factor” (RSF) based on the proposed formation mechanism of MCs_n^+ molecular ions. The novel methodology has successfully been applied in generating electron density profile (EDP) of an MBE grown Si/Ge superlattice structure and the results have been found to be in good agreement with EDP independently extracted through X-ray reflectivity. The talk will address the formation mechanisms of MCs_n^+ molecular ion complexes and potential applicability of the MCs_n^+-SIMS in precise quantitative analysis of Si/Ge superlattice and SiGe alloy compositions

---

* Corresponding author e-mail address: purushottam.chakraborty@saha.ac.in, purushottam.chakraborty@gmail.com

Tuesday
18 September 2012

HIGH SENSIVITY SNMS SURFACE ANALYSIS

B.V. King[1,*], *I.V. Veryovkin*[2], *J.F. Moore*[3], *AV Zinovev*[2], *S.V. Baryshev*[2], *C.E. Tripa*[2]

[1] School of Mathematical and Physical Sciences, University of Newcastle, Callaghan 2308, Australia
[2] Materials Science Division, Argonne National Laboratory, Argonne, IL 60439 USA
[3] .MassThink LLC, Naperville IL 60563, USA ..

1. INTRODUCTION

Sputter neutral mass spectrometry permits extremely sensitive analysis of solid surfaces, allowing for example depth profiling with sub-ppb sensitivity or the identification of large atomic clusters sputtered from the surface. We will discuss both aspects in this talk, with relevance to the analysis of magnesium in silicon wafers returned from the NASA Genesis space mission or the ejection of clusters containing up to 30 atoms from the CuAlAu ternary alloy as well as AuAl and CuAu binary alloys.

2. RESULTS

2.1. Depth profiling of Genesis samples

In the Genesis space return mission, silicon substrates were irradiated with solar wind (SW) for 27 months, causing implantation of SW atoms at ppm to sub ppb concentrations about 20nm below the surface. The samples effectively sat at a temperature of 200°C over that time period, causing radiation enhanced diffusion of solar wind impurity atoms. Unfortunately the spacecraft crashed on reentry causing surface contamination of wafers and a challenging analysis problem to separate SW atoms from surface contamination. Mg has however been depth profiled in Si Genesis wafers using laser postionisation SNMS giving an accumulated dose of 2.24×10^{12} cm^{-2} predominantly trapped at damage centers generated by 1keV H implantation [1,2]. The variation of contamination with position on the wafer measured by SNMS as well as other techniques (AFM, SRTXRF) and sample cleaning methods will be discussed.

2.2. Cluster Ejection

Figure 1 shows the relative signal from $Au_{n-x}Al_x$ clusters sputtered from an Au_4Al surface using normally incident 15keV Ar and illustrates that quite large clusters may be sputtered and survive until detection. The sensitivity of laser postionisation SNMS allows signals over many orders of magnitude to be detected. The cluster signals from Au_4Al follow at power law dependence on cluster size modulated by an odd-even variation related to the stability of cluster photoions.

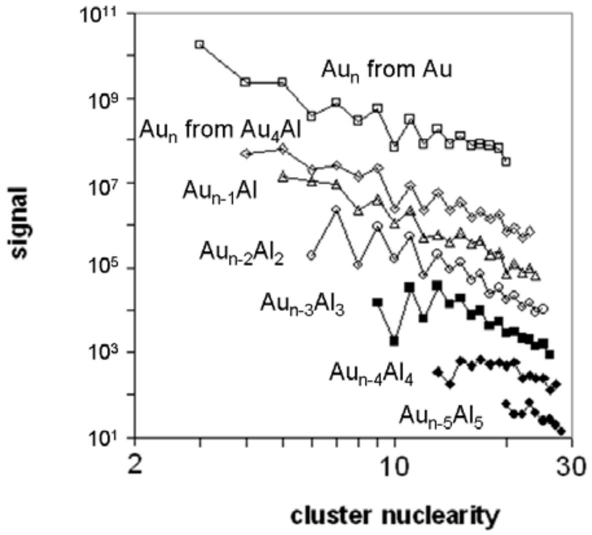

Figure 1: Neutral clusters sputtered from Au_4Al by 15keV Ar at normal incidence.

The power law parameter is related to the energy deposited into the cascade by the ion beam as well as to the cluster stability. We will discuss these dependences for binary alloys with high (AuAl) and lower (CuAu) binding energies as well as for the ternary alloy $Au_7Cu_5Al_4$.

3. REFERENCES

[1] BV King, JF Moore, AV Zinovev, IV Veryovkin, MJ Pellin, Nucl. Instr.Meth **B267**, 2757 (2009)
[2] SV Baryshev, AV Zinovev, CE Tripa, MJ Pellin, DS Burnett, IV Veryovkin, LPSC XLIII, Abstract #2909
[3] B.V. King, M.J. Pellin, DS Burnett, Appl Surf. Sci. **255** 1455 (2008)
[4] BV King, IV Veryovkin, JF Moore, WF Calaway, MJ Pellin, Surface Science **603** 819 (2009)

---

[*] Corresponding author e-mail address: bruce.king@newcastle.edu.au

SECONDARY ION FORMATION IN SPUTTERING OF METALS: EXPERIMENT AND THEORY

A.Wucher*

[1] Faculty of Physics, University Duisburg-Essen, 47048 Duisburg, Germany

1. INTRODUCTION

The formation of secondary ions in sputtering is still far from being completely understood. Even for the conceptually simplest case of a metal atom sputtered from a clean metallic surface, no theoretical model published so far can explain all available experimental data. Moreover, many different models result in very similar predictions, thereby greatly complicating the interpretation of measured data in terms of the underlying fundamental ionization mechanism. In addition, published experimental data appear partly contradictory, and the assessment of reliable information is difficult.

2. METHOD

2.1. Theory

We will first briefly review the main approaches to model secondary ion formation along with the resulting predictions with respect to key dependencies of the observed ionization probability. As a second step, we will present a microscopic, dynamic model [1,2] which takes into account the detailed lattice and electron dynamics following a projectile impact and allows to predict an individual ionization probability for each sputtered atom. The results will be used in order to discuss the validity of basic assumptions and approximations underlying the published analytical models. We will show that the dynamic model leads to novel predictions regarding, for instance, the dependence of ionization probabilities on projectile impact angle as depicted in Figure 1.

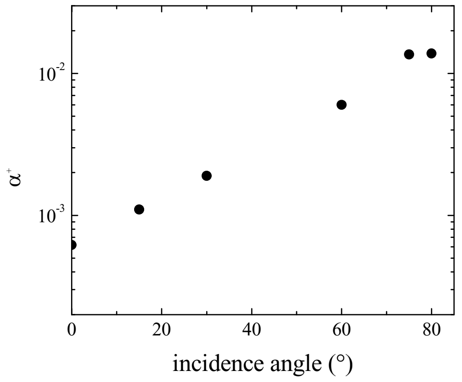

Figure 1: Calculated ionization probability of sputtered Ag atoms as a function of projectile impact angle [3].

2.2. Experiment

On the experimental side, we will briefly review the present status and discuss the available data on measured ionization probabilities particularly in terms of accuracy and reliability. We will demonstrate that a reliable assessment of a sputtered particle's ionization probability ultimately requires the detection of secondary ions along with their neutral counterparts, thereby ruling out a relatively large body of data measured on secondary ions alone [4] . The data deemed reliable are then used to test the model predictions, and the results will be compared to similar assessments based on, for instance, the electron tunneling model [5].

3. RESULT

As one of the most important results of this study, we find that the ionization probability of atoms sputtered from a clean metallic surface is significantly influenced by the kinetic excitation dynamics during the collision cascade. We will show that a seeming agreement between experimentally observed trends and simple model predictions may be fortituous, thereby misleading the interpretation in terms of the underlying ionization mechanism. Moreover, we demonstrate a significant change of the nature of the secondary ion formation process when switching from atomic to multi-atomic projectiles.

4. REFERENCES

[1] B. Weidtmann, A. Duvenbeck, and A. Wucher, Appl. Surf. Sci. **255**, 813 (2008).
[2] B. Weidtmann, S. Hanke, A. Duvenbeck, and A. Wucher, Surf. Interf. Anal. **43**, 24 (2011).
[3] B. Weidtmann et al., Phys. Rev. B (to be published)
[4] A. Wucher, Appl. Surf. Sci. **255**, 1194 (2008).
[5] K. Wittmaack, Mat. Fys. Medd. **52**, 465 (2007)

---

[*] Corresponding author e-mail address: andreas.wucher@uni-due.de

IN NEED OF A NOVEL SITE SPECIFIC MODEL OF ION FORMATION AT SURFACES

Klaus Wittmaack

Helmholtz Zentrum München, Institute of Radiation Protection, 85758 Neuherberg, Germany

1. INTRODUCTION

The processes controlling ion formation at ion bombarded surfaces have been of prime concern at all workshops of this series. However, a quantitative understanding of observed phenomena is still at a rudimentary level. This holds true for experimental data collected in ion scattering spectrometry (ISS) and, particularly, in secondary ion mass spectrometry (SIMS). Attempts to rationalize measured ion yields were commonly based on the semi-classical theory [1,2], also referred to as the tunneling model. In this one-electron picture of charge transfer, positive or negative ions can be formed near the surface, as long as the shifted ionization (affinity) level is above (below) the Fermi level. The ion yield actually measured at large distances from the surface is determined by the probability that the generated ion can escape neutralization after the respective level has crossed the Fermi level. The survival probability increases with decreasing transition rate, i.e., with decreasing level width, and with increasing velocity of the departing atom (shorter time for neutralization). Furthermore, positive (negative) ion yields should increase with increasing (decreasing) work function of the sample. Whereas issues of level shift and level width are the subject of theoretical studies [3], information concerning the predicted velocity dependence must be provided by properly designed experiments. To study the assumed correlation with the position of the Fermi level, the work function must be varied in a controlled manner. This is commonly achieved by depositing alkali atoms on the sample surface or by converting implanted alkali ions to adatoms [4].

This presentation summarizes the results of a comprehensive review on the charge state of ions formed in the presence of cesium. Essentially all information relevant to the problem was collected. The usefulness and reliability of available experimental data was explored in great detail with the aim of testing the applicability of the semi-classical model. Selected results gathered in course of this exercise have already been published very recently [4,5].

2. SUMMARY OF RESULTS

To explore the predicted dependence of ionisation probabilities on the velocity of sputtered atoms or ions, the performance characteristics of employed SIMS instruments need to be known very well. Only magnetic sector field mass spectrometers can be shown to allow measurements of secondary ion energy spectra with quantifiable transmission. Experimental data thus obtained on the yields of negative ions sputtered from metals or alloys exhibit no distinct velocity dependence, for Cs induced yield changes sometimes exceeding five orders of magnitude [6]. The tunnelling model cannot explain these results, see Fig. 1. Small velocity effects observed with species like O^- [7] are presumably caused by an ‘artefact’ associated with Cs-coverage dependent changes of the energy spectrum of sputtered neutral atoms.

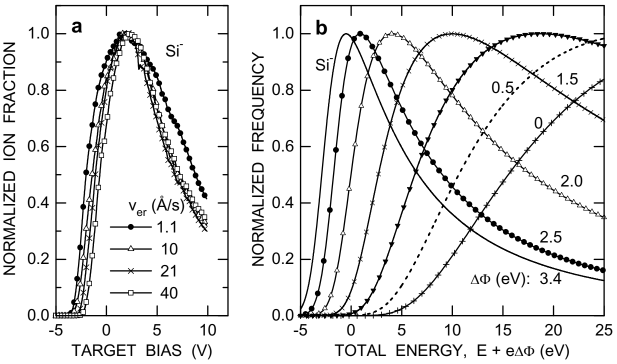

Figure 1: Comparison of energy spectra of Si^- secondary ions sputtered from Si. (a) Experimental data recorded for different fluxes of neutral Cs, (b) velocity dependence of energy spectra predicted by the tunneling model.

SIMS and ISS data leave little doubt that not the global but rather the local potential generated by the presence of Cs adatoms controls the efficiency of ion production. These results call for the development of a novel theoretical model describing secondary ion formation in site specific terms (local chemistry), with measured global WF changes predominantly serving to quantify the Cs coverage. Dynamic randomisation of the ion bombarded sample during the sputtering event could prevent neutralisation of sputtered ions, a line of thinking that might pave the way to explaining the absence of a velocity effect

3. REFERENCES

[1] J. K. Nørskov, B. I. Lundqvist, Phys. Rev. B **19**, 5661 (1979).
[2] R. Brako, D. M. Newns, Surf. Sci. **108**, 253 (1981).
[3] A. G. Borisov, G. E. Makhmetov, D. Teillet-Billy, J.P. Gauyacq, Surf. Sci. **350,** L205 (1996).
[4] K. Wittmaack, Int. J. Mass Spectrom. **313,** 68 (2012).
[5] K. Wittmaack, Surf. Sci. **606,** L18 (2012).
[6] M. Bernheim, F. Le Bourse, Nucl. Instrum. Methods B **27**, 94 (1987).
[7] M.L. Yu, Phys. Rev. Lett. **47,** 1325 (1981).

---

[*] Corresponding author e-mail address: wittmaack@helmholtz-muenchen.de

A MICROSCOPIC MODEL FOR TRACK FORMATION BY SWIFT HEAVY IONS

G. Wachter[1,*], K. Tőkési[2], G. Betz[3], C. Lemell[1] and J. Burgdörfer[1]

[1] Institute for Theoretical Physics, Vienna University of Technology, Wiedner
Hauptstraße 8-10, A-1040 Vienna, Austria, EU
[2] Institute of Nuclear Research of the Hungarian Academy of Science (ATOMKI),
H-4001 Debrecen, P.O. Box 51, Hungary, EU
[3] Institute for Applied Physics, Vienna University of Technology, Wiedner
Hauptstraße 8-10, A-1040 Vienna, Austria, EU

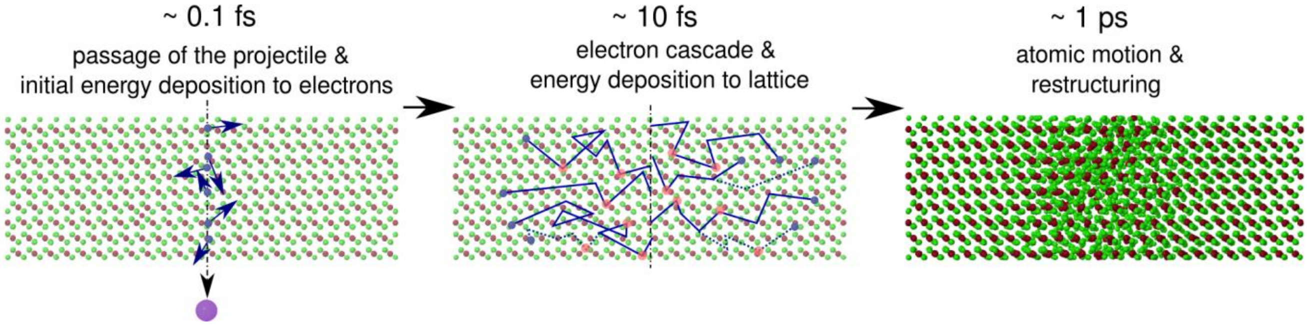

Figure 1: Sketch of the step sequence of processes leading to track formation, time scales as indicated.

1. SYNOPSIS

Collisions of swift heavy ions with insulator targets lead to a damage zone around the path of projectiles, the so-called tracks. We theoretically investigate track formation and propose a fully microscopic three-step model that incorporates processes on multiple time scales (see Fig. 1). The appearance of tracks is linked to melting of the target on a nanometric length scale.

2. MODEL FOR TRACK FORMATION

Experiments show that tracks in insulator targets appear only if above a threshold energy transfer per path length to the medium, i.e. above a critical stopping power. Earlier interpretation has associated this threshold with the melting temperature of the material. Theoretical work was largely based on a macroscopic description, the thermal spike model [1]. In this work, we focus on the microscopic processes that lead to track formation. We find that for a class of target materials the sequence of events leading to track formation can be well described by a three-step model due to the disparate time scales involved (see Fig. 1):

Excitation of the electronic subsystem of the target. The primary energy deposition from the swift projectile is modeled within time-dependent perturbation theory for binary ion-atom collisions (continuum distorted wave - eikonal initial state, CDW-EIS [2]).

Energy diffusion in the electronic system and energy transfer to the target lattice. The resulting electron cascade is modeled by a classical trajectory Monte Carlo simulation [3,4] incorporating lattice heating via electron-phonon-interaction. The energy transferred to the target lattice leads to an elevated temperature, allowing melting of the lattice around the ion path.

Nano-melting. In the third step we follow the temporal evolution of a heated region in a crystal at ambient temperature using a proof-of-principle classical molecular dynamics simulation.

Our simulation allows to link experimentally observed threshold behavior to melting on the nano scale. Results presented for the test system Xe → CaF_2 are found in good agreement with experiment.

3. REFERENCES

[1] A. Meftah et al, Phys. Rev. B **49** 12457 (1994)
[2] D. S. F. Crothers et al, J. Phys. B: At. Mol. Phys **16** 3229 (1983)
[3] B. Solleder et al, Phys. Rev. B **76** 075115 (2007)
[4] B. Gervais and S. Bouffard, Nucl. Instrum. Meth. B **88**, 355 (1994)

---

[*] Corresponding author e-mail address: georg.wachter@tuwien.ac.at

ION TRACKS PRODUCED BY SUB-MeV C_{60} IONS IN AMORPHOUS Si_3N_4

Y. Morita[1], K. Nakajima[1], M. Suzuki[1], K. Narumi[2], Y. Saitoh[2], N. Ishikawa[3], K. Hojou[4], M. Tsujimoto[5], S. Isoda[5] and K. Kimura[1]*

[1]Department of Micro Engineering, Kyoto University, Kyoto 606-8501, Japan
[2]Takasaki Advanced Radiation Research Institute, Japan Atomic Energy Agency, 1233 Watanuki-machi, Takasaki, Gumma 370-1292, Japan
[3]Nuclear Science and Engineering Directorate, Japan Atomic Energy Agency, Tokai, Naka, Ibaraki 319-1195, Japan
[4]Advanced Science Research Center, Japan Atomic Energy Agency, Tokai, Naka, Ibaraki 319-1195, Japan
[5]Institute for Integrated Cell-Material Sciences, Kyoto University, Kyoto 606-8501, Japan

1. INTRODUCTION

Since the first observation of ion tracks produced by fission fragments from ^{235}U in mica [1], the ion tracks have been extensively studied with various combinations of ions and materials. In case of crystalline materials, the structure of the ion track can be easily observed by TEM. The track interior is amorphized or comprised of defect clusters depending on the material. In case of amorphous materials, however, there has been no direct TEM observation of ion tracks. It is believed that direct TEM observation of ion tracks is difficult due to a lack of sufficient contrast. In this presentation, we will report on the first TEM observation of ion tracks produced in an amorphous material.

2. EXPERIMENTAL

Self-supporting amorphous Si_3N_4 (a-Si_3N_4) films of thickness 20 nm were irradiated with 120 - 720 keV $C_{60}^{+,2+}$ ions to fluences 1 – 5 × 10^{11} ions/cm^2. After the ion irradiation, transmission electron microscopy (TEM) and high-angle annular dark field scanning transmission electron microscopy (HAADF-STEM) observations were performed using a JEOL JEM-2200FS equipped with a field emission gun operating at 200 kV.

3. RESULTS

Figure 1(a) shows an example of the observed plan-view TEM images of the a-Si_3N_4 film irradiated with 720 keV C_{60}^{2+} ions. There are circular structures of almost uniform diameter. Each structure has a bright core which is surrounded by a dark shell. The radius of these quasi-monodisperse circular structures is several nm. The number of these structures agrees with the fluence of the C_{60}^{2+} ions, indicating that single C_{60}^{2+} impacts create individual circular structures. It is known that impact of energetic cluster ions may create crater-like structures on the surface, which might be seen as core-shell structures in the plan-view TEM images. In order to see if the observed structures are attributed to such surface structures or not, the sample was tilted and observed by TEM. Figure 1(b) shows an example of the TEM image of the a-Si_3N_4 film observed at a tilt angle of 25°. The observed structures are elongated along the tilt direction. The observed length (~ 9 nm) of the elongated structures agrees with the projected length of the ion tracks penetrating through the film, confirming that the observed structures are not surface craters.

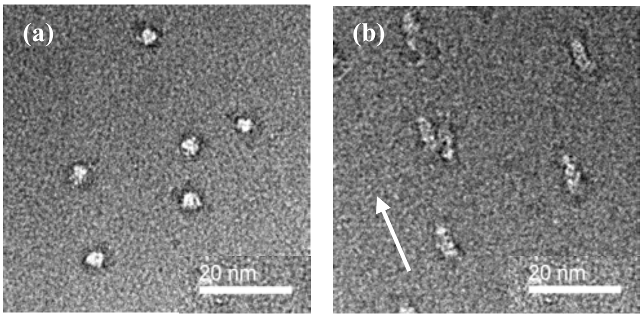

Figure 1: TEM images of a-Si_3N_4 film irradiated with 720 keV C_{60}^{2+} ions. A plan-view image (a) and an image observed with the film tilted by 25º (b).

The observed TEM images suggest that the ion track consists of a low density core and a surrounding high density shell. The TEM contrast, however, strongly depends on focusing conditions. The contrast is even reversed when the focusing conditions are changed. In order to deduce quantitative information without suffering from the focusing problem, the same samples were observed in HAADF-STEM mode. From the observed HAADF-STEM images, the radial density profiles of the ion tracks can be deduced. The obtained profile shows that the ion track consist of a low density core of ~5 nm in diameter and a surrounding shell of ~2.5 nm in width. The density at the track center is ~80% of the bulk density and the density of the shell is 1 – 2% larger than the bulk one. This core-shell structure is similar to the ion tracks in amorphous SiO_2 irradiated with high energy heavy ions observed by small angle x-ray scattering (SAXS) [2]. The role of the nuclear stopping power in the formation of ion tracks will be also discussed.

4. REFERENCES

[1] E.C.H. Silk and R.S. Barnes, Philos. Mag. **4**, 970 (1959).
[2] P. Kluth *et al*, Phys. Rev. Lett. **101** 175503 (2008).

---

* Corresponding author e-mail address: kimura@kues.kyoto-u.ac.jp

THERMAL SPIKE ANALYSIS OF HIGHLY CHARGED ION TRACKS

M. Karlušić[1,*], *M. Jakšić*[1]

[1] Ruđer Bošković Institute, Bijenička cesta 54, 10000 Zagreb, Croatia

The irradiation of material using swift heavy ion or highly charged ion causes excitation of the electron subsystem at nanometer scale along the ion trajectory. According to the thermal spike model, energy deposited into the electron subsystem leads to temperature increase due to electron-phonon coupling. If ion-induced excitation is sufficiently intensive, then melting of the material can occur, and permanent damage (i.e., ion track) can be formed upon rapid cooling. We present an extension of the analytical thermal spike model of Szenes for the analysis of surface ion track produced after the impact of highly charged ion. By applying the model to existing experimental data, more than 60% of the potential energy of the highly charged ion was shown to be retained in the material during the impact and transformed into the energy of the thermal spike. This value is much higher than 20% - 40% of the transferred energy into the thermal spike by swift heavy ion. Thresholds for formation of highly charged ion track in different materials show uniform behavior depending only on few material parameters.

---

[*] Corresponding author e-mail address: marko.karlusic@irb.hr

SURFACE STRUCTURE DETERMINATION VIA FAST ATOM DIFFRACTION

J. Seifert[*], *A. Schüller, and H. Winter*

Institut für Physik, Humboldt-Universität zu Berlin, Newtonstr. 15, 12489 Berlin, Germany

The recent development of “Fast Atom Diffraction” (FAD) and its application to surface structure determination is presented. Under axial surface channeling conditions, for sufficiently small angles of incidence ($\Phi_{\text{in}} \lesssim 1°$) and projectile energies ($E \lesssim 1\,\text{keV}$), diffraction patterns can be observed in the angular distribution of scattered atoms and molecules [1–3]. In analogy to established diffraction techniques, as LEED, RHEED, HAS, or SXRD from the splitting of diffraction spots the unit cell size and symmetry and from relative intensities atomic positions in the topmost layer can be deduced [4]. In combination with triangulation methods based on the transition between axial and planar surface channeling structural models are tested or established. The projectiles are detected by means of a microchannel-plate detector and the number of emitted electrons during scattering process is obtained by a surface barrier detector biased to a high voltage.

For the system of one monolayer of SiO_2/Mo(112) it could be unambiguously distinguished between two competing structural models. The positions of atoms can be determined with an accuracy of a few 0.01 Å [5].

The adsorption of oxygen on a Mo(112) surface was studied in-situ by detection of scattered He-atoms. From the intensity of specularly reflected atoms the formation of well-ordered adsorbate phases is observed. For scattering along axial channels the diffraction patterns provide information on the evolving surface geometry. For the c(2×4) and pg(2×1) adsorbate structure we demonstrate that not only a periodic lattice but also a separated pair of oxygen strings can be the origin of diffraction (Figure 1). The interference of matter waves from two equivalent rows within the unit cell can be analyzed in analogy to Young-type interference in a double-slit experiment. From the spot-splitting the distance of the atomic rows is derived [6]. Based on this information detailed structural models are established by means of triangulation methods. For higher coverages involving a c(4×2) and a p(1×2) surface unit cell, the gradual evolution of a “missing-row” reconstruction is revealed.

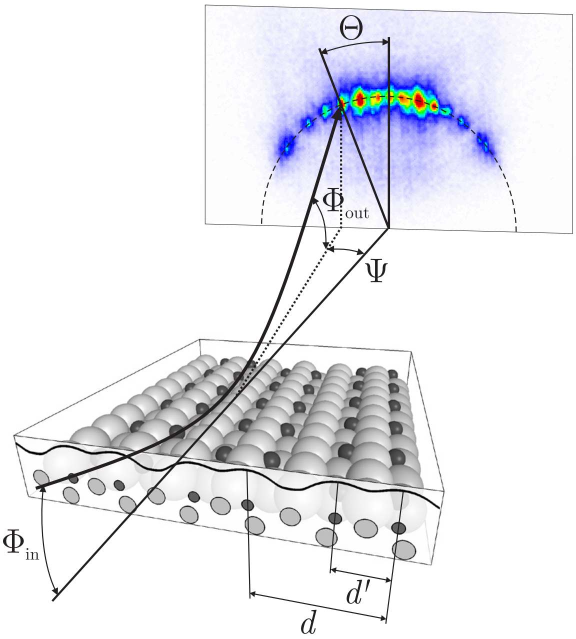

Figure 1: Sketch of scattering geometry and contour of averaged interaction potential in plane normal to beam axis. The scattering from a pair of oxygen rows (dark spheres) results in Young-type interference patterns.

1. REFERENCES

[1] A. Schüller, S. Wethekam, and H. Winter, Phys. Rev. Lett. 98, 016103 (2007).

[2] P. Rousseau, H. Khemliche, A.G. Borisov, and P. Roncin, Phys. Rev. Lett. 98, 016104 (2007).

[3] A. Schüller and H. Winter, Phys. Rev. Lett. 100, 097602 (2008).

[4] H. Winter and A. Schüller, Prog. Surf. Sci. 86, 169 (2011).

[5] J. Seifert, A. Schüller, H. Winter, R. Włodarczyk, J. Sauer, M. Sierka, Phys. Rev. B 82, 035436 (2010).

[6] J. Seifert and H. Winter, Phys. Rev. Lett. 108, 065503 (2012).

---

[*] E-mail: `jan.seifert@physik.hu-berlin.de`

TRANSITION FROM FAST TO SLOW ATOM DIFFRACTION

A. Zugarramurdi[1] *and A. G. Borisov*[1,*]

[1] Institut des Sciences Moléculaires d'Orsay, ISMO, UMR 8214 CNRS-Université Paris-Sud,
Bât. 351, Université Paris-Sud, FR-91405 Orsay CEDEX, France

In recent years a new experimental technique, grazing angle fast atom diffraction (GIFAD, also referred simply as FAD) has proven its power for the study of structural properties of metal, semiconductor and insulator surfaces [1, 2, 3, 4]. In GIFAD light projectiles such as He atoms of energies ∼0.1–2 keV are scattered from the surface under grazing incidence. If the beam is aligned along low index directions at the surface (axial surface channeling conditions), the scattered beam can show a diffraction pattern. This diffraction is possible because, under grazing angles, the de Broglie wavelength associated with the *slow* projectile motion normal to the surface is comparable to interatomic spacings at the surface. One of the advantages of GIFAD over other surface analysis techniques is the extreme sensitivity of the diffraction pattern to the details of the interaction potentials between the projectile and the topmost layer of the atoms at the target. Thus valuable information on the surface structure and reconstruction could be extracted [4, 5, 6].

From the point of view of the interpretation of the experimental data, most of the fully quantum (wave packet propagation) and all semi-classical approaches reported so far rely on the assumption that under axial surface channeling conditions the projectile only "feels" the potential averaged along the atomic strings in the direction of *fast* motion. The computational problem is then reduced to a two-dimensional (2D) scattering in the plane perpendicular to the surface and defined by the normal vector along the corresponding low index direction. Reduction of the three-dimensional (3D) problem to the 2D one allows to simulate diffraction patterns with relatively low computational cost.

Surprisingly, despite this approximation is routinely used, no quantitative assessment of its validity has been attempted so far. Our contribution tends to close this gap and to answer the question: what are the scattering conditions when the 3D structure of potentials becomes important? To this end we study theoretically the scattering of He atoms from the LiF(001) surface of the ionic crystal along the ⟨110⟩ and ⟨100⟩ directions. A large range of scattering conditions (energies and incident angles) is encompassed with fully quantum 3D and 2D calculations based on the wave packet propagation approach. Results (see figure 1) of our study show how the 2D approximation progressively breaks down with decreasing projectile velocity component parallel to the surface so that eventually 3D diffraction along the beam direction sets in.

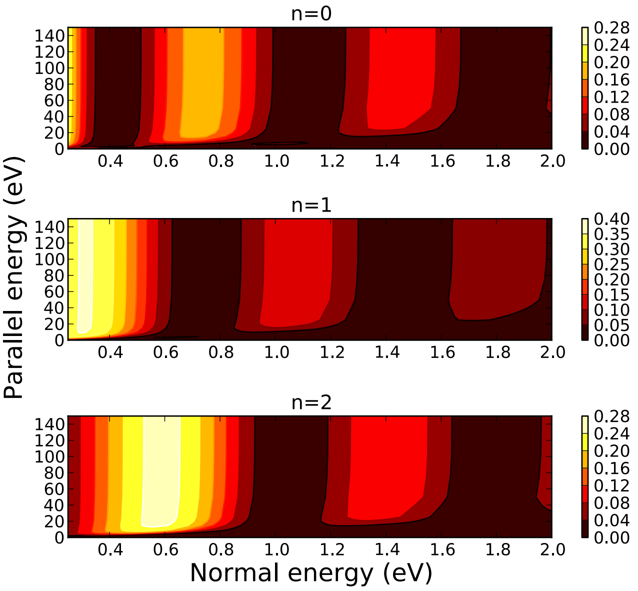

Figure 1: Calculated reflection probabilities of the first diffraction channels, with only exchange of momentum perpendicular to the beam direction, for the scattering of ^{3}He atoms from LiF(001) surface along the ⟨100⟩ direction. Results are shown as a function of the normal and parallel energies associated to the corresponding velocity components of the incident projectile with respect to the surface. The regime of validity of the 2D approximation is determined by the energies where the reflection probabilities are converged to those in the high parallel energy limit.

1. REFERENCES

[1] P. Rousseau, H. Khemliche, A. G. Borisov and P. Roncin, Phys. Rev. Lett. **98** 016104 (2007).

[2] A. Schüller, S. Wethekam and H. Winter, Phys. Rev. Lett. **98** 016103 (2007).

[3] N. Bundaleski, H. Khemliche, P. Soulisse and P. Roncin, Phys. Rev. Lett. **101** 177601 (2008).

[4] H. Winter and A. Schller, Prog. Surf. Sci. **86** 169 (2011).

[5] F. Aigner, N. Simonović, B. Solleder, L. Wirtz and J. Burgdörfer, Phys. Rev. Lett. **101** 253201 (2008).

[6] J. Seifert and H. Winter, Phys. Rev. Lett. **108** 065503 (2012).

---

[*] E-mail: `andrei.borissov@u-psud.fr`

LONGITUDINAL COHERENCE IN FAST DIFFRACTION AT SURFACES

M. Busch, J. Seifert, E. Meyer, and H. Winter

[1] Institut für Physik der Humboldt-Universität zu Berlin, Newtonstr. 15, D-12489 Berlin, Germany

1. INTRODUCTION

The recent discovery of diffraction effects during grazing scattering of fast light atoms and molecules from surfaces with energies up to some keV [1, 2] can be used to investigate the structure of clean surfaces, adlayers as well as ultrathin films [3]. In order to preserve quantum coherence in the scattering event, it is important to avoid excitations of the target and to provide sufficient coherence in the input channel by atomic beams well defined in their angular divergence and kinetic energy.

In the experiments reported so far it were primarily the splittings of Bragg peaks and their intensities which were exploited to deduce information on the periodic arrangement of atoms in the topmost surface layer. As a prominent example we mention here the determination of the “rumpling” of the LiF(001) surface [4]. So far, diffraction effects were present in the regime of surface channeling where quantum scattering is considered for the motion normal to the surface and to the direction of the fast beam which proceeds for channeling of keV beams at energies in the eV domain.

In the work presented here we will demonstrate that for specific cases also the longitudinal coherence is preserved so that so called “Laue circles” can be observed for fast atom diffraction. Then quantum scattering from surfaces gives rise to interesting features and enhances the transfer width of fast atom diffraction by more than one order of magnitude compared to scattering with transverse coherence only.

2. FAST ATOM DIFFRACTION FOR GRAZING SCATTERING FROM A SAPPHIRE SURFACE

In our experiments we have scattered H and He atoms with energies up to about 1 keV from a clean and flat $Al_2O_3(11\underline{2}0)$ surface under grazing angles of incidence from about 0.3° to 2°. Well defined diffraction patterns in the angular distributions are observed, after the surface was annealed under UHV conditions for several minutes at temperatures of about 1500 °C. Then a p(12x4) phase is formed [5] giving rise to rich diffraction patterns for scattering along the low indexed <0001> channel in the surface plane. Striking feature of the patterns is the presence of Bragg peaks located on a Laue circle of zeroth order.

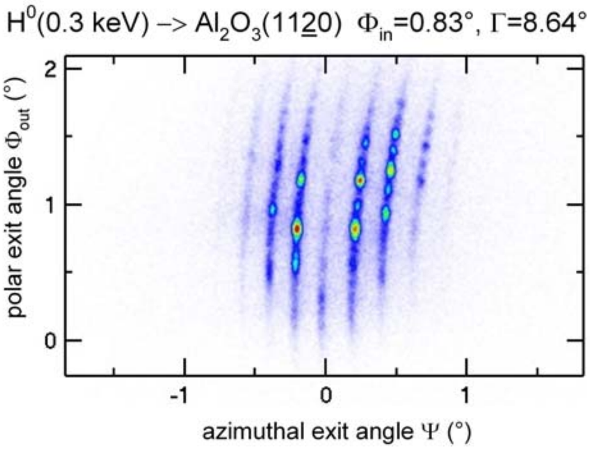

Figure 1: Angular distribution as recorded with position sensitive detector for scattering of 300 eV H atoms from $Al_2O_3(11\underline{2}0)$ surface under grazing angle of incidence of 0.83° and azimuthal offset to <0001> of 8.64°. Individual Bragg peaks are located on Laue circles. Splittings of circles correspond to periodicity interval of 33.4 Å.

Owing to the large angular splittings between Laue circles in view of the limited angular spread for the scattered beam, only the circle of order n = 0 can be observed for scattering along axial surface channels. However, for an azimuthal rotation of the target surface circles of higher orders can be identified (see Figure 1) and described by longitudinal coherence in terms of an “Ewald construction”. In this regime of scattering the periodicity interval of the p(12x4) arrangement of the reconstructed surface can be clearly resolved. From the data we deduce a transfer width of fast atoms diffraction for scattering under these conditions of several 100 Å.

3. REFERENCES

[1] A. Schüller, S. Wethekam, and H. Winter, Phys. Rev. Lett. 98 (2007) 016103.

[2] P. Rousseau, H. Khemliche, A.G. Borisov, and P. Roncin, Phys. Rev. Lett. 98 (2007) 016104.

[3] H. Winter and A. Schüller, Prog. Surf. Sci. 86 (2011) 169.

[4] A. Schüller, S. Wethekam, D. Blauth, H. Winter, F. Aigner, N. Simonovic, B. Solleder, J. Burgdörfer, and L. Wirtz, Phys. Rev. A82 (2010) 062902.

[5] T. Becker, A. Birkner, G. Witte, and C. Wöll, Phys. Rev. B65 (2002) 115401.

---

[*] Corresponding author e-mail address: winter@physik.hu-berlin.de

GRAZING INCIDENCE FAST ATOM DIFFRACTION APPLIED TO THIN FILM GROWTH

M. Debiossac[1], *P. Atkinson*[2], *A. Momeni*[1], *H. Khemliche*[*1], *P. Roncin*[1], *M. Eddrieff*[2], *V.H. Etgens*[2]

[1] Institut des Sciences Moléculaires d'Orsay, UMR 8214, CNRS - Université Paris-sud, Orsay, 91400 France
[2] Institut des NanoSciences de Paris, UMR 7588, CNRS – Université Pierre et Marie Curie Paris, 75005 France

We have developed a new surface sensitive technique, providing in seconds and with atomic resolution, topological images of the surface electronic density of crystalline surfaces. Grazing Incidence Fast Atom Diffraction (GIFAD) is a reciprocal space technique allowing determination of the surface topology of metals, semi-conductors and insulators [1]. Similar to RHEED in its geometry, we have recently installed GIFAD on a commercial MBE machine. We will present measurements of the surface reconstruction and GaAs growth on GaAs(001).

Figure 1 displays GIFAD images together with the corresponding RHEED images taken along the [1-10] direction at substrate temperatures 460 °C, 500 °C and 550 °C, which correspond to the well known c(4×4), $(2\times4)\gamma$ and $(2\times4)\beta$ reconstructions [2].

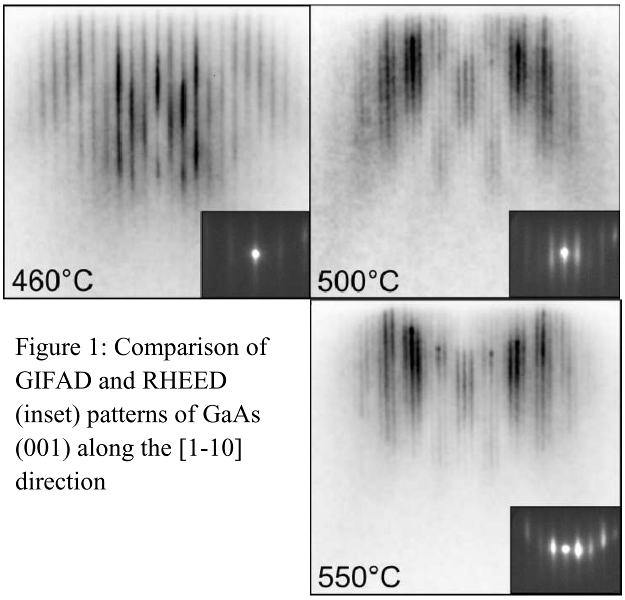

Figure 1: Comparison of GIFAD and RHEED (inset) patterns of GaAs (001) along the [1-10] direction

It can be seen that the change in the diffraction pattern for different reconstructions is much more marked using GIFAD than RHEED, highlighting the greater surface sensitivity of the GIFAD technique. The intensity distribution has two independent contributions. Within each Laue circle the intensity distribution is a Fourier-like transformation of the surface corrugation, as would be imaged by an AFM. The intensity distribution along the diffraction pattern streaks is governed however by the thermal movement of the surface atoms and by the finite length of the surface reconstructions. These two effects will be discussed in detail.

Importantly, for practical applications, GIFAD displays well resolved oscillations in the reflected beam intensity during layer-by-layer growth, as shown in figure 2, allowing growth dynamics to be probed.

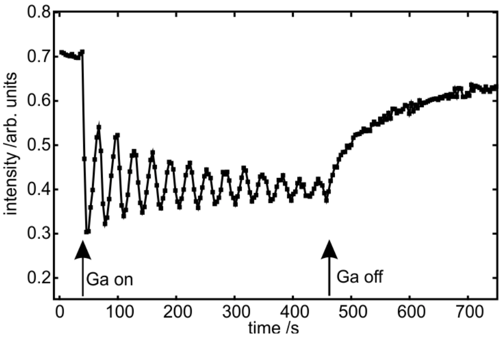

Figure 2 : GaAs(001) growth oscillations

New results will be presented showing both the fundamental progress of the technique and its application to thin film growth on semi-conductors.

Acknowledgement
This work has been supported by ANR contract ANR-07-BLAN-0160-0

REFERENCES

[1] see e.g. H. Khemliche et al, *Appl. Phys. Lett.* **95** 151901 (2009),
Schüller et al, *Nucl. Instr. Meth. Phys. Res.* B **267** 628 (2009)
[2] see e.g. Ohtake, Surf. Sci. Reports **63** 295 (2008)

---

[*] Corresponding author e-mail address: hocine.khemliche@u-psud.fr

Poster Session

NANO-HOLES MILLED IN 1 NM THICK CARBON NANOMEMBRANES WITH SLOW HIGHLY CHARGED IONS

R. Ritter[1], R. A. Wilhelm[2], M. Stöger-Pollach[3], A. Mücklich[2], U. Werner[4], A. Beyer[4],
S. Facsko[2], A. Gölzhäuser[4], and F. Aumayr[1,*]

[1] Institute of Applied Physics, TU Wien - Vienna University of Technology, 1040 Vienna, Austria, EU
[2] Helmholtz-Zentrum Dresden Rossendorf, 01314 Dresden, Germany, EU
[3] USTEM, TU Wien - Vienna University of Technology, 1040 Vienna, Austria, EU
[4] Fakultät für Physik, Universität Bielefeld, 33615 Bielefeld, Germany, EU

1. INTRODUCTION

We have recently discovered that the impact of individual slow highly charged ions (HCI) is able to cause permanent nano-sized hillocks on the surface of a CaF_2 single crystal [1]. The experimentally observed threshold of the projectiles potential energy necessary for hillock formation could be successfully linked to a solid-liquid phase transition (nano-melting) [1 - 3]. Meanwhile a variety of materials has been found, which are susceptible to nano-structuring by the impact of slow HCI [3]. The nature, appearance and stability of the created structures, however, depend heavily on the properties of the target material and the involved interaction processes (determined by the potential and kinetic energy of the projectiles) [3]. Not in all cases nano-hillocks but nano-craters or -holes are formed on a surface, like for KBr [4] or PMMA [5].

In this contribution we present the first investigations on the effect of individual slow highly charged ion bombardment of freestanding carbon nano-membranes [6].

2. EXPERIMENT

The carbon nanomembranes (CNMs) are produced by cross-linking of an aromatic self-assembled monolayer of biphenyl units with low-energy electrons. The substrate is then subsequently removed and the resulting nanosheet (1 nm thickness) transferred onto a holey carbon TEM grid.

CNMs produced in such a way are irradiated by slow highly charged Xe^{q+} ions of various charge states ($20 \leq q \leq 40$) and kinetic energies (4 keV $\leq E \leq 180$ keV). After irradiation the CNMs are inspected by high resolution imaging techniques, e.g. transmission electron microscopy (TEM), secondary electron microscopy (SEM), atomic force microscopy (AFM) and He-ion microscopy (HIM).

3. RESULTS

After irradiation by slow HCI we find nanoscopic holes (3 - 30 nm in diameter) at positions, where the sheet extends over holes in the carbon film (fig. 1). The number density of these nanopores corresponds well with the incident ion fluence, indicating that about every HCI produces a nano-hole in the CNM. These holes have so far been imaged in TEM, SEM as well as in AFM.

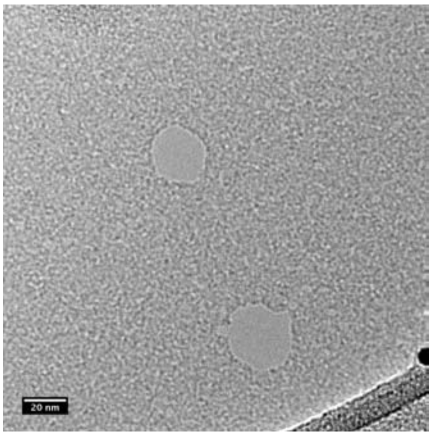

Figure 1: TEM image of 2 holes in a carbon nanomembrane induced by impact of two Xe^{40+} ions (E_{kin} = 40 keV, E_{pot} = 38.5 keV).

First evaluations of the size distribution of the created holes indicate that the average diameter of a pore induced by a given ion depends strongly on the potential energy of the projectile ion, but is also influenced by the kinetic energy.

4. ACKNOWLEDGEMENTS

This work has been supported by the EU Project SPIRIT under EC contract no. 227012. Support by ÖAW and by FWF is acknowledged. R. R. is a recipient of a DOC-fellowship of the Austrian Academy of Sciences at the Institute of Applied Physics of TU Wien.

5. REFERENCES

[1] A S El-Said, et al., Phys. Rev.Lett. **100**, 237601 (2008).
[2] C. Lemell, et al., Solid-State Electron. **51**, 1398 (2007).
[3] F. Aumayr, et al., J.Phys.: Cond.Mat. **23**, 393001 (2011)
[4] R. Heller, et al., Phys. Rev.Lett. **101**, 096102 (2008).
[5] R. Ritter et al., EPL **97**, 13001 (2012).
[6] C. Nottbohm et al., Ultramicroscopy **108**, 885 (2008)

---

[*] Corresponding author e-mail address: aumayr@iap.tuwien.ac.at

DEPTH-RESOLVED DEUTERIUM CONCENTRATION OF PLAMA-EXPOSED TUNGSTEN ALLOYS

J. Brinkmann[1,*], *F. Koch, and Ch. Linsmeier*[1]

[1] Max-Planck-Institut für Plasmaphysik, EURATOM Association, 85748 Garching b. München, Germany

1. INTRODUCTION

Tungsten alloyed with several other transition metals is a class of materials currently under consideration for application in the plasma-facing components of future fusion power plants [1]. The main benefit from such alloys is a substantial reduction of the oxidation rate in order to mitigate the effects of potential accidents under loss-of-coolant conditions with air ingress.

The choice of alloying elements is restricted to those which keep the compatibility of the resulting material with normal plasma operation close to that of pure tungsten. In this respect the implantation and retention of hydrogen isotopes within the surface layer and the bulk of the alloy are of interest both from fusion plasma vessel engineering and safety assessment points of view. Alloy films with varying composition are chosen to investigate both oxidation behavior and hydrogen isotope retention after plasma exposure.

2. SAMPLE PREPARATION AND EXPOSURE

The alloys are obtained via magnetron sputter deposition on silicon wafer pieces and quartz disks with tungsten being the major film component. The elements used for alloying are chromium, titanium, hafnium and tantalum. The film thicknesses range between 2 µm and 5 µm, and are determined using profilometry and Rutherford backscattering spectrometry (RBS).

Sputter films usually exhibit a microstructure and an intrinsic defect density different from bulk materials. Therefore pure elemental films of tungsten, chromium and titanium are investigated for comparison.

The samples are subjected to a series of RF deuterium plasma discharges varying both, the deuterium fluence (10^{23} D/m^2 - 10^{24} D/m^2) and the sample bias (10 V – 300 V, resulting in different ion energies) independently from each other. The sample temperature during each discharge was kept within several degrees at 290 K.

3. ION BEAM ANALYSIS AND DATA TREATMENT

The deuterium implanted into the samples during plasma exposure is analyzed using ion-beam analysis techniques at a 3 MV tandem accelerator. The deuterium concentration depth profile is probed by nuclear reaction analysis (NRA) using the

$$^{2}\mathrm{D}\left(^{3}\mathrm{He},\mathrm{p}\right)^{4}\mathrm{He} \tag{1}$$

reaction, which offers a high sensitivity due to an overall large cross section. Since the resonance width for (1) is very broad and its peak is less than a factor of ten above the off-resonance cross section [2], an inverse approach to deduce the deuterium depth profile is infeasible. Therefore the measured NRA spectra are evaluated using a forward modelling algorithm (NRADC) which in turn uses the SIMNRA code [3,4]. During the modelling process prior knowledge about the films is used together with the NRA spectra, namely to fix their composition inferred from RBS and energy dispersive X-ray micro-analysis (EDX) data, as well as their thicknesses obtained from RBS and profilometry data. The final output of NRADC is a quantitative deuterium depth profile for each alloy film as well as the total amount of detected deuterium within the information depth of the NRA depth scan.

4. RESULTS

The total deuterium retention in the samples is quantified using the total amount of deuterium detected by NRA and the quantified implantation fluences during the RF plasma exposure. The fluence and sample bias dependence of the retention is expected to be in agreement with a diffusive transport from the ion implantation range further into the bulk of the material. In such a scenario the implanted deuterium acts as a reservoir sustaining a concentration gradient which forces deuterium further into the depth of the sample. The concentration depth profiles for each sample are compared at different fluences and sample bias voltages.

We expect a strong dependence of the retained amount of deuterium from the alloying elements' tendencies to form hydrides, but also strong change of the alloy formation for the different elements alloyed with tungsten. Deuterium depth profiles are compared for different alloy compositions and conclusions are drawn with respect to their tendency to form hydrides.

5. REFERENCES

[1] F. Koch, J. Brinkmann, S. Lindig, T.P. Mishra, and Ch. Linsmeier, Physica Scripta **T145** 014019 (2011).

[2] V.Kh. Alimov, M. Mayer, J. Roth, Nucl. Instrum. Meth. **B 234** 169 (2005).

[3] K. Schmid and U. von Toussaint, Nucl. Instrum. Meth. **B 281** 64 (2012).

[4] M. Mayer, SIMNRA Users Guide, Report IPP9/113, MPI f. Plasmaphysik, Garching, Germany, 1997

---

[*] Corresponding author e-mail address: jens.brinkmann@ipp.mpg.de

FORMATION OF NEGATIVE IONS IN GRAZING SCATTERING OF HYDROGEN ATOMS FROM INSULATOR SURFACES

Yanling Guo, Hu Zhou, Lin Chen*, and Ximeng Chen*

School of Nuclear Science and Technology, Lanzhou University, Lanzhou 730000, China

Particle-surface interactions have been a subject of intensive research over the past decades. Most of these studies have focused on ion-induced electron emission, energy loss of the projectile, and charge transfer phenomena. In particular, recent studies on negative-ion formation in grazing scattering of neutrals from insulator surfaces have attracted considerable attention [1], due to its potential application in the development of new negative-ion sources.

In the past decades, Demkov model was successfully used to explain the formation of negative ions in grazing scattering of neutral atoms from insulator surface by H. Winter *et al* [2]. However, this model fails at relatively high velocities, since the electron detachment process is not included in the model. In fact, electron loss phenomena for insulators have been observed experimentally both in surface scattering [3] and nanocapillary transmission measurements [4]. Therefore, the understanding of the destruction of negative ions on insulator surfaces is highly desired.

In this work, as a complement of the Demkov model, we attempt to introduce an electron-tunneling model associated with electron loss processes to completely describe the kinematic dependence of negative-ion formation on oxide surfaces.

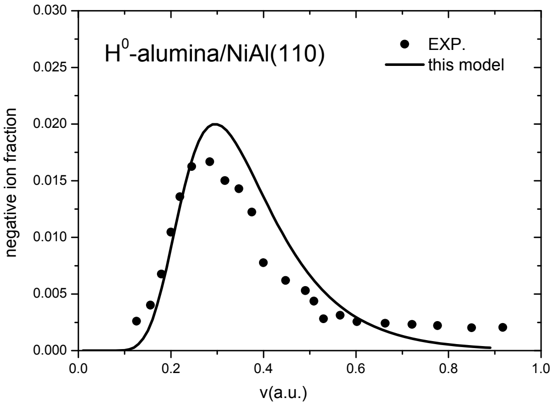

Figure 1: Negative-ion fractions as a function of velocity for H atoms in grazing scattering from an alumina/NiAl(110), surface. Experimental data [5]: solid circles. Theory: black solid line.

In Fig. 1, we present our theoretical result for H atoms in grazing scattering from an oxidized NiAl(110) surface, as well as the related experimental data [5]. It is shown that the good agreement is achieved.

In summary, the well-known quantum tunneling effect for electrons through the repulsive Coulomb barrier has been proposed to describe electron detachment from the formed negative ions. The combination of these two models results in excellent agreement with the experimental data in the overall impact velocity range.

REFERENCES

[1] C. Auth, A. G. Borisov, and H.Winter, Phys. Rev. Lett. **75**, 2292 (1995).

[2] C. Auth, A. Mertens, H. Winter, A. G. Borisov, and V. Sidis, Phys, Rev. A **57**, 351 (1998).

[3] M. Maazouz, L. Guillemot, S. Lacombe, and V. A. Esaulov, Phys. Rev. Lett. **77**, 4265 (1996); S. Ustaze, R. Verucchi, S. Lacombe, L. Guillemot, and V. A. Esaulov, *ibid.* **79**, 3526 (1997); A. G. Borisov and V. A. Esaulov, J. Phys.: Condens. Matter **12**, R177 (2000).

[4] Lin Chen, Y. Guo, J. Jia, H. Zhang, Y. Cui, J. Shao, Y. Yin, X. Qiu, X. Lv, G. Sun, J. Wang, Y. Chen, F. Xi, and X. Chen, Phys, Rev. A **84**, 032901 (2011); L. Chen et al., J. Phys. B **44**, 045203(2011).

[5] D. Blauth, H. Winter, Nucl. Instr. and Meth. B **269**, 1175 (2011).

---

* Corresponding author e-mail address: chenlin@lzu.edu.cn, chenxm@lzu.edu.cn

Electron emission due to impact of highly charged ions on C_{60} covered gold surfaces and HOPG

K. Dobes[1,*], *E. Bodewits*[2], *G. Kowarik*[1], *R. Hoekstra*[2] *and F. Aumayr*[1]

[1] Institute of Applied Physics, TU Wien, Vienna Austria, EU
[2] KVI-Atomic and Molecular Physics, University of Groningen, Groningen, The Netherlands

1. INTRODUCTION

Electron emission as a result of the interaction of highly charged ions (HCI) with solid surfaces is of substantial interest both with regard to fundamental research as well as technical applications such as controlled nanostructuring of surfaces or plasma surface interaction in e.g. thermonuclear fusion devices. The emission of electrons during the impact of a HCI on a solid surface is generally divided into two different regimes, i.e. kinetic emission (KE) and potential emission (PE). The former process is driven by the kinetic energy of the impinging projectile, while the latter is induced by the potential energy stored in a highly charged ion Z^{q+} due the removal of q electrons. A widely accepted model that describes the dissipation of the large amounts of potential energy, which are carried by a HCI, at the surface is the so-called hollow atom scenario [1,2]. It describes the neutralization and relaxation of the HCI upon surface impact. This process is not only governed by the potential energy of the projectile, i.e. its charge state q, but also depends on the electronic structure of the surface, the work function and electron transport properties of the target material [1].

To understand the influence of these properties on the electron emission yield and the hollow atom decay in greater detail, we studied and compared ion-induced electron yields from different target materials with different work functions. We investigated clean Au(111), a gold surface covered with 1 – 5 monolayer thin films of C_{60} and highly ordered pyrolytic graphite (HOPG) under the impact of highly charged Ar and Xe ions at different impact angles and energies.

2. EXPERIMENTAL SETUP

Experiments were performed at the setup IISIS at KVI Groningen [3]. The Au and HOPG target respectively were mounted within an UHV chamber at a base pressure of the order of 10^{-10} mbar. The Au surface was cleaned by cycles of sputtering and annealing. The HOPG sample was cleaved with a scotch tape before it was transferred to the vacuum chamber. Thin films of C_{60} were deposited onto the Au sample by means of an Omicron EFM3 evaporator. Single monolayers of C_{60} were deposited by first determining the deposition rate with a quartz crystal microbalance and then exposing the sample to the C_{60} beam for a corresponding time interval.

Ar^{q+} ions (q = 4, 6 - 13) and Xe^{q+} ions (q = 10, 12, 14, 16, 18, 20, 22, 24, 26, 28) were extracted from a 14 GHz ECR ion source. The Ar ion energies ranged from 3.9 keV up to 91 keV. The impinging Xe ions were in an energy range from 7.2 keV to 328 keV. The electron statistics detector [4] is mounted under 90° with respect to the incoming ion beam. It is an energy sensitive, passivated implanted planar silicon (PIPS) detector. Secondary electrons, which are emitted in an ion-surface collision event, are collected by a set of six different electrodes surrounding the target and are then accelerated towards the detector, which is biased to +30 keV. The number of electrons produced in a single ion impact event is determined by pulse height analysis. From this the electron number statistics is obtained in addition to the mean number of emitted electrons per incident projectile ion.

3. RESULTS

When comparing secondary electron yields from Au and Au covered with 1 – 5 ML of C_{60}, an increase in electron yield is found. This increase in electron yield is well described by an exponential gain function and is virtually independent of the potential energy of the projectiles between 0.5 and 10 keV. It saturates at 35%, when five monolayers of C_{60} are evaporated on the surface [5]. Also for a clean HOPG surface a higher yield is found as compared to a clean Au surface. A detailed comparison of the results obtained on the different targets will be presented and possible scenarios will be discussed that are able to explain this increase in electron yield.

4. REFERENCES

[1] J. Burgdörfer, P. Lerner and F.W. Meyer, Phys. Rev. A **44**, 5674 (1991).
[2] F. Aumayr and H.P. Winter, Springer Tracts Mod. Phys.**225**, 79 (2007).
[3] E. Bodewits et al., Nucl. Instrum. Meth. B **269**, 1203 (2011).
[4] G. Lakits, F. Aumayr and HP. Winter, Rev. Sci. Instrum. **60**, 165 (1989).
[5] E. Bodewits et al., Phys. Rev. A **84**, 042901 (2011).

---

[*] Corresponding author e-mail address: dobes@iap.tuwien.ac.at

Creation of Surface Nanostructures in Al_2O_3 by Slow Highly Charged Ions

A.S. El-Said[1,2,3*], *R.A. Wilhelm*[1], *and S. Facsko*[1]

[1] Institute of Ion Beam Physics and Materials Research, Helmholtz-Zentrum Dresden-Rossendorf,
01328 Dresden, Germany

[2] Physics Department, King Fahd University of Petroleum and Minerals, Dhahran 31261, Saudi Arabia

[3] Nuclear and Radiation Physics Lab, Physics Department, Faculty of Science, Mansoura University, 35516 Mansoura, Egypt

It is now well established that slow highly charged ions (HCI) can induce various surface nanostructures in different materials (e.g. hillocks on LiF, CaF_2, BaF_2, $SrTiO_3$, pits on KBr, craters on Si (111), and caldera like structures on TiO2 (110)). The creation, type and size of the surface nanostructures depends on the material as well as on ion parameters in particular charge state and kinetic energy [1,2]. Furthermore these structures often resemble the ones created by swift heavy ions in size and shape [3].

Among all investigated materials ionic alkali and alkaline-earth halides are considered as the most studied materials. For these crystals a model could be established, which describes the creation mechanism for surface nanostructures induced by the potential energy of HCIs. Recently, we investigated oxide materials including $SrTiO_3$ and SiO_2 single crystals [4].

In this contribution we extended this study to another oxide material, namely Al_2O_3. The selection is also motivated by the observation of surface nanostructures (mainly hillocks) after irradiation with swift heavy ions (SHI) by surpassing a threshold of electronic energy loss [5], which is higher than for other oxides (eg. SiO_2 and $SrTiO_3$).

Epi-polished Al_2O_3 single crystals were irradiated with slow highly charged Xe ions of various charge states from an EBIT (Electron Beam Ion Trap) source at the Dresden two source facility. The irradiations were performed at room temperature and under normal incidence. Scanning force microscopy (SFM) was utilized to investigate the topography of the irradiated surfaces. The measurements showed that above a potential energy threshold, each ion creates a nanohillock protruding from the surface, as shown in Fig. 1.

These structures will be compared to those created by SHI. The results will be discussed in terms of potential energy deposition of HCI and electronic energy loss of SHI.

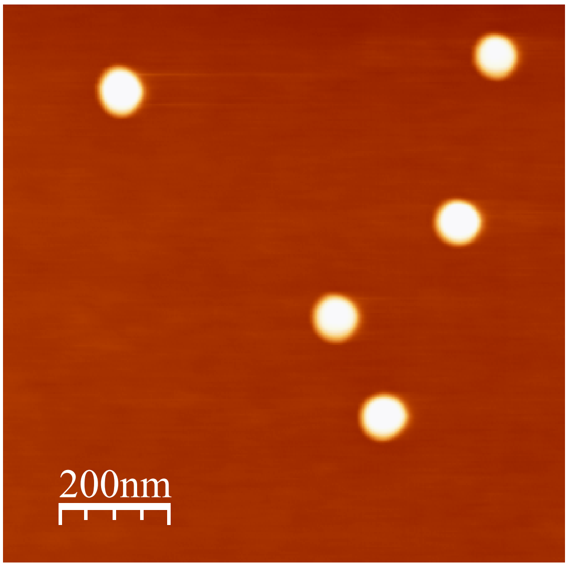

Fig. 1. Scanning force microscopy topographic image of Al_2O_3 surface irradiated with 1.15 keV/amu Xe^{36+} (fluence ≈ 5 x10^8 ions).

[1] A.S. El-Said, R. Heller, W. Meissl, R. Ritter, S. Facsko, C. Lemell, B. Solleder, I. Gebeshuber, G. Betz, M. Toulemonde, W. Möller, J. Burgdörfer, F. Aumayr, Phys. Rev. Lett. **100**, 237601 (2008).

[2] R. Heller, S. Facsko, R. A. Wilhelm, and W. Möller, Phys. Rev. Lett. **101**, 096102 (2009).

[3] F. Aumayr, S. Facsko, A. S. El-Said, C. Trautmann and M. Schleberger, J. Phys.: Condens. Matter 23, 393001 (2011).

[4] A.S. El-Said, R.A. Wilhelm, R. Heller, S. Facsko, F. Aumayr, C. Trautmann, Nucl. Instr. Meth. B 269, 1234 (2011)

[5] N. Khalfaoui , J.P. Stoquert b, F. Haas , C. Traumann , A. Meftah , M. Toulemonde, Nucl. Instr. Meth. B (2012) doi:10.1016/j.nimb.2011.11.047.

---

[*] Corresponding author e-mail address: a.s.elsaid@fzd.de, elsaid@kfupm.edu.sa

SYSTEMATIC INVESTIGATIONS OF ION BEAM SPUTTERING OF SI: FIRST EXPERIMENTAL AND SIMULATION RESULTS

R. Feder[1,*], *F. Frost*[1], *H. Neumann*[1], *C. Bundesmann*[1], *B. Rauschenbach*[1]

[1] Leibniz-Institut für Oberflächenmodifizierung e.V., Permoserstr. 15, 04318 Leipzig, Germany

1. ABSTRACT

Ion beam sputter (IBS) processes deliver some intrinsic features influencing the growing film properties, because ion properties and geometrical process conditions generate different energy and spatial distribution of the sputtered and scattered particles. Even though IBS has been used for decades, the full capabilities are not investigated systematically and used yet.

A UHV deposition chamber has been set up which allows ion beam sputtering different targets under variation of geometrical parameters (ion incidence angle, ion emission angle in respect to the target) and of ion beam parameters (ion species, ion energy) to make a systematic and comprehensive analysis of the correlation between the properties of the ion beam, the properties of the sputtered and scattered particles, and the properties of the deposited layers. An energy-selective mass spectrometer for energy and mass distribution measurements and a faraday cup for ion beam current density measurements were used in this work and the results are reported. A set of silica samples was prepared and characterized with respect to selected thin film properties, such as thickness, composition, strain, surface topography and optical properties. The experiments indicate a systematic influence of the deposition parameters on the film properties as hypothesized before [1].

Simulations of spatial and energetic distribution of sputtered and scattered particles with help of the well known TRIM.SP [2] code help supporting the explanation of the complex film properties in correlation to results of the particle measurements. A comparison of the experimental with the simulation data results in a validation of the code's basic parameters.

2. REFERENCES

[1] C. Bundesmann, I.-M. Eichentopf, S. Mändl, H. Neumann, Thin Solid Films **516**, (2008); 8604-8608.

[2] J. P. Biersack, W. Eckstein, Appl. Phys. A: Mater. Sci. Process. **34**, (1984); 73.

---

[*] Corresponding author e-mail address: rene.feder@iom-leipzig.de

A QUANTITATIVE INVESTIGATION OF QUASI-RESONANT NEUTRALIZATION OF HE$^+$ IONS AT A GERMANIUM SURFACE

D. Goebl[1,*], *D. Roth*[1], *D. Primetzhofer*[2] *and P. Bauer*[1]

[1] Institut für Experimentalphysik, Abteilung für Atom- und Oberflächenphysik, Johannes Kepler Universität Linz, 4040 Linz, Austria
[2] Institutionen för Fysik och Astronomi, Uppsala Universitet, Box 516, S-751 20 Uppsala, Sweden

1. INTRODUCTION

Low Energy Ion Scattering (LEIS) is an excellent tool to probe the composition and structure of the outermost atomic layers of a given sample [1]. However, to obtain quantitative information one needs detailed understanding of the involved charge exchange mechanisms. Typically, charge exchange may be due to Auger-Neutralization (AN) or resonant neutralization/reionization in a close collision (RN/RI). Additionally, there is a certain class of ion-target systems for which a different charge exchange process can be observed: quasi-resonant neutralization (qRN). This process was discovered by Erickson and Smith and occurs for materials with electrons of binding energy almost resonant with a projectile level, e.g., Ge*3d* – He*1s* [2]. A characteristic feature of this type of charge exchange is an oscillatory behavior of the ion yield with ion energy. Theoretical models explained these oscillations as consequence of quantum mechanical interference [3, 4]. Up to now, quantitative information on the efficiency of this process is astonishingly scarce.

2. EXPERIMENTAL RESULTS

We have measured the ion fraction, P^+, of He$^+$ scattered from a Ge(100) surface, by LEIS using time-of-flight (TOF) and electrostatic-analyzer (ESA) spectrometers. We used 1 – 8.5 keV He$^+$ ions and double alignment geometry to determine P^+ from the scattered yields of ions and neutrals, A_+ and A_0, as obtained by the TOF-LEIS setup ACOLISSA. This approach has the advantage that P^+ can be evaluated without detailed knowledge of surface structure and experimental parameters (e.g., primary current, scattering cross section). Complementary experiments performed with an ESA-LEIS setup were carried out to extend the energy range towards lower energies. In Fig. 1, deduced ion fractions are displayed as a function of the inverse initial velocity. One can clearly observe the oscillations in P^+, which are characteristic for charge exchange by qRN. Note, that for the He$^+$-Ge system P^+ is very low compared to results obtained for materials which do not feature qRN charge exchange. Cu is known to neutralize He$^+$ exclusively due to Auger-neutralization for He energies below 2 keV. In this case, the ion fraction is almost one order of magnitude higher than for He-Ge.

Additionally, we determined P^+ as a function of the polar angle of the incident beam. From such a polar scan the information depth can be estimated. These experiments revealed that only the outer atomic layer contributes to the ion yield.

These experimental results indicate that qRN is a very efficient neutralization mechanism, with considerably higher neutralization rate as compared to AN. To gain further insights, it would be interesting to disentangle the relative contributions of AN and qRN, and to determine the threshold energy for reionization.

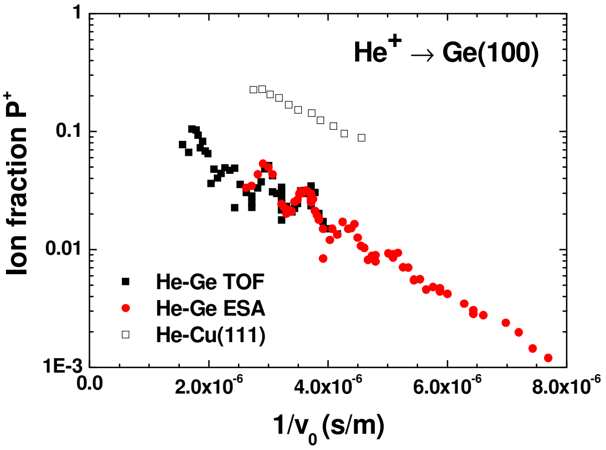

Figure 1: Ion fraction of He$^+$ scattered from a Ge(100) surface as a function of inverse initial velocity. Measurements were performed with TOF-LEIS (black) and ESA-LEIS (red) setups. P^+ for He$^+$-Cu (open squares) is shown to illustrate the efficiency of qRN.

3. REFERENCES

[1] HH. Brongersma, M. Draxler, M. De Ridder and P. Bauer, Surface Science Reports 62, 3, 63-109 (2007)
[2] R.L. Erickson, D.P. Smith, Phys. Rev. Lett. 34 (1975) 297.
[3] N. H. Tolk, J. C. Tully, J. Kraus, C. W. White, S. H. Neff, Phys. Rev. Lett. 36 (1976) 747.
[4] S. Kondo, J. Phys. Soc. Jpn. 80, 044717 (2011)

---

[*] Corresponding author e-mail address: dominik.goebl@jku.at

INTERACTION POTENTIALS FOR MULTI-ELECTRONIC ATOMS IN FRONT OF A LIF(001) SURFACE INVESTIGATED VIA RAINBOW SCATTERING

M.S. Gravielle[1,*], *J.E.Miraglia*[1], *A. Schüller*[2], *and H. Winter*[2]

[1] Instituto de Astronomía y Física del Espacio, CONICET-UBA, Buenos Aires, Argentina.
[2]Institut für Physik, Humboldt Universität zu Berlin, Newtonstrasse 15, D-12489 Berlin-Adlershof, Germany.

1. INTRODUCTION

Atom-surface interaction potentials play a crucial role in studies on inelastic processes in grazing scattering of fast particles from solid surfaces. For ionic crystals, several different models have been proposed to represent this interaction. Some of those fail to describe the angular distributions of swift atoms elastically scattered along low-indexed crystallographic directions. In particular, the angular positions of the outermost maxima of the projectile angular distribution, which originate from rainbow scattering, were found to be sensitive to the corrugation of the surface interaction, becoming a useful tool to probe surface potential models [1].

In this work, angular positions of rainbow maxima for grazing scattering of multi-electronic atoms - He, N, S, Cl and Kr – with a LiF(001) surface are investigated theoretically and experimentally. To represent the surface potential we use a model based on the sum of individual interatomic potentials, which include projectile polarization and second order contributions in terms of the electronic density.

2. THEORY AND EXPERIMENT

The projectile-surface potential is evaluated by adding the individual interactions with solid ions (*pairwise additive* hypothesis), reading

$$V_{SP}(\mathbf{R}) = \sum_i V_{bin}(\mathbf{R}_i), \qquad (1)$$

where the sum formally includes all ions of the target crystal and $V_{bin}(\mathbf{R}_i)$ represents the binary interaction between the projectile and the target ion i. In previous works we have derived binary atom-ion potentials making use of the local density approximation as given by the Abrahamson method [2]. Here we propose a modification of such binary potentials by incorporating second order corrections to the kinetic and exchange energies.

To describe the scattering process we employ a distorted-wave model - the surface eikonal approximation [3] - that makes use of the eikonal wave function to represent the elastic collision with the surface, while the motion of the fast projectile is classically described by considering axially channeled trajectories for different initial conditions.

The experiments were performed with a well prepared LiF(001) sample in a UHV chamber at a base pressure in the upper 10^{-11} mbar domain. Fast ions were produced in an ECR source, accelerated to voltages up to some 10 keV and neutralized in a gas target. The collimated beam was directed onto the target surface under grazing angles of incidence Φ_{in} ranging from a few 0.1° to some degrees. The normal energy for the collision with the surface $E_\perp$ was adjusted according to $E_\perp = E \sin^2 \Phi_{in}$ with E being the kinetic energy of the projectiles. The angular distributions of scattered atoms for scattering along the <100> or <110> axial channel were recorded with a position sensitive multi-channel-plate detector and reveal for the extreme of azimuthal angular deflection the so called "rainbow peaks".

3. RESULTS

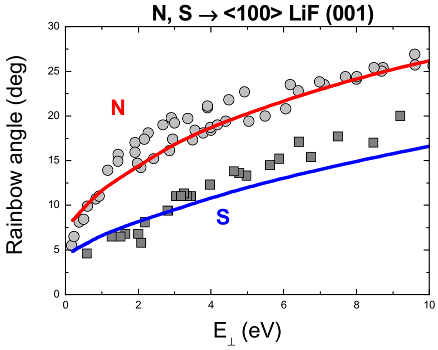

Figure 1: Rainbow angle for N and S atoms impinging on LiF(001) along <100> as function of $E_\perp$.

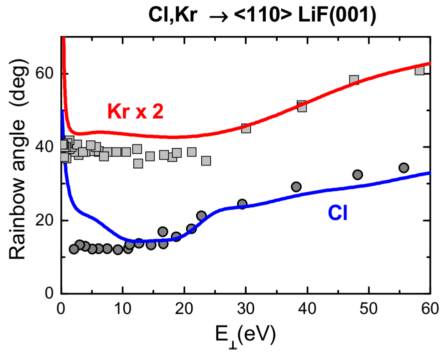

Figure 2: As Fig. 1 but for Cl and Kr atoms impinging along <110> direction.

4. REFERENCES

[1] U. Specht *et al.*, Phys. Rev. B **84**, 125440 (2011).
[2] A. A. Abrahamson, Phys. Rev. **133**, A990 (1964).
[3] M.S. Gravielle *et al.*, Nucl. Instr. Meth. B **269**, 1208 (2011).

---

[*] msilvia@iafe.uba.ar

GRAZING INCIDENCE FAST ATOM DIFFRACTION FOR HELLIUM ATOMS IMPINGING ON A Ag(110) SURFACE

C.A. Ríos Rubiano[1], *G. Bocan*[2], *and M.S. Gravielle*[1,*]

[1] Instituto de Astronomía y Física del Espacio, CONICET-UBA, Buenos Aires, Argentina.
[2]Centro Atómico Bariloche, Centro Atómico Bariloche (CNEA) and CONICET, Bariloche, Río Negro, Argentina.

1. INTRODUCTION

Diffraction of swift atoms due to grazing scattering from crystal surfaces has displayed an exceptional sensitivity to the projectile-surface interaction, which opens the way for the development of a powerful surface analysis technique. Even though the first experimental evidences of this phenomenon were reported at insulator surfaces, which provided a favorable scenery to prevent quantum decoherence, soon afterwards the effect was observed at metallic materials as well [1,2].

The aim of this work is to investigate the diffraction patterns produced by fast He atoms grazingly impinging on a Ag(110) surface. Since this collision system corresponds to the first atom-metal surface system experimentally studied with fast atom diffraction [1], it provides a useful benchmark to test both the theoretical method and the surface potential model.

2. THEORETICAL MODEL

The scattering process is described by means of the surface eikonal approximation [3], which is a distorted wave method based on the use of the eikonal wave function. This method takes into account the quantum interference originated by the coherent superposition of transition amplitudes corresponding to different projectile paths. It has been already applied to investigate fast atom diffraction from insulator surfaces, providing results in good agreement with experimental data [3].

The interaction potential of the He atom with the Ag(110) surface is described with a full adiabatic tridimensional Potential Energy Surface (PES) that depends on the atomic position. The PES is constructed from a grid of 252 ab initio energies over which an interpolation is performed.

All ab initio data are obtained from the Density Functional Theory-based "Quantum ESPRESSO" code [4], which uses a plane-wave basis set to expand the system wave functions and is particularly efficient to model metallic surfaces. The values of relevant Quantum ESPRESSO parameters are chosen so that ab initio energies are calculated to a prescribed accuracy (differences <5 meV with respect to the converged result). The exchange-correlation energy is calculated within the generalized gradient approximation [5].

3. RESULTS

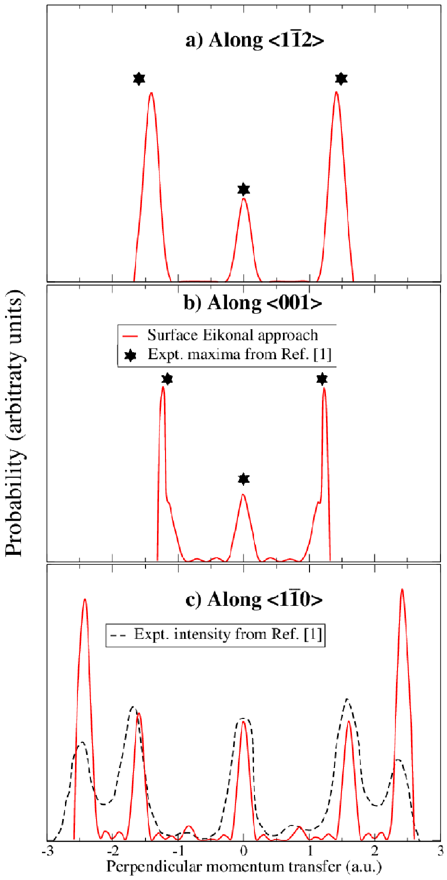

Figure 1: Perpendicular momentum transfer distribution for ^{3}He atoms impinging on Ag(110) along the crystallographic directions: a) <1-12>, b) <001>, c) <1-10>. The normal incidence energies are 360, 180, and 86 meV, respectively.

4. REFERENCES

[1] N. Bundaleski *et al.*, Phys. Rev. Lett. **101**, 177601 (2008).
[2] M. Busch *et al.*, Surf. Sci. **603**, L23 (2009).
[3] M.S. Gravielle *et al.*, Nucl. Instr. Meth. B **269**, 1208 (2011).
[4] P. Giannozzi *et al.*, J. Phys. Condens. Matter **21**, 395502 (2009).
[5] J.P. Perdew, K. Burke and M. Ernzerhof, Phys. Rev. Lett. **77**, 3865 (1996).

---

[*] msilvia@iafe.uba.ar

CONTROLLING ION GUIDING THROUGH TAPERED GLASS - CAPILLARIES WITH TEMPERATURE

E. Gruber[1], P. Hischenhuber[1], S. Wampl[1], M.J. Simon[2], and F. Aumayr[1,*]

[1]Institute of Applied Physics, TU Wien, 1040 Vienna, Austria, EU
[2]Labor für Ionenstrahlphysik, ETH Zürich, 8093 Zürich, Switzerland

1. INTRODUCTION

Guiding of highly charged ions (HCI) through tilted insulating capillaries, both straight and tapered ones [1-5], has developed from an area of basic research to a tool to efficiently collimate and focus ion beams. Applications range from nanoscale modifications of surfaces to irradiation of single living cells. Consequently, parameters are searched for to control and, possibly, optimize designer ion beams. One such parameter is the electrical conductivity of the insulating material [6]. Its strong temperature dependence is the key to transmission control and can be used to balance transmission instabilities arising from too high incident ion fluxes which otherwise would lead to Coulomb blocking of the capillary.

2. EXPERIMENTS

For our experiments we use a single tapered glass capillary made of Borosilicate. The entrance diameter of the conical shaped capillary is 0.86 mm, while the exit diameter is 82 µm. After a 5 mm long straight section the conical part of the capillary is about 5 cm long. The capillary is placed in a specially designed copper cylinder surrounded by stainless steel coaxial heaters and thermo shields. The temperature of the copper parts is monitored by a K-Type thermocouple and the heating power regulated by a PID controller. The current experimental set-up allows for a controlled and uniform temperature variation of the glass capillary between room temperature and +90°C. Within such a moderate variation of the temperature the conductivity changes by three to four orders of magnitude [6].

A beam of Ar^{7+} ions with a kinetic energy of typically 4.5 keV is collimated to a divergence angle of less than 0.7° and eventually hits a metallic entrance aperture directly in front of the capillary. Transmitted ions are registered by a position sensitive micro-channel-plate detector with wedge-and-strip anode, located about 14 cm behind the sample. Transmission rates are recorded for each capillary tilt angle after steady-state conditions (i.e. a dynamical equilibrium) are reached.

3. RESULTS

For our tapered capillary at room temperature we observe “guiding” of the incident ions up to several degrees tilt angle of the capillary with respect to the incoming ion beam. At very small tilt angles (close to the straight direction), however, we find a considerable suppression of the transmission of ions. Such a “blocking” effect has been reported previously by Nakayama et al. [7] and Kreller et al. [8] for ions transmitted through tapered glass capillaries at small angles, low beam energy and high beam intensity. It can be attributed to repulsive Coulomb forces of a uniformly charged ring-shaped region in the tapered part of the capillary. In our experiments we demonstrate, that by heating the tapered capillary (and thus increasing the conductivity of the glass capillary) the excess charge can be removed, and the blocking of the capillary can be terminated.

4. CONCLUSION

The strong temperature dependence of the conductivity of glass can be employed to successfully stabilize ion-guiding against Coulomb blocking due to a high incident ion flux.

5. REFERENCES

[1] N. Stolterfoht et al. Phys.Rev.Lett. **88**, 133201 (2002).
[2] R. J. Bereczky et al. Nucl.Instr.and Meth.B **267**, 317 (2009).
[3] G. Kowarik et al. Nucl.Instr.and Meth.B **267**, 2277 (2009).
[4] T. Ikeda et al. Appl.Phys.Lett. **89**, 163502 (2006).
[5] M. Kreller, et al. Nucl.Instr.and Meth.B **269**, 1032 (2011).
[6] G. Kowarik, et al. arXiv:1109.3953v1 [cond-mat.other] (2011).
[7] R. Nakayama et al., Nucl.Instr.and Meth.B **267**, 2381 (2009).
[8] M. Kreller et al. Nucl.Instr.and Meth.B **269**, 1032 (2011).

---

[*] Corresponding author e-mail address: aumayr@iap.tuwien.ac.at

Energy and Impact angle dependence of Sub-Threshold External Electron Emission

C.Heuser[1,*], *A. Wucher*[1]

[1] Faculty of Physics, University Duisburg-Essen, Germany

1. INTRODUCTION

When an ion impinges onto a solid surface, its energy is dissipated via different channels, which briefly can be separated in nuclear and electronic stopping mechanisms. The first one describes the scattering processes of the projectile ion with the target atoms, which can lead to collisional cascades and to the emission of paticles into vacuum, which is called “sputtering”.

The second mechanism deals with the interaction of the penetrating ion with the electronic subsystem, which manifests in a spacially and temporally localized heating of the valence electrons in the solid. If an electron gains enough excitation energy to overcome the work function, it can be emitted into vacuum, leading to ion-induced external electron emission.

In the case of normal incidence of the projectile, the energy of the ion is deposited along the track of the moving ion, leading to a certain energy loss distribution as a function of the penetration depth. Due to inelastic scattering processes only electrons close to the surface can be detected, which limits the amount of electrons contributing to the external electron yield. By changing the impact angle of the impinging ion from normal to grazing incidence, the penetrating ion spends more time close to the surface, so that the energy loss distribution is compressed towards the surface, which results in an impact angle-dependent increase of the electron yield [1].

The excitation energy of the electrons is directly connected to the kinetic energy of the ion, leading to a kinetic threshold energy as the lower limit for the projectile ion to excite electrons, that can still be emitted. However even below this classic threshold electron emission is observed, giving rise to sub-threshold electron emission models.

The goal of this work is to adapt the sub-threshold hot-spot model by Sroubek [2] in order to describe and understand the impact angle dependence of the external electron yield.

2. EXPERIMENT

The external electron emission experiments are carried out in an UHV-chamber under a pressure of 10^{-9} mbar. The Ar^+ projectile ions with a kinetic energy of several keV are created in a commercial rare gas ion source and accelerated onto the polycrystalline silver surface, which can be rotated towards the ion beam.

The determination of the electron emission yield is achieved by the current measuring method [3], in which the sample current is measured. In order to distinguish between the signal contributions a shielding collector is biased with positive and negative voltages to suppress or support the emission of electrons.

3. RESULTS

Figure 1 shows the external electron yield measured for different kinetic energies and different angles of incidence of the projectile ion (see Figure 1).

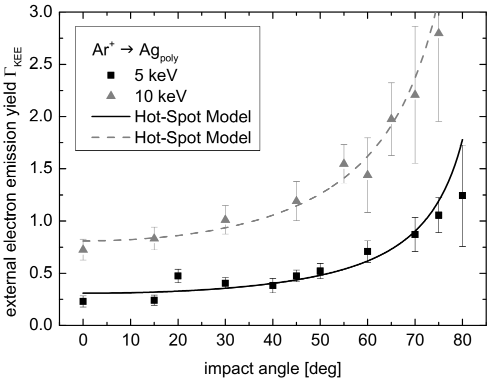

Figure 1: impact angle dependence of the external yield for the impact of argon ions onto a polycrystalline silver surface. The solid and the dashed line represent a fit with Sroubek’s hot-spot model [2].

The experimental results are compared to data from literature and different theoretical approaches are made to understand the observed behavior. Thereby an attempt is made to adapt Sroubek’s hot-spot model to describe the impact angle dependence of the yield of secondary electrons. Furthermore the electronic excitation is estimated by introducing a local electron temperature, which can be obtained from the model and the resulting values are compared to results from molecular dynamics simulations, carried out in our group [4].

4. REFERENCES

[1] J. Ferrón, E. V. Alonso, R. A. Baragiola, and A. Oliva-Florio, Physical Review B **24**, 8 (1981).

[2] Z. Sroubek, Nuclear Instruments and Methods in Physics Research Section B: Beam Interactions with Materials and Atoms **268**, 21 (2010).

[3] H. Eder, W. Messerschmidt, H. Winter, and F. Aumayr, Journal of Applied Physics **87**, 11 (2000).

[4] B. Weidtmann, S. Hanke, A. Duvenbeck, and A. Wucher, Surface and Interface Analysis **43**, 1-2 (2011).

---

[*] Corresponding author e-mail address: Christian.Heuser@uni-due.de

HIGHLY CHARGED ION IRRADIATION OF TWO-DIMENSIONAL SYSTEMS

J. Hopster[1,*], J. Krämer [1], R. Kozubek [1], M. El Kharrazi[1], O. Osmani[2], M. Karlusic[3], and M. Schleberger[1]

[1] Universität Duisburg-Essen, Fakultät für Physik, 47057 Duisburg, Germany
[2] Donostia International Physics Center (DIPC), 20018 Donostia-San Sebastian, Spain
[3] Ruder Boskovic Institut, 10000 Zagreb, Croatia

1. INTRODUCTION

Highly charged ions (HCI) are a well known tool to induce nano-scaled modifications on a variety of surfaces ranging from insulators like CaF_2 to half-metals like graphite [1]. The energy deposition of a HCI is very localized and limited to a volume of a few nm^3 only. From this, one could conclude, that HCI irradiation of volume material or very thin films of the same material should yield similar results. On the other hand, the two-dimensional (2D) forms of several bulk materials show intriguing new properties completely different from the bulk properties. For example, graphene, the 2D form of graphite, is a semiconductor with an unusually high mobility [2] and MoS_2 becomes a direct bandgap semiconductor if prepared as a single layer [3]. To study how these 2D materials are affected by HCI irradiation we have investigated single layer MoS_2 and graphene on insulating substrates.

2. EXPERIMENT AND MODELLING

The samples were prepared by mechanical exfoliation of HOPG and MOS_2 crystals onto single crystals of $CaF_2(111)$ and KBr(100), see fig. 1. The arbitrary distributon of the flakes offers several advantages: At first, crystallites with different numbers of layers are prepared on the same sample and are thus irradiated under exactly the same conditions. Second, because of their unique shape the exact same spot on the sample surface can be accessed before and after irradiation by an atomic force microscope (AFM). The two substrate materials, as well as HOPG, are very well investigated [4, 5, 6] and ensure that any results for these materials can be directly compared to literature values.

The samples were irradiated by Xe ions from a EBIT ion source (setup described in [7]). The maximum charge state was $q = 40+$ supplying a potential energy of 38 keV. The kinetic energy was kept fixed at 260 keV. After irradiation the samples were investigated by AFM in contact mode. The corresponding threshold charge states for damage of the respective materials are calculated using a thermal spike model [8, 9]. The results are compared to the experimental data.

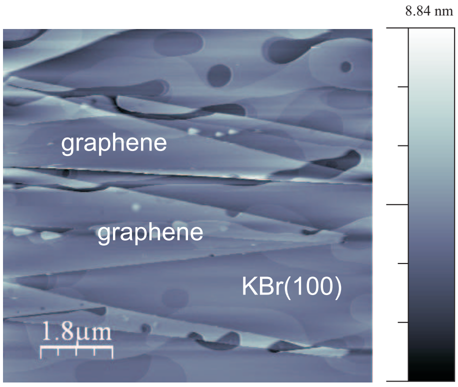

Figure 1: AFM image (tapping mode) of single layer graphene exfoliated on KBr before irradiation. Round step edges are typical for cleaved KBr(100), straight edges are characteristic for graphene layers.

3. REFERENCES

[1] F. Aumayr, *et al.*, J. Phys. Cond. Matt. **23**, 393001 (2011)

[2] K.S. Novoselov, *et al.*, PNAS **102**, 10451 (2005)

[3] K.F. Mak, *et al.*, Phys. Rev. Lett. **105**, 136805 (2010)

[4] A.S. El-Said, *et al.*, Phys. Rev. Lett. **100**, 237601 (2008)

[5] R. Heller, *et al.*, Phys. Rev. Lett. **101**, 096102 (2008)

[6] R. Ritter, *et al.*, Nucl. Instrum. Meth. B **268**, 2897 (2010)

[7] T. Peters, *et al.*, Nucl. Instrum. Meth. B **267**, 687 (2009)

[8] M. Karlusic, *et al.*, Thermal spike analysis of highly charged ion track. Nucl. Instrum. Meth. B in print

[9] O. Osmani, *et al.*, Phys. Rev. B **84**, 214105 (2011)

---

[*] Corresponding author e-mail address: johannes.hopster@uni-due.de

ENERGY DISTRIBUTION OF SPUTTERED ATOMS AND IONS FROM ENERGETIC ION BOMBARDMENT OF GaAs

Angelin Ebanezar John[1], Satyaranjan Bhattacharyya[2], and Rainer Hippler[1]

[1] Institut für Physik, Universität Greifswald, Greifswald (Germany)
[2] Surface Physics Division, Saha Institute of Nuclear Physics, Kolkata (India)

The energy distributions of secondary neutral Ga and As atoms and positively and negatively charged ions sputtered from a GaAs(100) surface after energetic Ar^+ ion bombardment are reported. The incident ion energy was 150keV. A charge analysis shows that Ga species are preferentially sputtered as neutral Ga atoms or as positively charged Ga^+ ions. By contrast, As is preferentially sputtered as negatively charged As^- ions (table 1).

	Negative Ions	Neutral atoms	Positive Ions	Prediction
Ga-69	0.02	0.59	0.58	0.3005
Ga-71	0.01	0.41	0.39	0.1995
As-75	0.97	0.00	0.03	0.5000

Table 1: Measured relative abundances of sputtered neutral atoms and of positively and negatively charged ions.

The energy distribution of sputtered Ga and As monomers was investigated up 100 eV. Asymptotically, it is close to an E^{-3} dependence (E is the kinetic energy), while binary collision theory predicts an E^{-2} dependency.

Sputtering of small clusters was also investigated. In general, the energy distribution of sputtered Ga_n, As_n and of mixed Ga_nAs_m clusters is significantly steeper than compared to the monomers. Results will be presented at the Conference.

---

* Corresponding author e-mail address: hippler@physik.uni-greifswald.de

CALCULATIONS OF NEUTRAL FRACTIONS AND ANGULAR DISTRIBUTIONS FOR H(1s) AND H$^+$ IMPINGING ON Al(111) AT GRAZING INCIDENCES

H. Jouin[1,*] *and F.A. Gutierrez*[2]

[1] Univ. Bordeaux, CNRS, CEA, CELIA, UMR 5107, F-33400 Talence, France
[2] Departamento de Física, Universidad de Concepción, Casilla 160-C, Concepción, Chile

1. INTRODUCTION

In recent works [1-2], we have computed outgoing H(1s) neutral fractions (NF) and the related angular distributions (AD) for protons impinging on Al(111) at grazing incidences (around 0.5°) with incident energies in the range 1 keV – 100 keV. The role of capture and loss for both resonant (R) and Auger (A) processes has been investigated together with the relevance of the surface-plasmon-assisted electron capture channel (P). For H$^+$ beams, consideration of all these mechanisms together (RAP) yield a good agreement between experimental NF [3] and AD [4] and a set of calculations performed by using various theoretical results [5-7] for the resonant process.

Furthermore, comparison between computed NF corresponding to an H(1s) ingoing beam and those obtained for H$^+$ projectiles allows us to show [8] that neutral fractions keep the memory of the initial charge state in the intermediate impact energy range 2 keV - 43 keV, whereas in the extreme domains of low (< 2 keV) and high (> 43 keV) impact energies, the outgoing NF do not depend on the charge state of the initial beam. A detailed analysis of these findings may be found in [8].

In order to complete our previous works [1-2,8], AD corresponding to incident neutrals have been computed here and compared to the available experimental data [4].

2. CALCULATIONS and RESULTS

The ETISC1D code [9] has been used to perform dynamical calculations. Since resonant [5-7] and Auger rates [10] have been so far obtained only in the static case, we use the approximate “kinematic factor” approach proposed in [11] to compute velocity-dependent capture and loss resonant and Auger transition rates. Velocity-dependent rates for surface-plasmon assisted electron capture process have been obtained as detailed in [12]. Furthermore, we use a fitted representation [1] of the dynamical image potential reported in [13] while the purely repulsive potential is described by means of the ZBL screening function [14].

We report in Fig. 1, a comparison between calculated AD for 25 keV impinging H(1s) and H$^+$ at an angle of incidence of 0.56° and the available experimental results [4]. Reported calculations correspond to the use of the H(1s) energy and width (supplemented with the kinematic factors) of [5]. We obtain a pretty good agreement between our calculations and experimental results with, in particular, a good description of the image shift for charged projectiles although the calculated AD is slightly shifted towards large angles with respect to its experimental counterpart. Similar theoretical results (not shown in Fig. 1) are obtained by using the static resonant results reported in [6-7] in such a way that the present comparison at 25 keV do not allow to clearly discriminate between the various theoretical reports for the resonant process in spite of the large differences between them, both in magnitude for the static width or in shape for the H(1s) energy shift.

Comparisons between theory and experiments similar to the present one for both AD and NF for a smaller impact energy like 9 keV would be very useful since for AD the image shift would be greater allowing to better discriminate as shown in [2] and since it has been predicted [8] that NF depend on the projectile charge state for this impact energy.

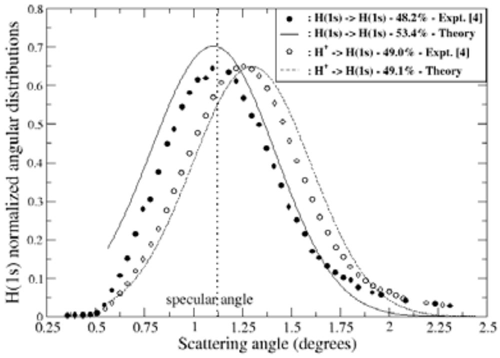

Figure 1: Comparison between experimental [4] and theoretical (this work) angular distributions of scattered H(1s) after grazing incidence (0.56°) collisions of 25 keV H(1s) (● : experiments, full line: theory) and H$^+$ (○: experiments , dashed line: theory).

3. REFERENCES

[1] H. Jouin and F.A. Gutierrez, Phys. Rev. A **80**, 042901 (2009).
[2] F.A. Gutierrez and H. Jouin, Phys. Rev. A **81**, 062901 (2010).
[3] H. Winter, Phys. Rep. **367**, 38 (2002).
[4] H. Winter and M. Sommer, Phys. Lett. A **168**, 409 (1992).
[5] P. Nordlander and J.C. Tully, Phys. Rev. B **42**, 5564 (1990)
[6] A.G. Borisov, D. Teillet-Billy and J.P. Gauyacq, Nucl. Instrum. Methods Phys. Research B **78**, 49 (1993).
[7] S.A. Deutscher, X. Yang and J. Burgdörfer, Phys. Rev. A **55**, 466 (1997).
[8] H. Jouin and F.A. Gutierrez, Phys. Rev. A **84**, 014901 (2011).
[9] S. Jequier, H. Jouin, C. Harel and F.A. Gutierrez, Surf. Sci. **570**, 189 (2004).
[10] R. Hentschke, K.J. Snowdon, P. Hertel and W. Heiland, Surf. Sci. **173**, 565 (1986).
[11] Z.L. Mišković and R.K. Janev, Surf. Sci. **221**, 317 (1989).
[12] F.A. Gutierrez and H. Jouin, Phys. Rev. A **68**, 012903 (2003).
[13] F.J. Garcia de Abajo and P.M. Echenique, Phys. Rev. B **48**, 13399 (1993).
[14] J.P. Ziegler, J.P. Biersack and U. Littmark, The stopping and range of ions in solids (Pergamon, New-York, 1985).

---

[*] Corresponding author e-mail address: jouin@celia.u-bordeaux1.fr

SYNTHESIS OF LIGHT-EMITTING Si NANOCRYSTALS IN Si/SiO$_2$ MULTILAYERS STIMULATED BY INELASTIC LOSSES OF SWIFT HEAVY IONS

G.A. Kachurin[1*], *S.G. Cherkova*[1,2], *V.A. Volodin*[1,2], *A.G. Cherkov*[1,2] *D.V. Marin*[1,2], *A.H. Antonenko*[1,2], *G.N. Kamaev*[1,2], *and V.A. Skuratov*[3]

[1] A.V. Rzhanov Institute of Semiconductor Physics SB RAS, 630090 Novosibirsk, Russia
[2] Novosibirsk State University, 630090 Novosibirsk, Russia
[3] Joint Institute for Nuclear Research, 141980 Dubna, Russia

Stopping of swift heavy ions in the near-surface layers occurs predominantly by the ionization losses. That leads to formation of the tracks, nm-scale in diameters, where the carrier concentrations may reach 10^{22} cm^{-3} and the temperature may exceed 5000 K for 10^{-13}–10^{-11} s. Thus, the structural transformations in the target may be stimulated either by heat or by ionization. We used swift heavy ions as a tool for formation of light-emitting quantum-size Si nanocrystals. They are very prospective for Si-based optoelectronics. Commonly exploited thermal annealing of the Si-rich SiO$_2$ layers results in a relatively broad size distribution of the synthesized nanocrystals. Moreover, the size and density of the quantum dots cannot be controlled independently. Six pairs of the alternating ~8 nm-thick amorphous Si and ~10 nm-thick SiO$_2$ layers have been deposited on the crystalline Si substrates. The layers were irradiated with 167 MeV Xe ions to the doses ranging between 10^{12} cm^{-2} and 10^{14} cm^{-2}. The ionization and nuclear losses of the ions were ~14.5 keV/nm and ~0.3 displacements/nm, respectively. It was supposed that thickness of the Si layers and the diameters of the tracks will define the sizes of the synthesized nanocrystals. Spectral photoluminescence (PL), infrared absorption, Raman scattering and high resolution cross-sectional electron microscopy were used for the characterizations. It was found, that irradiation made the the Si-SiO$_2$ borders less sharp (Fig. 1) and in the absorption spectra the line at 1090 cm^{-1}, belonging to Si-O bonds of perfect SiO$_2$, decreased, while the 1040 cm^{-1} line, usually ascribed to the damaged oxide, increased. Broad yellow-orange PL band appeared from the irradiated layers, which intensity grew with the ion dose. Such emission is traditionally considered as belonging to the different non-crystalline Si nanoinclusions in SiO$_2$. The electron microscopy supported that idea, revealing an appearance of numerous 3-5 nm size dark spots (Fig. 1, inset). After annealing the SiO$_2$ network restored and the PL strongly increased with a shift of maximum intensity to ~800 nm, typical wavelength region of the Si nanocrystals emission. The highest intensity was observed after 1100 °C anneal. Its post-annealing intensity still remained to be proportional to the Xe ion dose (see Fig. 2), and Raman spectroscopy evidenced in parallel the disappearance of the amorphous Si phase, also in compliance with the ion doses. It is concluded, that irradiation with swift heavy ions stimulates synthesis of the light-emitting Si nanocrystals in SiO$_2$ during the subsequent annealing. The roles of inelastic losses in the synthesis is discussed.

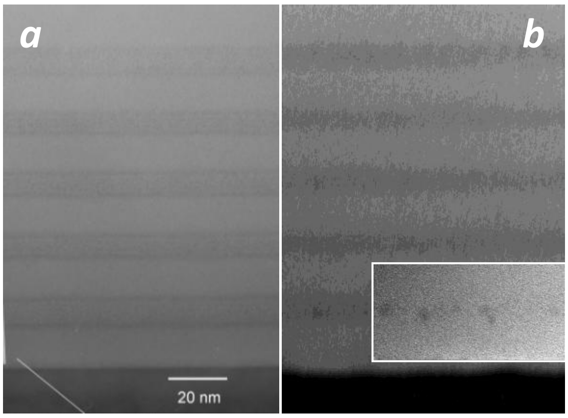

Figure 1: Cross-sectional HREM image of Si/SiO$_2$ heterostructures before (*a*) and after irradiation with the dose of $3x10^{13}$ cm^{-2} (*b*). Inset – more thin cross-section of the irradiated structure.

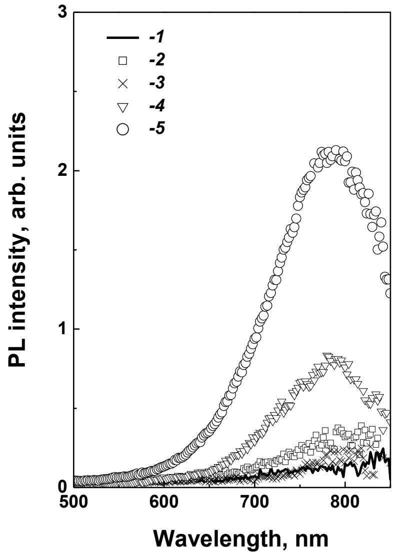

Figure 2: PL spectra before (*1*) and after irradiation with Xe ions and subsequent annealing at 1100 °C. Xe doses, 10^{12} cm^{-2}: *2* – 1, *3* – 3, *4* – 10, *5* – 30.

---

[*] Corresponding author e-mail address: kachurin@isp.nsc.ru

ENERGY AND TIME DEPENDENCE OF GUIDED ELECTRONS THROUGH PET NANOCAPILLARIES

D. Keerthisinghe[1], B. S. Dassanayake[1], S. Wickramarachchi[1], A. Ayyad[1], N. Stolterfoht[2] and J. A. Tanis[1]*

[1] Department of Physics, Western Michigan University, Kalamazoo, MI 49008, USA
[2] Helmholtz-Zentrum Berlin für Materialien und Energie, D-14109, Berlin, Germany

In 2002 the transmission and guiding of slow highly charged ions (HCIs) through insulating polyethylene terephthalate (PET) nanocapillaries was reported [1]. The first electron transmission and guiding through alumina and PET nanocapillaries was published in 2007 [2,3], and later electron transmission through single glass microcapillaries was also studied [4]. The aim of the present work is directed towards the energy and time dependence of electron transmission through PET nanocapillaries. The PET foil used in this study, from the GSI and the Helmholtz-Zentrum, Berlin, had capillaries with diameters of 100 nm and an aspect ratio 120. Data were acquired for sample tilt angles ψ (with respect to the incident beam direction) of 0.0^0 to -4.5^0 for energies of 500 and 800 eV at Western Michigan University.

The present results show three electron transmission regions corresponding to the direct beam, guiding, and the transition region between the two. The spectra for the intensities vs. the observation angle were fit with Gaussian functions having different centroid angles θ, and for the transition region two Gaussians were fit to the spectra. For the direct beam region with sample tilt angles ψ near zero degrees, the observation angle θ is constant for the both incident energies and equal to about zero. In the guiding region ψ θ, while in the transition region there are two observation angles showing characteristics of both. These results are shown in Fig. 1. The linear relationship of the centroid of the observation angle θ as a function of sample tilt angle ψ is evidence for guiding of electrons through PET nanocapillaries. The characteristic guiding angle ψ_c, i.e., the angle at which the transmission falls to 1/e of its initial value, is found to increase in the guiding region with increasing energy in contrast to the previous results [3], and in agreement with the results found for glass capillaries [4]. Comparison with single glass micro-capillaries [4] shows higher ψ_c values for PET as expected from it being a better insulator than glass.

Time dependence measurements were performed by blocking the beam for ~24 hours for a particular sample tilt angle ψ and the corresponding spectrometer centroid angle θ. Measurements (not shown) were made for sample tilt angles $\psi = 0.0^0$, $\pm1.7^0$ and $\pm2.5^0$ for both energies. Results for both 500 and 800 eV, normalized to the current on the sample, clearly show that the transmission of electrons through PET strongly depends on the time (charge) with the transmission eventually reaching equilibrium.

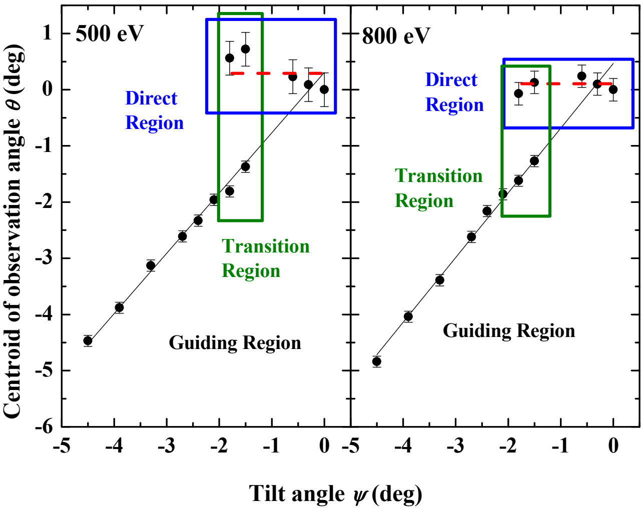

Figure 1: Centroid of the observation angle θ as a function of sample tilt angle ψ for incident energies of 500 and 800 eV showing the existence of the direct, guiding, and the transition regions. The line through the guiding data is a linear fit, while the red dashed line through the direct data is drawn to guide the eye.

REFERENCES

[1] N. Stolterfoht, J.-H. Bremer, V. Hoffmann, R. Hellhammer, D. Fink, A. Petrov and B. Sulik, Phys. Rev. Lett. **88,** 133201 (2002).

[2] A. R. Milosavljević, Gy. Víkor, Z. D. Pešić, P. Kolarž, D. Šević and B. P. Marinković, Phys. Rev. A **75** 030901(R) (2007).

[3] S. Das, B. S. Dassanayake, M. Winkworth, J. L. Baran, N. Stolterfoht and J. A. Tanis, Phys. Rev. A **76** 042716 (2007).

[4] B. S. Dassanayake, S. Das, R. J. Bereczky, K. Tőkési and J. A. Tanis, Phys. Rev. A **81** 020701 (R) (2010).

---

* Corresponding author e-mail address: darshika.keerthisinghe@wmich.edu

FORMATION AND EMISSION OF GOLD AND SILVER CARBIDE CLUSTER IONS IN A SINGLE C_{60}^{-} SURFACE IMPACT AT keV ENERGIES: CHARACTERIZATION AND MECHANISMS

*Y. Cohen, V. Bernshtein , E. Armon, A. Bekkerman and E. Kolodney**

Schulich Faculty of Chemistry, Technion-Israel Institute of Technology, Haifa 32000, ISRAEL

1. INTRODUCTION

We have studied a reactive surface scattering event where a large molecule/cluster projectile ion is disintegrating upon 10-15 keV impact , resulting in the impulsive formation and emission of product cluster ions. This can be considered as a generalized Eley-rideal (ER) type scattering event where target atoms (or aggregates) are being picked up by parent fragments during impact disintegration at energies well above shattering threshold. Single impact of C_{60}^{-} ions on surfaces at keV energies can also be used for generating new carbide cluster ions in the gas phase. This approach is applied to the late transition metal targets, gold and silver, resulting in unique cluster ions with a relatively wide range of stochiometries (1,2).

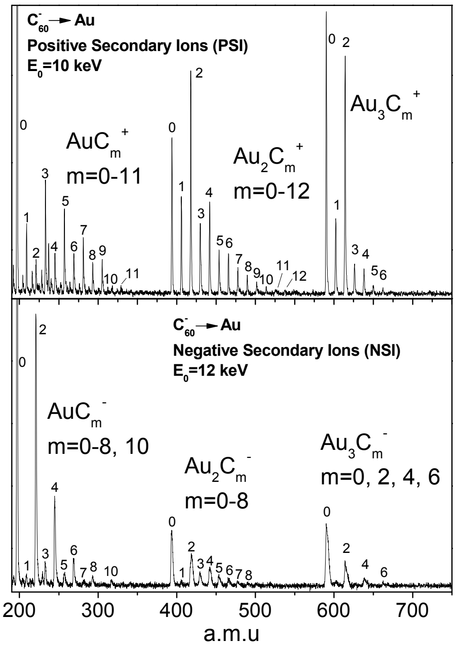

Fig.1. Positive and negative secondary ion mass-spectra.

2. RESULTS AND DISCUSSION

The fullerene ion bombardment led to the formation of positively and negatively charged cluster ions $Au_nC_m^+$ (n=1-5, 1≤m≤12), $Ag_nC_m^+$ (n=1-7, 1≤m≤7), $Au_nC_m^-$ (n=1-5, 1≤m≤10) and $Ag_nC_m^-$ (n=1-3, 1≤m≤6). The impact synthesis of these unique gold-carbon and silver-carbon compounds was demonstrated under very low flux conditions (pulsed beam) where the whole process (impact, cluster formation and surface emission) is clearly a single impact event and for much higher fluxes (continuous beam) where the single event nature of the impact induced process is demonstrated by following the instantaneous formation kinetics of the sputtered/emitted ions. We conclude that under both low and high flux conditions the process leading to the combined formation/ejection of the carbide ions is a single impact pick-up of one-to-several metal atoms. The process is taking place mainly during the shattering stage (of the incoming C_{60}^{-} projectile) and the initial phase of the non-linear collision cascade (thermal spike) evolving within the impact/sputtering volume (completed within one psec). Due to effective mixing (or tight contact) between projectile fragments and target atoms and the very high temperatures obtained within the impact zone, the most abundant carbides produced have relatively balanced stoichiometries. Both gold-carbon and silver-carbon cluster ions were rarely explored before and their general structure therefore pose an intriguing open question .We have carried out density functional theory (DFT) calculations aimed at identifying optimal geometries of the AuC_m^+ series (m=1-7), $Au_2C_m^+$ series (m=1-6), the highly abundant $Au_3C_2^+$, $Ag_3C_2^+$ species and the $Ag_5C_4^+$ structure. For the AuC_m^+ series we were able to explain the odd/even intensity alternation in terms of corresponding alternations of AuC_m adiabatic ionization energies (rather than dissociation energies). Both $Au_3C_2^+$ and $Ag_3C_2^+$ were found to have a similar π-complex bonding $[M(\pi\text{-}M\text{-}C\equiv C\text{-}M)]^+$ (M=Ag, Au) between the metal d electrons and the π electrons of the carbon-carbon triple bond. We will also present measurements of kinetic energy distributions (KEDs) of the different species emitted (focusing on several outgoing carbide ions) and discuss possible emission mechanism.

3. REFERENCES

[1] Y. Cohen , .V. Bernstein, E. Armon, A. Bekkerman and E. Kolodney, J. Chem. Phys. 134 (2011) 124701

[2] Y. Cohen and E. Kolodney, Nuclear Instr. And Meth. B, 269 (2011) 985.

---

* Corresponding author e-mail address: eliko@tx.technion.ac.il

HIGH DEPTH ANALYSIS WITH ION BEAM AND NANO-AREA ANALYSIS WITH NOVEL COMPACT HIGH BRIGHTNESS AND HIGH SPIN-POLARIZED SPLEEM

*T. Koshikawa**, *M. Suzuki, T. Yasue, E. Bauer*[1], *Y. Takeda*[2] *and T. Nakanishi*[3]

Osaka Electro-Communication Univ., Neyagawa, Osaka, Japan
[1] Arizona State Univ.Tempe, Arizona, USA
[2] Nagoya Univ.Chigusa, Nagoya, Japan

Ion beam technique makes us very high depth resolution analysis which is important for application to new memory devices, however it is difficult to make nano-order special resolution analysis. We need another technique. Here we will present novel idea of a compact high brightness and high spin-polarized LEEM. Memory size has been tremendously enlarged after the development of GMR. Recently new concept MRAM (magnetic random access memory) has been proposed, in which the magnetic domain wall can be driven with current (current-induced domain wall motion: CWM) using perpendicular magnetic anisotropy. $[Co/Nix]_y$ multi-layer nano-wires might be an important candidate, which has strong perpendicular magnetic anisotropy [1]. In order to clarify the detailed magnetic thin film formation and their property, we need more sophisticated magnetic microscopy instrument which gives us high spatial resolution, dynamic observation and so on. The magnetic images of $Co/Ni_2/W(110)$ and 1 ML Au on $Co/Ni_2/W(110)$ show that Au ultra thin film conducts to the strong perpendicular magnetic anisotropy shown in Fig. 1. W(110) substrate gives also big effect on the perpendicular magnetization of $CoNi_2$ thin film. This means that combination of ultra thin Au film and W substrate could be used as the cap materials.

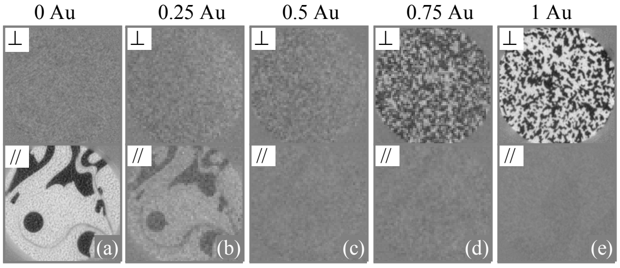

Fig. 1. Magnetic domain contrast of Au/1Co/2Ni/W (110)

Additional development are carried out in order to improve the high quantum efficiency of the photo-cathode with reducing the absorption of the laser light at the GaAs inter-layer and the reflection of the laser beam at the back-side surface, which makes us now improving the factor four. We are also making a compact spin gun with new idea in which we can reduce the devices for spin manipulation and rotation from two to one. This novel device can operate the spin direction in 3 dimensional ways.

---

* Corresponding author e-mail address: kosikawa@isc.osakac.ac.jp

ENERGY AND ANGULAR RESOLVED DETECTION OF SPUTTERED IONS AND NEUTRALS

M.Marpe[*]*,M.Mai*[2]*, and A. Wucher*[3]

[1-3] University of Duisburg-Essen, Faculty of Physics, Lotharstr. 1, D-47048 Duisburg

1. INTRODUCTION

During ion/surface interaction processes a variety of species is emitted into the vacuum. It is a well known fact that most of the emitted particles leave the surface as neutrals while only about 1% (depending on the atomic species) are emitted as ions. Due to the fact that principally only ionized particles are detectable in **T**ime-**o**f-**F**light **M**ass **S**pectrometers, a post-ionization e.g. with a laser field is frequently applied. Under certain circumstances the post-ionization can be driven into saturation that nearly all emitted particles can be detected.
By comparing the signal of detected ions with and without post-ionization it is possible to determine the ionization probability of sputtered particles - a quantity of crucial importance in Secondary Ion Mass Spectrometry.
Although this field has been intensively studied through the last two decades the dependence of ionization probabilities on parameters like, e.g. the impact angle is still not well understood.
We present a method in which the ionization probability as a function of the impact angle can be determined. This is interesting because there are theoretical predictions that this quantity depends on the impact angle. Corresponding experimental data testing that prediction, however, is still lacking.
Basically a ToF-MS with resonant laser post-ionization is applied for those measurements.

2. Experiments

The method to determine the ionization probability is based on the EARN (**e**nergy and **a**ngular **r**esolved **n**eutrals) experiment developed in the Winograd group. The idea is to accelerate secondary ions and post ionized secondary neutrals through the application of an electric field. These ions travel through a grounded grid which limits the acceleration field and then pass a field-free flight path until they reach a Chevron-stack MCP combined with a phosphor screen. Impinging ions produce a light flush on the phosphor screen, which is filmed by a CCD-camera and digitized using a frame-grabber. The applied software is used to deconvolute the recorded two-dimensional data into an energy and emission-angle resolved spectrum.
The applied instrument was developed and built in the Winograd lab at the Pennsylvania State University. It was previously just used for the detection of neutral particles [1] while secondary ions created during the emission process were suppressed. Without this suppression the instrument can detect secondary ions and secondary neutrals (post-ionized) as well. For that purpose the timing scheme of the instrument has to bee changed.
In our experiments a 5keV Ar^+-beam is used for the sputtering of a polycrystalline In foil. The applied resonant laser post-ionization scheme for post-ionization of sputtered neutral In atoms is described elsewhere [2]. The general experimental scheme and also first experimental results will be presented.
These measurements performed with the EARN apparatus will also be compared with measurements recently performed in our laboratory using a conventional reflectron-type ToF-MS with a different post ionization technique which are both described elsewhere [3]. While the experiments done on the EARN instrument utilize resonant multi-photon laser post-ionization, the reflectron type experiments use a single photon post-ionization scheme with 157 nm laser pulses produced by a commercial excimer laser; the projectile is in both cases a pulsed 5 keV Ar^+-beam and the target also a polycrystalline In foil.

3. REFERENCES

[1] J. P. Baxter, G. A. Schick, J. Singh, P. H. Kobrin and N. Winograd, J. Vac. Sci. Technol. A, Vol. 4, No. 3 (May/Jun 1986)

[2] F. M. Kimock, J. P. Baxter and N. Winograd, Nuclear Instruments and Methods in Physics Research 218 (1983) 287-292

[3] *Laser Postionization: Fundamentals* A. Wucher in ToF-SIMS: Surface Analysis by mass spectrometry, Ed. J. C. Vickerman, D. Briggs, IM Publications and Surface Spectra 2001, 347-374

---

[*] Corresponding author e-mail address: mario.marpe@uni-due.de

AUGER NEUTRALIZATION OF HE$^+$ ON CU SURFACES: SIMULATION OF AZIMUTHAL SCANS

R. C. Monreal[1,*], *D. Goebl*[2], *D. Primetzhofer*[3], *E. Abad*[1] *and P. Bauer*[2]

[1] Departamento de Física Teórica de la Materia Condensada, Universidad Autónoma de Madrid, E-28049 Madrid
[2] Institut für Experimentalphysik, Abteilung für Atom- und Oberflächenphysik, Johannes Kepler Universität Linz, 4040 Linz, Austria
[3] Institutionen för Fysik och Astronomi, Uppsala Universitet, Box 516, S-751 20 Uppsala, Sweden

1. INTRODUCTION

Charge exchange between ions and surfaces is a topic of great interest in many research fields, e.g. catalysis, plasma-wall interactions or surface analysis. When an ion approaches a surface, charge exchange can occur due to two-electron Auger-processes or due to resonant processes. This investigation is focused on Auger-Neutralization (AN). In an AN-process an electron from the conduction band tunnels to an unoccupied level of higher binding energy of the approaching ion. The gain in potential energy is dissipated by excitation of another electron (Auger-electron) or by excitation of a plasmon.

Since the pioneering work of Hagstrum [1], many theoretical investigations were devoted to the understanding of AN. Recently, a study of AN in Low-energy ion scattering (LEIS) revealed that the AN probability strongly depends on the binding energy of the He 1s level [2]. This is insofar of importance, as interactions between projectile and target do modify the binding energy as a function of the ion-atom distance. The aim of the present investigation is to verify whether the obtained results for Cu(111) are also valid for other Cu surface orientations and if this model correctly predicts second layer contributions.

2. RESULTS AND DISCUSSION

We present simulations of LEIS experiments for He ions scattered from Cu(110) and Cu(100) surfaces in the energy regime $E_0 < 2$keV, where neutralization is exclusively due to AN. In this regime, the fraction of ions amongst the backscattered particles, P^+, depends on the AN-rate, Γ, and the projectile trajectory, $\vec{r}(t)$, in the following way:

$$P^+ = \exp(-\int \Gamma(\vec{r}(t))dt) \qquad (1)$$

Γ was calculated using the above mentioned model and projectile trajectories were obtained employing the MD-simulation package KALYPSO [3].

We performed two different kinds of calculations: Calculations of P^+ as a function of energy for fixed geometries and calculations of ion yields for a fixed energy as a function of the azimuthal exit angle of the backscattered projectiles. For the energy dependent calculations, geometries are selected where He trajectories comprise a single-scattering event from a first or second layer atom. Results for Cu(110) are shown in Fig.1 for exit in $[1\bar{1}2]$ direction (1st layer visible) and in $[1\bar{1}0]$ direction (1st and 2nd layer visible). Scattering from the 2nd layer contributes more to the neutral yield than to the ion yield. Therefore, P^+ is reduced by 2nd layer contributions.

From the exit angle dependent calculation, we can extract the specific influence of scattering geometry and neutralization rates on the resulting ion yield.

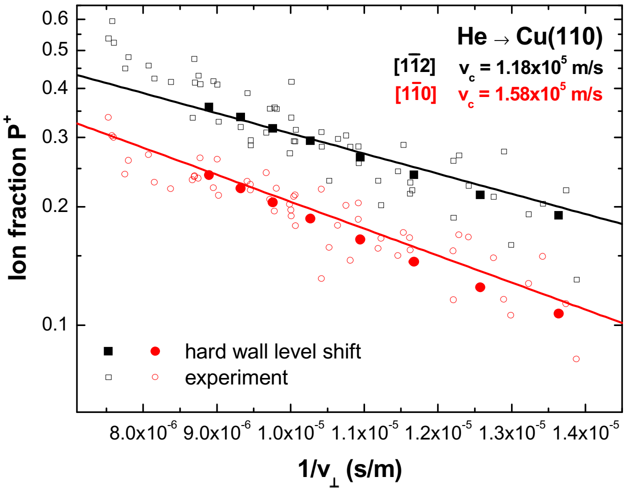

Figure 1: Ion fraction of He$^+$ scattered from Cu(110) in $[1\bar{1}2]$ and $[1\bar{1}0]$ azimuth directions (squares and circles, respectively). Calculations were performed with the hard wall level shift model to approximate the distance dependent He 1s level shift (for details, see [2]).

3. REFERENCES

[1] H.D. Hagstrum, Phys. Rev. 96 (1954) 336.
[2] D. Goebl, R. C. Monreal, D. Valdes, E. Abad, D. Primetzhofer, and P. Bauer, Phys. Rev. B. 84 (2011) 165428.
[3] MA. Karolewski, Nucl. Instr. Meth. B 230, 1-4, 402-405 (2005).

---

[*] Corresponding author e-mail address: r.c.monreal@uam.es

ENERGY DEPENDENCE OF NONLINEAR EFFECT ON SPUTTERING YIELDS OF Si BOMBARDED WITH 10-540 keV C_{60} IONS

K. Narumi[1, 2, *], *H. Naramoto*[2], *K. Yamada*[1], *A. Chiba*[1], *Y. Saitoh*[1], *and Y. Maeda*[2, 3]

[1] Takasaki Advanced Radiation Research Institute, Japan Atomic Energy Agency, Takasaki, Gumma 370-1292, Japan
[2] Advanced Science Research Center, Japan Atomic Energy Agency, Tokai, Ibaraki 319-1195, Japan
[3] Department of Energy Science and Technology, Kyoto University, Sakyo-ku, Kyoto 606-8501, Japan

1. INTRODUCTION

The sputtering yield of a polycrystalline or amorphous single-element solid bombarded with monatomic ions is well described by the linear-collision-cascade theory by Sigmund [1]. When the atomic numbers of the projectile and the target become large, however, the deviation of experimental sputtering yields from the theoretical predictions, which is called nonlinear effect, is found; especially, it is more significant in the case of cluster-ion bombardment [2]. In the case of Au self-sputtering by Au$_n$-ion (n 13) bombardment, it has been reported that the sputtering yield is proportional to n^2 in the energy range where the nuclear stopping is dominant [3]. This nonlinear effect can be attributed to an elastic-collision thermal-spike model [4]. In the present study we have determined Si sputtering yield as a function of energy of C_{60} ions in the energy range from 10 to 540 keV in order to investigate nonlinear effects on the sputtering yield.

2. EXPERIMENTAL AND RESULTS

Pieces of Si(100) wafer were irradiated with 200-keV Ar^+ ions at the fluence of 5 10^{15} /cm^2 to make an amorphous layer at the surface. Then, the samples were irradiated with 10-540 keV C_{60}^+ or C_{60}^{2+} ions. After the C_{60}-ion irradiation, the thickness change of the amorphous layer was measured with Rutherford-backscattering spectrometry using 2-MeV He^+ ions. Sputtering yields were evaluated with the change in the thickness of the amorphous layer. Figure 1 shows the obtained sputtering yield of Si bombarded with C_{60} ions as a function of the energy of a C_{60} ion. The observed sputtering yield has the maximum around 100 keV, which is approximately 600 Si/C_{60} or 10 Si/C. They were compared with those bombarded with a C monatomic ion calculated both based on Sigmund's theory [1] and using the SRIM2008 code [5]. The results are shown in Fig. 1 as the solid line and the open diamonds, respectively. Comparing with the calculated sputtering yield for an equi-velocity monatomic ion, nonlinear effect on the sputtering yield has been found. Here, we introduce the sputtering-yield ratio $Y_{60}/(60\ Y_1)$, which gives the magnitude of the nonlinear effect. The ratio depends on the energy of C_{60} ions as shown in Fig. 2: It is very large around the energies where the sputtering yield has the maximum and hardly observed at 10 keV. No n^2 dependence is observed. The present results support that the observed nonlinear effect is not attributed to "the thermal spike" but to "the dense collision cascades".

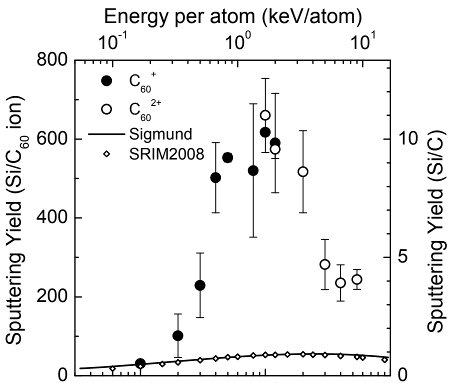

Figure 1: Energy dependence of the Si sputtering yield for C_{60}-ion bombardment. The solid line shows the sputtering yield for monatomic-ion bombardment calculated with Sigmund's theory. The result simulated with SRIM2008 is also shown.

3. REFERENCES

[1] P. Sigmund, Phys. Rev. **184**, 383 (1969).
[2] H.H. Andersen and H.L. Bay, Rad. Effects **19**, 139 (1973).
[3] S. Bouneau *et al.*, Phys. Rev. B **65**, 144106 (2002).
[4] P. Sigmund and C. Claussen, J. Appl. Phys. **52**, 990 (1981).
[5] J.F. Ziegler, SRIM version 2008, <http://www.srim.org> (2008).

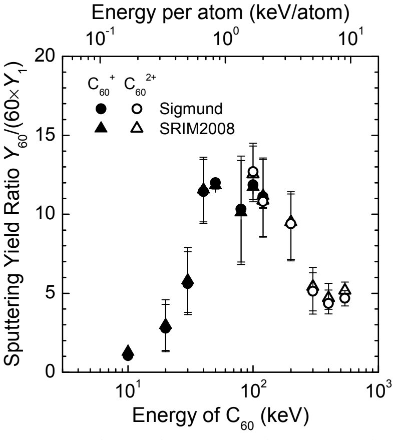

Figure 2: Energy dependence of the sputtering-yield ratio $Y_{60}/(60\ Y_1)$, where Y_{60} is the present sputtering yield for a C_{60} ion and Y_1 is the sputtering yield for a monatomic ion.

---

[*] Corresponding author e-mail address:narumi.kazumasa@jaea.go.jp

TRANSIENT METAL-LIKE ELECTRICAL CONDUCTIVITY IN SWIFT HEAVY ION IRRADIATED SIO$_2$

O. Osmani[1,*], N. Medvedev[2], M. Schleberger[3] and B. Rethfeld[4]

[1] Donostia International Physics Center, 20018 Donostia-San Sebastian, Spain
[2] Center for Free-Electron Laser Science, DESY, 22607 Hamburg, Germany
[3] Fakultät für Physik, Universität Duisburg-Essen, 47048 Duisburg, Germany
[4] Department of Physics and OPTIMAS Research Center, Technical University of Kaiserslautern, 67653 Kaiserslautern, Germany

1. INTRODUCTION

The irradiation of insulators with swift heavy ions is known to induce structural modifications in the target material such as nanometric hillocks or craters on the surface and so called tracks in the bulk. Commonly, the creation of these modifications is studied by means of the so-called two temperature model (TTM) [1]. In the framework of this model, the strong electronic excitation induced by the ions energy loss is transferred to the lattice via electron-phonon coupling. One drawback of the TTM is, that critical parameters, like the number of excited electrons are often not known and thus treated as fitting parameters. The application of the Monte Carlo method (MC) [2] allows for a detailed study of the dynamics of the electron system. Combining both methods, i.e. using the results of the MC simulation as input for the TTM gives the means to predict track radii in a fit free manner. Here it will be demonstrated how the combined MC-TTM model [3] is capable of predicting additional properties of the irradiated insulator, like the transient electrical conductivity for the exemplary irradiation of 456 MeV Ca in SiO$_2$.

2. MODEL

Intrinsically, insulators like SiO$_2$ exhibit very low electrical conductivity σ due to the almost empty conduction band. However, during the irradiation of insulators with swift heavy ions, a significant number of electrons can be excited into the conduction band, thus giving rise to an increasing transient electrical conductivity.

The electrical conductivity can be described using the law of Wiedemann and Franz

$$\frac{\kappa_e}{\sigma} = LT \ , \tag{1}$$

where κ_e is the electron thermal conductivity, T is the temperature and L is the Lorentz number. Thus in order to compute the electrical conductivity, the thermal conductivity must be known. However, this quantity is difficult to compute and experimental measurements are rare. In order to determine κ, another approximation will be employed

$$\kappa = C_e D_e \ , \tag{2}$$

where C_e and D_e are the electron heat capacity and diffusivity respectively. Both can be obtained using our Monte Carlo computer code. Thus with eq. (2) σ is given as

$$\sigma = \frac{C_e D_e}{LT} \ . \tag{3}$$

The electrical conductivity shown in Fig. 1 is calculated at 100 fs after the ion impact for different radii from the ion impact point. The electron density in the conduction band, that governs the electrical conductivity is of transient nature. The electron density distribution will broaden in time, while electron-hole recombination processes will reduced the number of electrons in the conduction band. Thus, the electrical conductivity presented here is of transient nature.

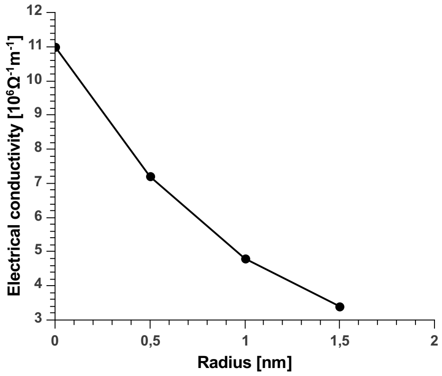

Figure 1: Electrical conductivity at different radii from the ion impact point calculated 100 fs after the impact.

3. REFERENCES

[1] E. Akcöltekin, S. Akcöltekin, O. Osmani, A. Duvenbeck, H. Lebius and M. Schleberger, New J. Phys. **10**, 053007 (2008).

[2] N. Medvedev, A. Volkov, N. Shcheblanov and B. Rethfeld, Phys. Rev. B **82**, 125425 (2010).

[3] O. Osmani, N. Medvedev, M. Schleberger, and B. Rethfeld, Phys. Rev. B **84**, 214105 (2011).

---

[*] Corresponding author e-mail address: orkhan_osmani@ehu.es

HEAVY ION ELASTIC RECOIL DETECTION AND NUCLEAR REACTION ANALYSIS IN STUDIES OF NITROGEN-15 TRANSPORT MARKER IN TOKAMAKS

P. Petersson[1,*], M. Rubel[1], G. Possnert[2], S. Brezinsek[3], A. Hakola[4], J. Likonen[4], M. Mayer[5], V. Rohde[5], ASDEX Upgrade team

[1]Alfvén Laboratory, KTH Royal Institute of Technology, Association Euratom-VR, SE-100 44 Stockholm, Sweden
[2]Tandem Laboratory, Association Euratom-VR, Uppsala Universitet, P. O. Box 256, 751 05 Uppsala, Sweden
[3]IEK-4, Forschungszentrum Jülich, Association EURATOM, Jülich, Germany
[4]VTT, Association Euratom-Tekes, P. O. Box 1000, 02044 VTT, Finland.
[5]Max-Planck-Institut für Plasmaphysik, Euratom Association, Boltzmannstr. 2, 85748 Garching, Germany.

1. INTRODUCTION

Accelerator-based ion beam methods are the most efficient tools for qualitative and quantitative characterization of plasma-facing components (PFC) in controlled fusion devices. Wall components undergo severe modifications by plasma-wall interactions (PWI) which cause material migration that involves erosion of wall material, its transport in hot hydrogen plasma and subsequent re- and co-deposition. A conclusive approach to the determination of migration processes is based on the application of tracer elements. These can be radioactive or rare isotopes of elements being of interest in PWI studies, i.e. first wall materials (C, Be, W) or gases such as N_2 or Ne used for cooling the plasma edge, essential in high power plasma operations with tungsten PFC. Parts of the injected gases remain in a tokamak and their inventory must thus be quantified. This is a challenging task because of the presence of a large number of light isotopes: H, D, T, ^{9}Be, ^{10}B, ^{11}B, ^{12}C, ^{13}C, ^{14}N, and ^{19}F. This paper focuses on the development of experimental and analytical procedures for Nitrogen-15 which was used as a marker in the TEXTOR [1,2] and ASDEX-Upgrade (AUG) [3] tokamaks.

2. EXPERIMENTS AND ANALYSES

Nitrogen-15 injection experiments have been accompanied by seeding other tracers: ^{13}C-labelled methane and, in the case of TEXTOR, also tungsten fluoride, WF_6. A targe number of various probes and wall components were retrieved from the tokamaks and then analysed.

Two different ion-beam techniques have been applied to study the resulting ^{15}N distribution: (i) Nuclear reaction analysis (NRA) with a 900-keV proton beam using the $^{15}N(p,\gamma^{4}He\ ^{12}C$ reaction and (ii) Time of Flight Heavy Ion Elastic Recoil Detection Analysis (ToF HIERDA). Both techniques have sufficient resolution ($<10^{15}$ at/cm^2) for global migration investigations. In addition, ToF HIERDA has the advantage of not being selective and can show several elements simultaneously such as ^{15}N, ^{13}C and oxygen whereas the proton beam will only result in nuclear reactions with certain isotopes. However, due to the large cross-section NRA measurements are NRA fast, thus allowing measurements of a large number of data points. Moreover, the method is also less dependent on the structure and geometry of the samples. Both methods have good depth resolutions so that ^{15}N on the surface can be separated from ^{15}N further in the bulk.

3. RESULTS

Fig. 1 shows a HIERDA spectrum recorded after an experiment involving ^{15}N, ^{13}C and WF_6 puffing. Most significant results are summarised as follows:

(i) nitrogen retention is quite significant as proven by analyses of the ^{15}N tracer in TEXTOR and ASDEX Upgrade,

(ii) high-Z volatile compounds can be effectively used in migration studies,

(iii) only small quantities of fluorine from the WF_6 remain in PFC, while, (iv) helium is trapped in deposits.

The presentation of surface studies will be accompanied by discussion of local and core spectroscopy data from those tracer experiments.

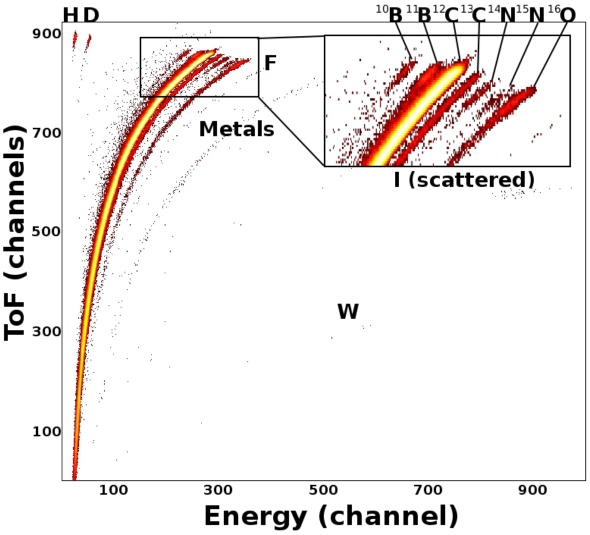

Figure 1: Time-of-flight HIERDA spectra recorded with a 26 MeV $^{127}I^{7+}$ beam for co-deposits on a graphite plate exposed to plasma in TEXTOR.

4. REFERENCES

[1] P. Petersson et al., Nucl. Instr. Meth. B**273**, 113 (2012).
[2] M. Rubel et al., J. Nucl. Mater., submitted.
[3] P. Petersson et al., J. Nucl. Mater., submitted.

---

[*] Corresponding author e-mail address: Per.Petersson@ee.kth.se

ANALYSIS OF Mo/Si MULTILAYERS BY MEANS OF RBS

W.Roessler[1,*], *D. Primetzhofer*[1,2], *and P.Bauer*[1]

[1] Johannes-Kepler-Universität Linz, Institut für Experimentalphysik, A-4040 Linz, Austria
[2] Institutionen för Fysik och Astronomi, Uppsala Universitet, Box 516, S-751 20 Uppsala, Sweden

1. INTRODUCTION

Samples consisting of 50 Mo/Si double layers on Si were analyzed by Rutherford Backscattering Spectrometry (RBS) using protons and deuterons at different experimental conditions. From measurements at high energies (400 - 650 keV) and perpendicular incidence, the absolute amount of Mo and Si in the multilayers was determined. Under these conditions the individual layers cannot be resolved, but from the different slopes of the plateaus corresponding to Mo and Si, it can be deduced that there is a gradient in the thickness ratio d_{Mo}/d_{Si}. Quantitative information on the individual layer thicknesses can be deduced from a comparison with a SIMNRA [1] simulation: from the surface to the interface the thickness of d_{Mo} increases from 2.08 nm to 2.72 nm, and d_{Si} decreases from 5.49 nm to 3.90 nm. Thus, we are able to evaluate this gradient even if the thickness successive Mo and Si-layers varies only by 0.3%. Figure 1 shows the measured and simulated spectra for 600 keV protons.

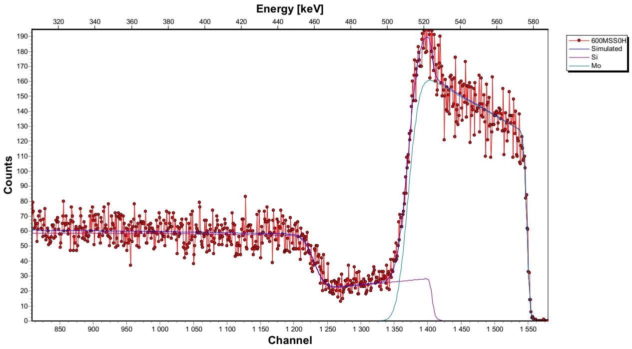

Figure 1: RBS spectrum for 600 keV H+. The solid lines are fits obtained by SIMNRA.

In order to obtain information on the Mo layers next to the surface, we performed further experiments with optimized depth resolution. For this purpose, spectra were recorded using 250 keV deuterons as projectiles, and a Si-detector of optimized energy resolution (2.5 keV FWHM particle resolution) [2]. As an angle of incidence, 74° were chosen. As shown in Fig. 2, with these conditions chosen, we can resolve at least the first four Mo layers individually. Also shown is the corresponding SIMNRA spectrum, which has been obtained for the same target model as used in Fig.1, and only the scattering conditions were modified. Perfect agreement to experiment has been obtained, giving confidence in experiment and evaluation procedure.

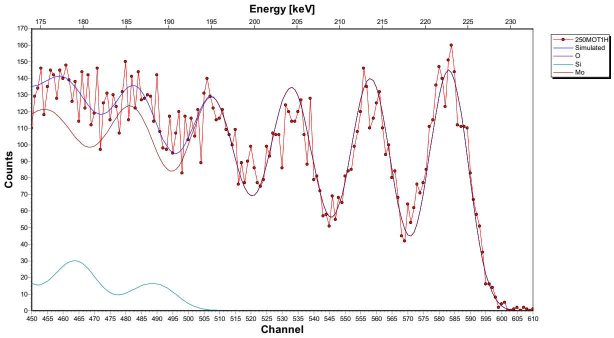

Figure 2: RBS spectrum for 250 keV d+. The solid lines are fits obtained by SIMNRA.

2. Acknowledgement

We are grateful to Dr. Martin Weiser, Carl Zeiss SMT GmbH, who provided the Mo/Si Multilayers used in this work.

3. REFERENCES

[1] M. Mayer, *SIMNRA, a Simulation Program for the Analysis of NRA, RBS and ERDA*, Proceedings of the 15th International Conference on the Application of Accelerators in Research and Industry, J. L. Duggan and I.L. Morgan (eds.), American Institute of Physics Conference Proceedings 475, p. 541 (1999)

[2] M. Geretschläger, *A simple low-noise cryogenic preamplifier for silicon surface barrier detectors*, Nuclear Instruments and Methods in Physics Research Volume 204, Issues 2–3, 1 January 1983, Pages 479–483.

---

[*] Corresponding author e-mail address: wolfgang.roessler@jku.at

New experimental setup to measure slow ion-induced sputter yields in graphite

P. Salou[1], *H. Lebius*[1], *A. Benyagoub*[1] *and B. Ban-d'Etat*[1,*]

[1] CIMAP (CEA-CNRS-ENSICAEN-UCBN)
Boulevard Henri Becquerel, BP5133 Caen Cedex 14070, France

1. INTRODUCTION

The walls of tokamaks are experiencing an influx of heat and particles from the plasma. The ensuing erosion, which is partially enhanced due to chemical reactions, leads on one hand to a surface modification of the plasma wall elements, and on the other hand to the introduction of high-Z materials into the plasma. This introduction induces plasma cooling, which contributes to its instability. The choice of the plasma-facing material is thus essential for the reactor design. Due to their thermal properties, carbon components are one of the selected materials. However the effect of the plasma interacting with carbon components, in particular due to sputtering, is still not well known.

Many studies have been done, using plasma immersion. Their application is limited to basic plasmas, which do not simulate the plasma in tokamaks very well.

We propose to simulate the particles influx of the plasma by means of ion beams. To achieve this goal we designed a set up in order to study the sputtering induced by ion – surface interaction. This set-up is based on the catcher method with the specificity of an "in situ" analysis by Auger spectroscopy in order to avoid problems linked to hydrocarbon pollution of the catchers during transport in air.

2. A New Experimental Set up

In the early eighties the comprehension of sputtering on fusion plasma facing materials has been pointed out as one of the main needs for the design of future plasma devices [1]. Although a lot of data has been collected [2], there are still needs for specific fields, such as the study of carbon sputtering.

We have studied sputtering by the so-called catcher method [3]. For carbon sputtering, this method should be restricted to an in situ measurement; the hydrocarbons present in air would pollute the catcher. An in situ analysis of the catcher material has already been done by means of Auger electron spectroscopy [4].

To study slow ion-induced sputtering on graphite, we propose a dedicated device, PULSAR.

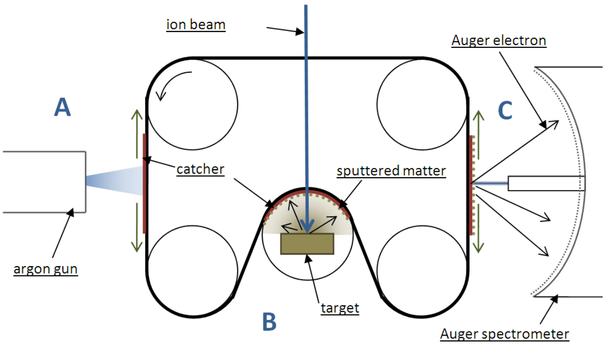

Figure 1: Schematic view of PULSAR device.

Figure 1 shows a schematic view of the PULSAR device. A catcher is fixed on a belt which is stretched by a system of pulleys. By rotating these pulleys it is possible to move the catcher in front of different areas. The first area (A) is dedicated to surface cleaning by means of sputtering. When the catcher surface is atomically clean, the target is moved to a second area (B), where the sputter experiment is performed. Then the catcher is moved to the last area (C) where it is analyzed by Auger spectroscopy.

Figure 2 shows the PULSAR device which will be used in a first sputtering experiment with low energy, low charge argon ions.

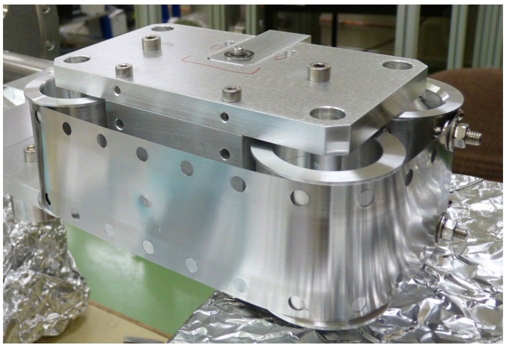

Figure 2: Picture of PULSAR device.

3. REFERENCES

[1] H. Vernickel et al., Phys. Rep., **37**, 93-110 (1978).
[2] J. Roth et al., J. Nucl. Mater., **390-391**, 1-9 (2009).
[3] F. Haranger et al., Eur. Phys. J. D, **38**, 501-506 (2006).
[4] H. Ohtsuka et al., J. Nucl. Mater., **76-77**, 188-189 (1978).

---

[*] Corresponding author e-mail address: Brigitte.Bandetat@ganil.fr

AN ULTRA-COMPACT SETUP FOR MEASURING ION-INDUCED ELECTRON EMISSION STATISTICS

D. Schrempf, W. Meissl, and F. Aumayr*

Institute of Applied Physics, TU Wien, 1040 Vienna, Austria, EU

1. INTRODUCTION

Impact of heavy particles as atoms, molecules, positive or negative ions on solid surfaces gives rise to electron emission, which is of great importance for many applications, e.g. surface and space science, sensitive particle detection/counting, plasma wall interaction, electrical discharges, etc. Particle-induced electron emission is of special relevance for the registration of extremely small particle currents, for which the statistics of the electron emission plays a crucial role. The emission statistics (ES), i.e. the probabilities W_n for emission of a given number n of electrons due to a single impact event immediately permits evaluation of the related total electron yield γ as the mean number of emitted electrons

$$\gamma \equiv \bar{n} = \sum_{n=1}^{\infty} n \cdot W_n \; ; \qquad \sum_{n=0}^{\infty} W_n = 1$$

as well as the fraction of projectiles, which do not emit at least one electron and which are therefore not registered by electron emission.

2. EXPERIMENTAL SETUP

To measure the ES distribution during ion-surface interaction usually the electrons emitted from the interaction region are extracted by a weak electric field through a highly transparent grid and accelerated onto a surface barrier type detector biased at +30 kV [1 - 6]. The n electrons emitted due to a particular ion impact will be registered like one electron of n times 30 keV rather than n individual 30 keV electrons. The number of electrons emitted in a particular ion-impact event can therefore be deduced from the detector's pulse height distribution. More details on this ES detection method and its appropriate evaluation can be found in [1 - 3] and refs. therein.

The usual setup for ES measurements involves a NIM crate with detector bias, spectroscopy amplifier and power supply operated at HV potential and a suitable data transfer from HV to ground potential. We have now designed and constructed a novel light and ultra-compact electronics replacing this heavy and bulky equipment by small and light components, which can be operated using a battery pack only. Even the pulse height analysis is now performed at high voltage and just the resulting pulse height spectrum is communicated by optical fibers to the measurement PC at ground potential. A photo and the schematics of the new electronics is shown in fig. 1.

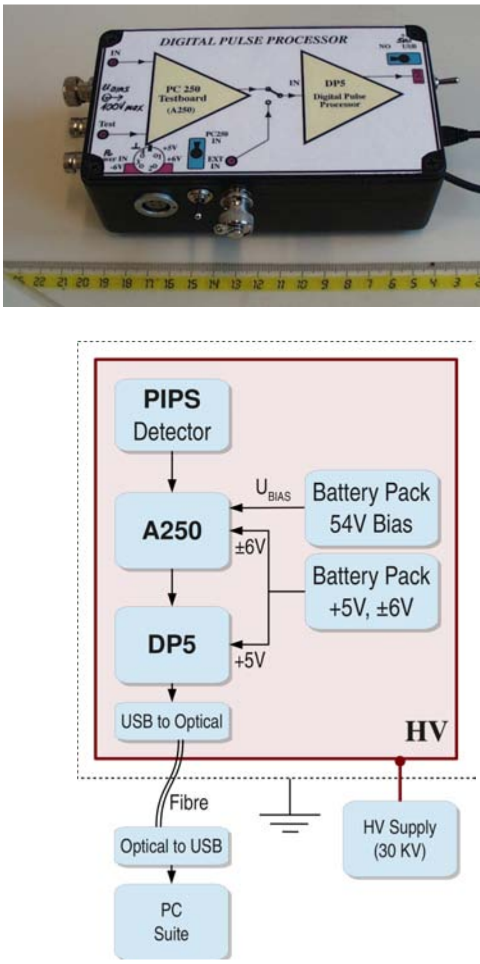

Figure 1: New ultra-compact ES detection electronics

Not only the compact design but also the low cost of the new electronics presented in this contribution, will allow other groups to easily employ the ES technique at their beam lines and use it e.g. to determine the composition of their HCI or cluster ion beams as described in [4, 6] or for basic ion-surface collision studies.

3. REFERENCES

[1] G. Lakist et al., Rev. Sci. Instrum. **60**, 3151 (1989).
[2] F. Aumayr et al., Appl. Surf. Sci. **47**, 139 (1991).
[3] F. Aumayr et al., Rev. Sci. Instrum. **64**, 3499 (1993).
[4] F. Aumayr et al., Int. J. Mass Spectr. **163**, 9L (1997).
[5] C. Lemell et al., Rev. Sci. Instrum. **70**, 1653 (1999).
[6] W. Meissl et al., Rev. Sci.I nstrum. **77**, 093303 (2006).

---

[*] Corresponding author e-mail address: aumayr@iap.tuwien.ac.at

(e, 2e) TRIPLE DIFFERENTIAL CROSS SECTIONS OF Ar AND Xe ATOMS

Prithvi Singh [*], *Vinod Patidar, and G. Purohit*

Department of Physics, School of Engineering, Sir Padampat Singhania University, Bhatewar, Udaipur-313 601, India

The charged particle impact ionization studies of fundamental atomic and molecular systems have been of great interest since the early days of quantum mechanics. Extensive theoretical and experimental investigations have been carried out to understand the electron impact single ionization (i. e. (e, 2e) processes) of various targets. [1-6]. Being able to provide the information about momentum vectors of both final state continuum electrons, the (e, 2e) processes are very important in understanding the dynamical behavior of quantum mechanical systems and also provide the stringent tests of the theoretical models.. Such type of studied is important in many areas, such as understanding the processes in the earth's upper atmosphere, in the development of new lasers and novel forms of lighting, as well as in the treatment of cancers that use radiotherapy. Accurate cross sections for Xe atom target ionization by electron impact are very important for the understanding of the complex interactions involved in the plasma process .

We will report triple –differential cross section of Ar and Xe atoms for low energy (e,2e) ionization for the incident electron energies ranging from 5 to 40 eV above the ionization threshold. The range of geometrics is from coplanar to perpendicular plane .The present investigation is done in the modified distorted wave Born approximation and it has been observed that post collision interaction and polarization of target are important in the perpendicular plane ionization of atoms. Thus we are able to see the effect of target polarization and post collision interaction in coplanar as well as the perpendicular plane geometrical condition. The result of our calculation for Ar and Xe have been compared with the very recent measurements of Nixon et al. [K. L. Nixon, A. J. Murray Physical Review A 85, 022716 (2012)].

REFERENCES

[1] I. E. McCarthy and E. Weigold, Phys. Rep. C27 (1976) 275.
[2] A. Lahmam-Bennani, J. Phys. B: At. Mol. Opt. Phys. 24 (1991) 2401.
[3] F. W. Byron Jr and C. J. Joachain, Phys. Rep. 179 (1989) 211.
[4] G. Purohit, Prithvi Singh, Vinod Patidar, Y. Azuma, and K. K. Sud1, Phys. Review A 85, 022714 (2012)
[5] W. Nakel and C. T. Whelan, Phys. Rep. 315 (1999) 409.
[6] I. Bray, Phys. Rev. Lett. 89 (2002) 273201.
[7] I. Bray, J. Phys. B 33 (2000) 581.

---

[*] Corresponding author e-mail address: prithvipurohit@gmail.com

ELECTRON EMISSION AND SURFACE ETCHING BY SLOW AND MEDIUM HIGHLY CHARGED IONS ON HOPG SURFACE

Y. Y. Wang[*], *Y. T. Zhao, J. R. Sun, R. Cheng, J. R. Ren, Y. Yu, X. M. Zhou, Y. Lei, X. Wang, Y. F. Li, G. Q. Xiao*

Institute of Modern Physics, Chinese Academy of Sciences, Lanzhou 730000, China

1. INTRODUCTION

Impact of ions on solid surfaces is of genuine interest in plasma- and surface physics and related applications, like electrical discharges, plasma–wall interaction in controlled thermonuclear fusion devices, surface analysis and single-particle detection. Highly charged ions carry several tens of keV potential energy. Most of the potential energy is deposited within a few nm of first few atomic layers of the surface on the fs time scale, effective energy deposition rates can exceed about 10^{14}W/cm^2. How the potential energy is deposited into the surface and the respond of the surface are the most considerable topics in recent years. Secondary electron emission and surface modification in the interaction of slow ($v < v_{\mathrm{Bohr}}$) and medium ($v \sim v_{\mathrm{Bohr}}$) highly charged ions with surfaces are dominated by the deposition of potential energy of the ions. Studying both theoretically and experimentally the correlated electron emission from a single dot would be of considerable interest, both for the understanding of nanostructure formation and for diagnostic purposes [1, 2].

2. EXPERIMENT AND RESULTS

2.1. Experiment

Experiments on electron emssion and surface nanostructure formation have been carried out at No.1 physics experimental terminal by using ion beams extracted from the 320 kV ECR platform in the Institute of Modern Physics, Lanzhou. Xenon ions with different charge states and incident energies were selected to study the combination of electron emission and surface nanostructuring formation.

2.2. Results

Total secondary electron yield of a HOPG target induced by highly charged xenon ion (^{129}Xe^{q+}, q=10-30) was measured and contributions of potential electron emission and kinetic electron emission yields were obtained. The potential electron yield is proportional to the potential energy of the ion [3]. In addition, surface nanostructures created by individual ions were investigated by AFM. The results show that high potential energy of the incident ions is responsible for the observed hillock-like nanostructures. However, the sizes of nanostructures are independent with incident kinetic energy, see Fig.1. Our results indicate that only about 8% potential energy of the highly charged ions is utilized in potential electron emission and rest of its potential energy is most probably deposited in first few monolayer of the target that produce etching.

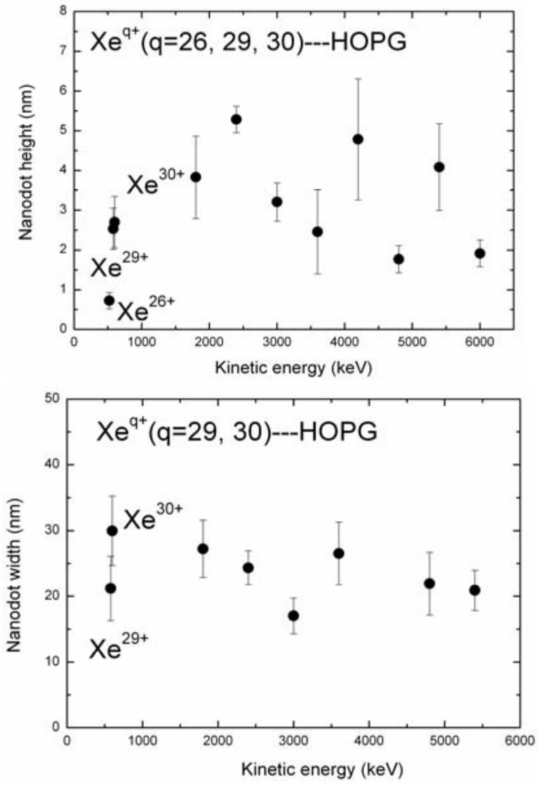

Figure 1: The height and width of nanostructures on HOPG created by xenon ion as a function of incident kinetic energy.

3. REFERENCES

[1] F. Aumayr and HP. Winter, in Slow Heavy-Particle Induced Electron Emission, edited by HP. Winter and J. Burgdoerfer, Chapter 3, pp 79-112, Springer tracks in modern physics, 2007.
[2] F. Aumayr, HP. Winter, Nuclear Inst. and Methods in Physics Research, B 233, 111(2005).
[3] Y. Y. Wang, et al., Nucl. Instr. and Meth. B 269, 977 (2011) and 265, 474 (2007).

---

[*] Corresponding author e-mail address: wangyuyu@impcas.ac.cn

Wednesday 19 September 2012

NITROGEN INTERACTIONS AT METAL SURFACES

A.W. Kleyn

FOM Institute DIFFER - Dutch Institute for Fundamental Energy Research
Postbox 1207, 3430 BE Nieuwegein, The Netherlands
and
Van 't Hoff Institute for Molecular Sciences, Faculty of Science, University of Amsterdam, The Netherlands

Molecular beam experiments with specially prepared beams allow the study of the interaction of very reactive species and surfaces. In the present case the interaction of N-atoms is studied. The energy of the atoms is around 5 eV, precisely between the classical energy regimes of seeded molecular beams and low energy ion scattering. In this work questions will be addressed as:

- Can N-atoms lead to a passive layer, that is not reactive to N-atoms?
- Can N-atoms remove N-atoms in an Eley-Rideal reaction?
- Does the electronic state of the atoms matter?
- Can the interaction already be described by state-of-time art theory?

The methods used will be introduced with examples of fast, 5 eV Ar scattering from Ru(0001) and Ag(111).

Subsequently, the interaction of N-atoms with the same surfaces will be discussed in order to address the questions listed above. Some work with reactive N_2 will be shown. Here it is remarkable that the usually very inert N_2 molecules become reactive at energies of 5 eV.

The systems studied experimentally can also be investigated theoretically by DFT and molecular dynamics methods. Comparisons between theory and experiment will be shown. The work to be discussed is also very relevant for several applications, that will be summarized briefly.

---

* Corresponding author e-mail address: A.W.Kleijn@uva.nl

MULTIFRAGMENTATION MODES IN CLUSTER-SURFACE COLLISIONS: EXPERIMENT AND SIMULATIONS

*E. Kolodney**

Schulich Faculty of Chemistry , Technion-Israel Institute of Technology, Haifa 32000 , ISRAEL

1. INTRODUCTION

When a large molecule or cluster is impacting a solid target at kinetic energies in the range of 100-1000 eV , it experiences a strong deformation which eventually leads to a variety of fragmentation phenomena , manifested by the abundances pattern of the outgoing fragments ,their kinetic energy distributions and angle distributions . Up to a certain impact energy and vibrational excitation (well below its total cohesion energy) the energized cluster is assumed to recoil intact and undergo a statistical unimolecular delayed emission of its subunits. At higher impact and internal energies, multifragmentation (multiparticle break-up) dynamics will start to dominate, eventually reaching complete disintegration of the system into its smallest units (the shattering limit). We have studied different intermediate multifragmentation modes by scattering C_{60}^{-} ions from surfaces (gold and nickel) at a few hundreds of eV impact energies . The results were in good agreement with model calculations based on the emission of fragments from a superhot outgoing precursor. Microscopic insight into the nature of the new, velocity correlated multifragmentation process was obtained by molecular dynamics (MD) calculations.

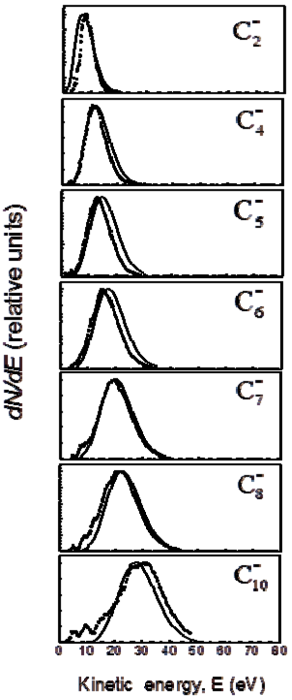

Fig.1. Kinetic energy distributions of outgoing C_n^- fragments (experiment and model calculations). (600 eV C_{60}^- impact on nickel).

2. RESULTS AND DISCUSSION

By analyzing kinetic energy and angle distributions of outgoing C_n^- (n=2-15) fragments for different incidence angles and impact energies we have observed multifragmentation events which occur at the surface ("during-collision') and events which occur away from the surface ("post-collision") [1,2]. Also positively charged fragments were measured and analyzed [3]. The post-collision multifragmentation results in velocity correlated emission of all outgoing fragments and gradual narrowing of incidence angle dependences of the C_n^- fragment yield as a function of the fragment size *n.* A predicted $1/\sqrt{n}$ narrowing law is found to be in good agreement with the experimental results [2]. Molecular dynamics (MD) simulations will also be reported, providing deeper understanding into the details of the post-collision multifragmentation event [4]. Finally, we will present results related with the collisional formation of the larger C_{60-2n}^{+} (n=1-5) ionic cage fragments [5].

REFERENCES

[1] A. Kaplan, A. Bekkerman, B. Tsipinyuk and E.Kolodney , Phys. Rev. B 79, 233405 (2009).

[2] A. Kaplan, A. Bekkerman, B. Tsipinyuk and E. Kolodney , Phys. Rev. B 82, 245421, (2010).

[3] M.Fleischer , V.Bernstein , O.Glozman ,B.Tsipinyuk A. Bekkerman and E.Kolodney , Nuclear Instr. And Meth. B, 269 , 919 (2011).

[4] V. Bernstein and E. Kolodney ,submitted

[5] M.Fleischer, A. Bekkerman, B.Tsipinyuk and E.Kolodney, Phys. Rev. B 85 , 165407 (2012).

---

* Corresponding author e-mail address: eliko@tx.technion.ac.il

EFFECTS OF CHEMISTRY IN C_{60} BOMBARDMENT OF Si

K. D. Krantzman[*] *C. A. Briner* and Barbara J. Garrison*[§]

[*]Department of Chemistry and Biochemistry, College of Charleston, Charleston, SC 29424, USA
[§]Department of Chemistry, The Pennsylvania University, University Park, PA 16802, USA

1. INTRODUCTION

Molecular depth profiling with cluster secondary ion mass spectrometry (SIMS) has become a state-of-the-art analytical technique for characterizing organic and biological solids. C_{60}^{+} is one of the commonly used ion beam sources because of its commercial availability, high sputtering yield and minimal damage to the surface. However, some experiments have shown damage to the sample that appears to be the result of the chemical reactivity of the carbon atom in the C_{60}^{+} projectile and the cumulative results of chemical effects are not well understood.

Previous molecular dynamics (MD) simulations of single impacts of C_{60} on a Si surface demonstrate that strong bonds are formed between projectile C atoms and substrate Si atoms, which lead to nearly all of the atoms from the projectile being incorporated into the surface [1]. Recently, a "divide and conquer" scheme has been developed by Russo, Postawa and Garrison [2] to treat successive bombardment. In this paper, the results of multiple-impacts of 20-keV C_{60} at normal incidence on a single Si microcrystallite are presented.

2. MD SIMULATIONS

The Si sample is successively bombarded by 20-keV C_{60} projectiles at normal incidence on a set of 550 impact points chosen randomly over the entire surface of the large master Si crystal. The trajectory for each impact point is run using a smaller cylindrical sample extracted from the master crystal and then reinserted after the trajectory is complete. An empirical many body potential developed by Tersoff [3] is used to model the Si-Si, Si-C and C-C interactions. Specific details about the simulations are described in a previous paper [4]. The effects of increasing carbon content as a result of successive impacts of Si with C_{60} are investigated.

3. RESULTS

Simulations with 550 successive impacts, corresponding to a fluence of 9.69 10^{13} impacts/cm^{2}, have been performed. As more carbon atoms are incorporated into the solid, the relative contribution of carbon atoms to the sputtered species increases and the sputtering rate of Si decreases as that of C increases. The sputtering rate of the total number of substrate atoms still shows a linear dependence on fluence in this fluence regime. Surface topography develops as a result of successive bombardment. The average surface height decreases by 2.5 nm after 550 impacts. The root mean square roughness reaches a steady state value of about 2 nm after 100 impacts, corresponding to a fluence of 1.76 10^{13} impacts/cm^{2}. The average carbon concentration is defined as a weighted percent carbon average, in which the percentage of carbon in the surface as a function of height is weighted by the probability of an atom being sputtered with this height. It is found that the partial sputter yield of carbon from the simulations is directly proportional to the average carbon concentration on the surface.

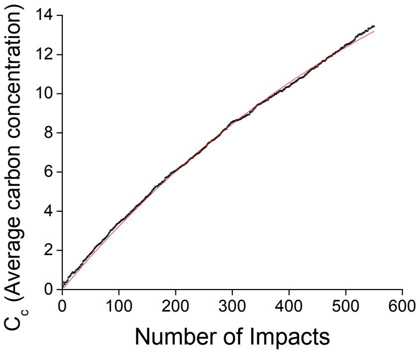

Figure 1: Average carbon concentration, calculated as the weighted percent carbon average, plotted as a function of the number of impacts. The red curve represents a functional fit to the data from the simulations.

In Fig. 1, the average carbon concentration is plotted as a function of the number of impacts. A function of the form $C_C = a\left(1-e^{-bN}\right)$ is fit to the curve and the values for the parameters *a* and *b* are determined to be 24 and 0.0144. From this data, we predict that the percent carbon concentration will reach a steady state value of 24 % and it will take 1600 impacts (2.9 10^{14}impacts/cm^{2}) to reach a concentration equal to 90 % of the steady state value.

4. REFERENCES

[1] K.D. Krantzman, D. Kingsbury, B.J. Garrison, App. Surf. Sci. **252**, 6463 (2006**).**
[2] M. F. Russo, Jr., Z. Postawa, B.J. Garrison, J. Phys. Chem. C **113**, 3270 (2009).
[3] J. Tersoff, Phys. Rev. B **39**, 5566 (1989).
[4] K.D. Krantzman, A. Wucher, J. Phys. Chem. C **114**, 5480 (2010).

---

[*] Corresponding author e-mail address: krantzmank@cofc.edu

Sputtering of fusion relevant surfaces by seeding impurities

K. Dobes[1,*], *J. Pyszkowski*[1], *T. Schäfer*[1] *and F. Aumayr*[1]

[1] Institute of Applied Physics, TU Wien, Association EURATOM-ÖAW, Vienna Austria, EU

1. INTRODUCTION

The interaction of a fusion plasma with the walls of its containing vessel will constitute one of the key challenges in the successful realization of a future fusion power plant. A profound knowledge about sputtering yields of plasma facing components under the impact of fusion relevant ion species is hence desired. Besides the evolution of plasma facing materials like tungsten, beryllium and possibly also carbon in the environment of a burning fusion plasma and especially the mixing of materials is of considerable interest. In addition also the retention of hydrogen isotopes in plasma facing components is of major concern. Particularly the build-up of a tritium inventory within the plasma vessel imposes operational limits due to safety considerations.

ASDEX Upgrade was the first fusion machine to operate with a full tungsten wall [1]. Also in future fusion devices like ITER tungsten is foreseen as a divertor target [2]. In order to reduce the power load to the divertor target plates to acceptable values, radiation cooling is essential [3]. Especially in all-metal fusion machines, where no carbon is present in the vessel, radiation due to intrinsic impurities is no longer sufficient and has to be replaced by seeding of additional impurities [3]. At ASDEX Upgrade nitrogen seeding with feedback control has meanwhile matured into a standard operational scenario [1]. Using nitrogen, the divertor target power flux could be mitigated by high radiation to a technically acceptable level, and the performance of the plasma was even increased compared to discharges without impurity seeding [1]. At ITER heavier seeding impurities like Ne and Ar will be necessary and used for radiative cooling. It is hence of considerable interest to study the interaction of different seed impurity ions (N^+, N_2^+, Ne^+, Ar^+) with tungsten and other fusion relevant surfaces.

2. EXPERIMENT & RESULTS

In our studies we are using a quartz crystal microbalance (QCM) technique [4 - 7] that has been designed at Vienna University of Technology. The experimental technique has been optimized for extreme high sensitivity and accuracy. It is capable of determining mass changes of as small as 2 amu/ion·nA/mm^2 or accordingly $3 \cdot 10^{-4}$ tungsten monolayers per second. Total sputtering yields for N^+, N_2^+, Ne^+ and Ar^{q+} ions on tungsten have been investigated under controlled laboratory conditions. The high sensitivity of our QCM [7] allows us to study the change in surface composition during seed impurity impact and its influence on the sputtering yield in-situ and in real-time. The code TRIDYN [8], which takes into account a change of the surface under ion impact due to implantation and erosion, is used to model and better understand the investigated sputtering phenomena.

We will present the flux dependence of tungsten erosion by different seed impurity ions at fusion relevant impact energies. In addition sputtering of tungsten-nitride surfaces, which are formed as a result of high flux nitrogen bombardment of tungsten [9], were investigated. Furthermore a comparison of sputtering yields under the impact of singly and multiply charged ions at the same impact velocities will be presented and discussed.

3. ACKNOWLEDGEMENT

This work, supported by the European Commission under the Contract of Association between EURATOM and the Austrian Academy of Sciences, was carried out within the framework of the European Fusion Development Agreement. The views and opinions expressed herein do not necessarily reflect those of the European Commission.

4. REFERENCES

[1] A. Kallenbach et al., Plasma Phys. Control. Fusion **52**, 055002 (2010).
[2] A. Loarte et al., Nucl. Fusion **47**, S203 (2007).
[3] J. Rapp et al., J. Nucl. Mat. **337 – 339**, 826 (2005).
[4] G. Hayderer et al., Rev. Sci. Instrum. **70**, 3696 (1999).
[5] G. Hayderer et al., Phys. Rev. Lett. **83**, 3948 (1999).
[6] A. Golczewski et al., Nucl. Instr. And Meth. B **267**, 695 (2009)
[7] K. Dobes et al. Phys. Scr. **2011**, 014017 (2011).
[8] W. Möller, W. Eckstein and J.P. Biersack, Comp. Phys. Commun. **51**, 355 (1988).
[9] K. Schmid et al., Nucl. Fusion **50**, 2 (2010).

---

[*] Corresponding author e-mail address: dobes@iap.tuwien.ac.at

COLLISIONS OF SEEDING GAS IONS Ar^+ AND N_2^+ WITH TUNGSTEN AND BERYLLIUM SURFACES

A. Keim[1,*], *M. Harnisch*[1], *P. Scheier*[1], *and Z. Herman*[2]

[1] Institute for Ion Physics and Applied Physics, University of Innsbruck, Technikerstraße 25b, 6020 Innsbruck, Austria
[2] J. Heyrovský Institute of Physical Chemistry, Academy of Sciences of the Czech Republic, Dolejškova 3,
18223 Prague 8, Czech Republic

1. INTRODUCTION

Research and development of feasible fusion reactors require reliable fundamental data quantifying plasma-wall interactions. Modeling and computational science for the pioneering project ITER depend on the determination of erosion and deposition coefficients of the involved plasma projectiles on the materials of choice: beryllium, tungsten and carbon, in the form of carbon fibre composite (CFC). Ion-surface collisions are a useful means to investigate the processes which occur in plasma-wall interactions. Recently the attention of material studies in fusion science has shifted from interactions of hydrocarbon projectiles [1] to those of seeding gas ions, namely N_2^+ and Ar^+.

2. EXPERIMENTAL SETUP

The experimental setup BESTOF in Innsbruck is described in large detail in previous publications [2]. It consists of two mass spectrometers arranged in tandem geometry (Fig. 1).

Ions are produced in a Nier-type electron ionization ion source and extracted into the first mass analyzer, a reverse-geometry two-sector-field mass spectrometer. The m/z-selected beam of projectile ions (N_2^+ or Ar^+) is then directed onto the target surface (Be or W) at well-defined incident energies in the range of 10-100eV and at an angle of 45° with respect to the surface normal.

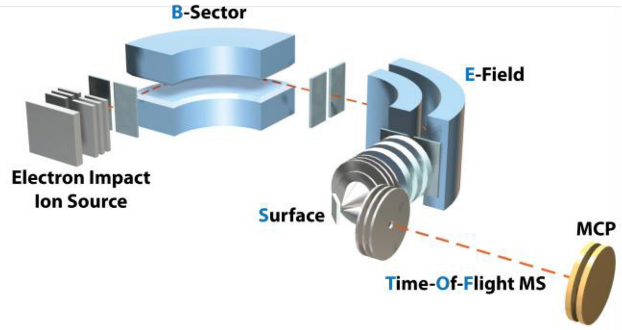

Figure 1: Experimental setup BESTOF: an m/z-selected ion beam interacts with a surface, the product ions are detected by a TOF mass spectrometer.

Product ions formed on impact are analyzed in a linear time-of-flight mass spectrometer positioned at a total scattering angle of 90°.

In order to simulate more realistic fusion reactor conditions and to investigate the dependence of product ion signals on surface temperature, the surface samples can be heated up to 600°C.

3. RESULTS

For all combinations of the two projectiles with the two surfaces we present collision energy resolved mass spectra showing relative ion intensities of product ions as a function of incident energy at different surface temperatures.

3.1. Interactions with a tungsten surface

In case of the tungsten surface kept at room temperature, the main product ions for both projectiles investigated can be attributed to hydrocarbons adsorbed on the surface. Furthermore we witness notable contributions from oxygen-containing compounds originating from the oxides on the tungsten surface.

For elevated surface temperatures we observe the well-known decrease in ion intensities of both these components [3].

3.2. Interactions with a beryllium surface

Ion-surface interactions for both projectiles with beryllium show similar product ions as in the tungsten case. The relative intensities of the peaks, however, change. In addition we observe sputtering products Be^+, BeH^+, Be_2H^+, CH_3Be^+ and $BeHO^+$ even at incident energies as low as 15eV.

For all surfaces we observe substantial contributions from alkali metal ions Na^+ and K^+ when heating the surface.

4. REFERENCES

[1] A. Keim, B. Rasul, N. Endstrasser, P. Scheier, T.D. Märk, Z. Herman, IJMS **306**, 204-209 (2011).
[2] C. Mair, T. Fiegele, F. Biasioli, Z. Herman, T. D. Märk, J. Chem. Phys. **111**, 2770 (1999).
[3] J. Roithova, J. Žabka, Z. Dolejšek, Z. Herman, J. Phys. Chem. B **106**, 8293 (2002).

---

[*] Corresponding author e-mail address: alan.keim@uibk.ac.at

DEPTH RESOLUTION OF NUCLEAR REACTION ANALYSIS OF BURIED HYDROGEN-CONTAINING LAYERS

S. Bielesch[1], M. Oberkofler[1,*], H. Maier[1], H.-W. Becker[2], D. Rogalla[2] and Ch. Linsmeier[1]

[1] Max-Planck-Institut für Plasmaphysik, EURATOM Association, 85748 Garching b. München, Germany
[2] Dynamitron Tandem Labor des RUBION, Ruhr-Universität Bochum, 44780 Bochum, Germany

1. ABSTRACT

In many areas of research, hydrogen in metals plays an important role. One of the most common possibilities of detecting hydrogen is the ion beam analysis. Many of these experiments show that the depth resolution deteriorates with increasing depth, due to geometrical and electronic straggling. Therefore, it is necessary to find a way to calculate this deterioration. With increasing depths, the electronic straggling plays the most important role. The contribution of the electronic straggling can be calculated by using the Bohr formula (1) [1], which depends on the atomic density or thickness (Δx [10^{18} at/cm^2]) and the atomic numbers of the incoming (Z_1) and the target element (Z_2). To investigate the influence of the atomic number on the depth resolution, a light (Ti) and a heavy element (W) are compared.

$$\sigma_{\mathrm{Bohr}}[\mathrm{keV}] = \sqrt{0.26 \cdot \mathrm{Z_1}^2 \cdot \mathrm{Z_2} \cdot \Delta \mathrm{x}} \qquad (1)$$

The two investigated nuclear reactions are shown in (2) and (3). They are chosen because they can detect hydrogen and deuterium. Their large cross sections provide high sensitivity.

$$^{2}\mathrm{D}(^{3}\mathrm{He}, {}^{1}\mathrm{H})^{4}\mathrm{He} \qquad (2)$$

$$^{1}\mathrm{H}(^{15}\mathrm{N}, {}^{4}\mathrm{He}, \gamma)^{12}\mathrm{C} \qquad (3)$$

In this work we show how the depth resolution of nuclear reaction analysis measurements changes with increasing depth. As test samples thin (10 nm) deuterium (a:C-D) or hydrogen (a:C-H) containig carbon layers are produced. The thickness of 10 nm is chosen since it is below the depth resolution and therefore can be considered as a delta function layer.

To assess the depth resolution of reaction (2), the a:C-D layers are covered with tungsten and titanium of various thicknesses between 500 nm and 8 μm. The samples are then analyzed using different ^{3}He energies at the 3 MV tandem accelerator at the IPP in Garching. In reaction (2), the resonance is very wide and the cross section in the resonance area is only one order of magnitude larger than off resonance [2]. Because of the large non-resonant contributions it is impossible to determine the depth profile through shifting the resonance to greater depths, by increasing the beam energy. Due to the overlap in depth of the measurements at different energies, it is necessary to optimize the primary energies for a given number of measurements. These calculations are performed with the program "'experimental design"[3]. The deconvolution of the measured spectra is done with the program NRADC [4]. At first this program performs a forward calculation by linearization and creates a design matrix with SimNRA [1]. To extract the depth profile from this matrix it is necessary to deconvolute it. NRADC uses Bayesian statistics to determine the most probable profile.

For analyzing the depth resolution of reaction (3), a:C-H layers of different thicknesses are produced and then measured at the RUBION in Bochum. The reaction (3) has a very narrow resonance width and the cross section at the on- and off- resonance regions differ by orders of four magnitudes [5]. Therefore it is sufficient to vary the beam energy to get a depth profile, since every beam energy probes exactly one depth.

The measurements show as expected, that the depth resolution is getting worse with increasing thickness of the coating. They also show, that the depth resolution of different elements deteriorates with increasing atomic number. From the measurements performed with the different sets of reference samples a quantitative determination of the depth resolution at different depth is possible.

2. REFERENCES

[1] M. Mayer, SIMNRA Users Guide, Report IPP 9/113, Max-Planck-Institut für Plasmaphysik, Garching, Germany, 1997. <http://www.rzg.mpg.de/∼mam/, mailto:matej.mayer@ipp.mpg.de>

[2] V.Kh. Alimov, M. Mayer, J. Roth, Nucl. Instrum. Meth. B 234 (2005) 169

[3] U. von Toussaint, T. Schwarz-Selinger, M. Mayer and S. Gori, Nucl. Instrum. Meth. B 268 (2010) 2115

[4] K. Schmid and U. von Toussaint, Nucl. Instrum. Meth. B 281 (2012) 64

[5] W.A. Lanford, Nucl. Instrum. Meth. B 66 (1992) 65

---

*Corresponding author e-mail address: martin.oberkofler@ipp.mpg.de

RADIOLYSIS OF ASTROPHYSICAL ICES BY ENERGETIC HEAVY IONS (COSMIC RAYS)

Ph. Boduch[1], *A. Domaracka*[1], *X. Lv*[1], *H. Rothard*[1,*], *E. Dartois*[2], *D. Andrade*[3], *A.L.F. de Barros*[4], *V. Bordalo*[5], *S. Pilling*[3], *E. Seperuelo-Duarte*[6], *E.F. da Silveira*[5], *M.E. Palumbo*[7], *G. Strazzulla*[7]

[1]Centre de Recherche sur les Ions, les Matériaux et la Photonique (CEA/CNRS/ ENSICAEN/Université de Caen-Basse Normandie), UMR 6252 CIMAP-CIRIL-Ganil, Boulevard Henri Becquerel, BP 5133, 14070 Caen Cedex 05, France.
[2]Institut d'Astrophysique Spatiale, Astrochimie Expérimentale, UMR-8617 Université Paris-Sud, bâtiment 121, 91405 Orsay, France.
[3]Universidade do Vale do Paraíba (UNIVAP), Instituto de Pesquisa e Desenvolvimento (IP&D), São José dos Campos, SP, Brazil.
[4]Departamento de Disciplinas Básicas e Gerais, CEFET-RJ, Av. Maracanã 229, 20271-110 Rio de Janeiro, RJ,Brazil.
[5]Departamento de Fiısica, Pontifícia Universidade Católica do Rio de Janeiro, Rua Marquês de São Vicente 225, 22451-900, Rio de Janeiro, RJ, Brazil.
[6]Grupo de Física e Astronomia, CEFET/Química de Nilópolis, 2653-060 Nilópolis, RJ, Brazil.
[7]INAF-Osservatorio Astrofisico di Catania, 95123 Catania, Italy.

1. INTRODUCTION AND EXPERIMENT

In the solar system and in dense regions of the interstellar medium, icy layers (e.g. grain mantles) formed from a mixture of small molecules are exposed to ionizing irradiation (UV photons, electrons, ions). The interaction of radiation with the ices induces several physic-chemical processes (fragmentation/radiolysis, followed by chemical reactions and formation of new molecules; structural/phase changes; desorption/sputtering of molecules from the surface).

The experiments were performed with thin layers (microns) layers formed from condensed gases on a CsI window at 15K (interstellar medium) and 80K (solar system), which allowed to measure infrared absorption spectra (FTIR) before and after irradiation with ions at different fluences.

2. RADIOLYSIS AND SPUTTERING

Although protons and helium are several orders of magnitudes more abundant in the cosmic ray spectrum than heavy ions, the high electronic energy loss of heavy ions can compensate for the lower flux and yield to non-negligible contributions of heavy ion induced physico-chemistry. In particular, we observed a strong non-linear increase of sputtering yields Y with deposited energy $Y \sim S_e^{\,2}$ in CO and CO_2 ices bombarded with Ni ions of different energies. [1,2]. This clearly shows that the contribution of heavy ion induced desorption from grains must be taken into account for understanding the presence of gas phase molecules in dense interstellar clouds.

Another interesting result related to the specificities of the strong electronic energy deposition by heavy ions concerns ion bombardment of frozen Methanol CH_3OH. Its destruction cross sections by fast heavy ion irradiation (Zn and Kr beams) were found to be considerably larger than those for lighter ions (O, He or H beams) [3]. As a scaling law, we found that destruction cross sections σ increase with the electronic stopping power roughly as $\sigma \sim S_e^{\,3/2}$.

The laboratory experiments allow studying the production of oxidants such as hydrogen peroxide and ozone on icy moons by ion bombardment [4]. The formation of organic compounds seems to be favored at lower temperature [5]. Finally, in the case of H_2O-CO-NH_3 mixed ices irradiated with swift heavy ions, we have observed strong indications for the formation of glycine, the simplest proteinaceous amino acid, considered as pre-biotic molecule in the infrared absorption spectra of the residues (after thermal desorption of volatile small molecules) [6].

3. REFERENCES

[1] E. Seperuelo Duarte, P. Boduch, H. Rothard, T. Been, E. Dartois, L. S.Farenzena, E.F. da Silveira, Astronomy & Astrophysics **502**, 599 (2009).

[2] E. Seperuelo Duarte, A. Domaracka, P. Boduch, H. Rothard, E. Dartois, E. F. da Silveira, Astronomy & Astrophysics **512**, A71 (2010).

[3] A. L. F. de Barros, A. Domaracka, D.P.P. Andrade, P. Boduch, H. Rothard, E. F. da Silveira, Monthly Notices of the Royal Astronomical Society **418**, 1363 (2011).

[4] P. Boduch, E. F. da Silveira, A. Domaracka, O. Gomis, X.Y. Lv, M. E. Palumbo, S. Pilling, H. Rothard, E. Seperuelo Duarte, G. Strazzulla, Advances in Astronomy, Article ID 32764, Volume 2011.

[5] S. Pilling, E. Seperuelo Duarte, A. Domaracka, H. Rothard, P. Boduch, E. F. da Silveira, Phys. Chem. Chem. Phys. **13**, 15755 (2011).

[6] S. Pilling, E. Seperuelo Duarte, E. F. da Silveira, E. Balanzat, H. Rothard, A. Domaracka, P. Boduch, Astronomy & Astrophysics **509**, A87 (2010).

---

[*] Corresponding author e-mail address: rothard@ganil.fr

Thursday
20 September 2012

ION-SURFACE INTERACTION PROCESSES AND THEIR IMPLICATIONS FOR FUSION DEVICES

K. Krieger[1,2,*] *and JET EFDA contributors*[1,+]

[1] JET-EFDA, Culham Science Centre, OX14 3DB, Abingdon, UK
[2] Max-Planck-Institut für Plasmaphysik, EURATOM Association, Garching, Germany
[+] See App. of F. Romanelli et al., Proc. of the 23rd IAEA Fusion Energy Conf. 2010, Daejeon, Korea.

In a nuclear fusion device with magnetic plasma confinement both energy and particles from the plasma must be extracted through the walls of the reaction vessel to meet the requirements of energy exhaust, fuel recirculation and ash removal. Plasma-wall interactions (PWI) are therefore of fundamental importance for design and operation of such devices. These interactions are to a large extent determined by the properties of ion-surface processes at the interface of plasma and plasma exposed "first wall": The bombardment of the first wall by plasma ions (and neutral atoms) leads to sputtering of wall material and at the same time to retention of implanted fuel species in the first wall.

In the plasma the eroded material leads to increased power loss by line radiation, which is undesirable particularly in the confined plasma. At the plasma boundary, however, radiation losses might even be required to spread heat exhaust over large areas. To this end, suitable impurity species can be seeded but will, like the intrinsic wall impurity ions, eventually end up at the first wall at locations, which may be far from their source.

At the plasma exposed material surface one will find, depending on material migration paths and local plasma conditions, areas with net erosion and net deposition respectively. In erosion dominated areas, sputtering and chemical erosion rates ultimately determine the life time of the corresponding plasma facing components. In deposition dominated areas, material mixing will occur if the affected area is made of a different element than the incident species. The mixed materials will suffer from degraded thermo-mechanical properties and detrimentally affect fuel retention and release rates. Ultimately, the on-going deposition results in formation of material layers. Fuel (i.e. deuterium+tritium) retention by co-deposition in these layers can, depending on the material, significantly contribute to the growth rate of the fuel inventory bound in the vessel, which must not exceed a certain T-level imposed by radiation safety requirements.

Component life time, tritium retention and material mixing have become key issues of fusion research with the advent of ITER, which will be the first device with a burning fusion plasma. In ITER the main chamber first wall will be made of beryllium for optimal plasma compatibility while the divertor where particle and heat exhaust are concentrated will be made of tungsten. The plasma wall interaction properties of this configuration are currently studied at JET, which for this purpose has been equipped with an "ITER-Like Wall" (ILW) [1].

The first ILW campaign already provided important new results on ITER relevant PWI key issues. Based on studies of co-deposition with Be and carbon in linear plasma devices it was predicted that replacement of C walls by a Be/W wall would significantly reduce T-retention [2]. The experiment confirmed the prediction [3] and also demonstrated the continuous decrease of residual carbon after switching from the carbon dominated JET wall to the ILW configuration [4]. The unique opportunity of starting with well-defined initial conditions of clean Be and W wall areas was used to study both material migration and the resulting evolution of plasma facing surfaces by mixing processes. It turned out that significant Be migration occurs already during limiter discharge phases, which had previously been neglected in predictive modelling for ITER [5]. The erosion of tungsten, which is mainly caused by light impurities could for the first time be studied with the ITER relevant combination of Be and seeded nitrogen as main sputtering species [6,7].

REFERENCES

[1] G. F. Matthews et al., Phys. Scr. **T145**, 014001 (2011), doi:10.1088/0031-8949/2011/T145/014001.
[2] J. Roth et al., J. Nucl. Mat. **390–391** (2009) 1–9.
[3] T. Loarer et al., PSI-20 Aachen (2012), submitted to J. Nucl. Mat.
[4] S. Brezinsek et al., PSI-20 Aachen (2012), submitted to J. Nucl. Mat.
[5] K. Krieger et al., PSI-20 Aachen (2012), submitted to J. Nucl. Mat.
[6] G. van Rooij et al., PSI-20 Aachen (2012), submitted to J. Nucl. Mat.
[7] M. Oberkofler et al., PSI-20 Aachen (2012), submitted to J. Nucl. Mat.

---

[*] Corresponding author e-mail address: krieger@ipp.mpg.de

Synergistic effect during simultaneous steady-state and transient plasma loads

G. De Temmerman[1,*], H.Y. Xu[2], T.W. Morgan[1], B.J. Hensen[1], J.J. Zielinski[1]

[1] FOM Institute DIFFER, Dutch Institute For Fundamental Energy Research, Ass. EURATOM-FOM, Trilateral Euregio Clusters, PO Box 1207, 3430BE Nieuwegein, The Netherlands
[2] Department of Material Science and Engineering, Tsinghua University, Beijing 100084, China

1. Introduction

The interaction of energetic particles with solid surfaces is at the core of numerous applications such as thin film deposition or materials processing. Ion-beam processing, for example, allows nanostructure formation on metal and semiconductor surfaces, while reactive ions can be used to chemically modify surfaces during nitriding for example. Those processes usually involve ions with energies above 100eV where ion-induced damage creation and physical sputtering are expected, and are relatively well documented. In a fusion reactor, at locations where the plasma intersects with the solid surfaces, plasma-facing surfaces are bombarded by extreme particle fluxes (up to 10^{24}m^{-2}s^{-1} or 1.6x10^{5}A.m^{-2}), albeit with energies below 50eV. While the ion energy is below the damage threshold for the incoming ions, the particle flux is high enough to cause a local supersaturation of mobile gas particles within the implantation zone and strong surface morphology changes as a result of cluster/bubble growth. In addition to being bombarded by a high flux continuous plasma, plasma instabilities mean that the surface will also be subjected to repetitive high transient heat and particle fluxes. In order to study how the superimposition of those effects would affect the response of a metal surface, a new experimental setup has been developed.

2. Magnetized pulsed arc discharge

The setup is based on the Pilot-PSI linear device, which produces plasma parameters relevant to the study of steady-state plasma-surface interactions in the ITER divertor. The plasma source has been modified to allow for transient heat and particle pulses superimposed on the steady-state plasma . Peak surface heat fluxes of up to 1 GW.m^{-2} have been generated with pulse duration of about 1 ms (up to 1MJ.m^{-2}). To provide more flexibility, the shape and the duration of the pulse can be adapted to the needs. In addition, a pulsed bias system has been developed to vary the ion energy during the pulse. Importantly, the steady-state and pulsed plasma conditions can be varied independently. The pulsed plasma properties have been studied using Thomson scattering, fast visible and infrared imaging for H, He and Ar operations. In addition, a high power laser (LASAG FLS 352N-302) with variable pulse duration is used to disentangle the effect of the increased particle flux during a pulse on the surface response.

3. Overview of the main results

Repeat pulsing using the combined system at Pilot-PSI on polycrystalline tungsten targets shows significant release of tungsten at lower energy density thresholds (7 MW m^{-2} s$^{1/2}$) than for cracking from repeat electron beam pulsing at JUDITH (~9 MW m^{-2} s$^{1/2}$), laser ablation experiments with pre-bombarded targets (12 MW m^{-2} s$^{1/2}$) and the cracking threshold for quasi-stationary plasma accelerators (15 MW m^{-2} s$^{1/2}$). The surface also shows roughening and cracking when exposed to the combination of steady state and low energy transient pulses compared to an absence of morphology changes for a steady state-only exposed reference sample.

Laser ablation studies in combination with steady state plasmas stress the role of steady-state plasma exposure on the material behaviour during transients. Experiments were performed with successive and simultaneous plasma and laser irradiation to identify the role of mobile gas particles on the surface response to the transient heat load. The most drastic effects are found during simultaneous exposures where the surface roughening and cracking is significantly enhanced.

These results indicate that synergistic effects can produce a significant enhancement of plasma-induced material modifications.

---

[*] Corresponding author e-mail address: g.c.detemmerman@differ.nl

TEM OBSERVATIONS OF RADIATION DAMAGE IN SELF-IRRADIATED TUNGSTEN

Ł.Ciupiński[1*], *O.V.Ogorodnikova*[2], *T.Płociński*[1], *M.Andrzejczuk*[1], *M.Rasiński*[1], *M.Mayer*[2], *K.J.Kurzydłowski*[1]

[1] Warsaw University of Technology, ul. Woloska 141, PL-02507 Warsaw, Poland
[2] Max-Planck-Institute für Plasmaphysik, Boltzmannstr. 2, D-85748 Garching, Germany

1. INTRODUCTION

Tungsten (W) will be used in the high-flux region of the divertor in ITER and is a candidate material for plasma facing components in future fusion devices [1]. This is mainly due to its favorable physical properties under high heat and particle fluxes loading, i.e. low sputtering yield which can minimize the impurity generation and also good thermal properties, i.e. high melting point and high thermal conductivity required from efficient plasma facing materials. Neutron (n) irradiation of materials leads to a significant modification of their crystal structure due to introduction and accumulation of radiation induced structural defects. This radiation-induced damage will influence tungsten properties important from the point of view of fusion power plant operation, e.g. fuel retention [2].

As the sources of fusion neutrons for materials irradiation are still not existent and irradiation of materials in fast nuclear reactor is not very practical due to the long time required for accumulation of relevant dpa level in this work, devoted to the study of microstructural defect in tungsten, heavy tungsten ions with energy of 20 MeV were used to simulate displacement damage created by fast neutrons.

2. EXPERIMENTAL

2.1. Material

The polycrystalline W samples were cut into 10 x 10 mm^2 plates of the thickness of c.a. 0.5 mm and mechanically polished to mirror like finish. Prior to self-implantation with tungsten ions the plates were recrystallized at 1800 ˚K for 1 hour. The radiation damage was made by implantation with 20 MeV W^{6+} ions up to different dpa level. The implantation was carried out at IPP Garching in a chamber connected to the 3 MV tandem accelerator.

2.2. TEM investigations

The transmission electron microscopy (TEM) observations have been performed on lamellae cut as cross-sections perpendicular the implanted sample surface. Focused Ion Beam system - Hitachi FB2100 has been used for samples milling and extraction. Prior TEM analyses the lamellae were subjected to low energy Argon ions polishing with LINDA Gentle Mill device aiming at sample thinning and reduction of structural damage additionally introduced in tungsten during FIB processing. The TEM observations have been carried out with scanning-transmission electron microscope STEM HD2700 made by Hitachi with accelerating voltage of 200 kV.

3. RESULTS

Figure 1 shows the bright field STEM image of the damaged zone in tungsten sample implanted up to 0.89 dpa.

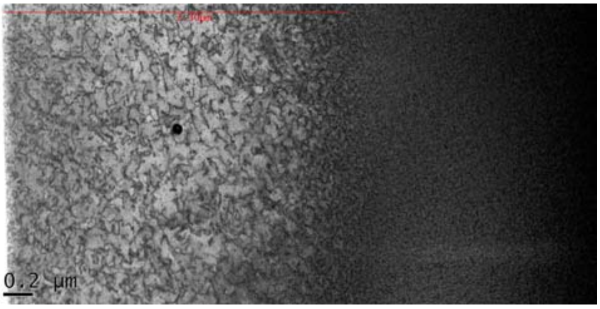

Figure 1: Damaged zone (left) in polycrystalline tungsten implanted by 20 MeV W^6 ions.

The observed damaged zone depth (c.a. 2.4 microns) is in a good agreement with SRIM calculations and the observed defects density and morphology varies with the distance form sample surface.

The damaged zone can be divided into 3 sub-regions:

1) near surface area with high density of dislocations up to 0.4 microns,
2) intermediate area with lower density of “long” dislocations and “sub-grain” regions free from dislocations from 0.5 microns up to 1.7 microns,
3) deep region with high density of “short” dislocations from 1.7 microns to 2.4 microns.

Below this damaged zone defects introduced by FIB milling can be observed (see Fig. 1 right).

4. REFERENCES

[1] V. Philipps, J. Nucl. Mater. **415**, Issue 1, Supplement, pp. S2-S9, (2011).

[2] O.V. Ogorodnikova, B. Tyburska, V.Kh. Alimov, K. Ertl,’ Journal of Nuclear Materials, Volume 415, Issue 1, Supplement, 2011, pp. S661-S666

---

[*] Corresponding author e-mail address: lukas@inmat.pw.edu.pl

Li^+ ION NEUTRALIZATION ON METAL SURFACES AND THIN FILMS

Lin Chen,[1,2,] Jie Shen,[1] Juanjuan Jia,[1] Thirunavukkarasu Kandasamy,[1] Kirill Bobrov,[1] Laurent Guillemot,[1] Javier. D. Fuhr,[3] Maria Luz Martiarena,[3] and Vladimir A. Esaulov[1,]*

[1]*Institut des Sciences Mol´eculaires d'Orsay, (UMR8214, CNRS—Universit´e Paris-Sud), F-91405 Orsay Cedex, France*
[2]*School of Nuclear Science and Technology, Lanzhou University, Lanzhou 730000, China*
[3]*Consejo Nacional de Investigaciones Cientificas y T´ecnicas (CONICET) and Instituto Balseiro, Centro At´omico Bariloche,*

1. INTRODUCTION

The studies of alkali-metal ion neutralization on small gold clusters and thin films have recently revealed very large probabilities of neutralization. Furthermore a very curious feature was the observation of large neutralization on related some large workfunction surfaces like those of Au(111) and Cu(111), which is not understandable in "standard" models [1]. In an endeavor to better understand this large neutralization we performed measurements of Li^+ neutralization on Cu(100), Cu(111), Au(111), and Au(100) surfaces. These experiments revealed that, consistently, neutralization is "anomalously" large on these surfaces and also the energy dependence was found to be at variance with expectations.

When considering alkali ion neutralization, one usually considers an upward shift of the atomic level near the surface, which would lead to ionization at close atom-surface distances. However more recent theoretical work [2] has indicated that neutralization in alkali ion scattering can occur for small ion-surface distances, because the atomic level lies below the Fermi level because of specific short range interactions. This feature could explain large neutralization for an atom receding rapidly from the surface after close approach. However, the existing modeling remains incomplete and has been unable to reproduce the overall features of neutralization for these systems.

In view of all these developments and as a concluding sequel to our earlier study of some noble metal surfaces, we decided to investigate Li^+ neutralization on Au(110), Pd(100), and Ag layers grown on Au(111) [3]. The experiments are complemented by a theoretical study using density functional theory (DFT) .

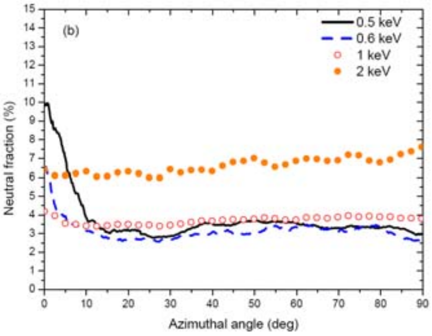

Figure 1: Neutral fraction obtained in scattering on a Au(110) surface as a function of the azimuthal angle for different incident energies of Li^+. The results correspond to a scattering angle of 83° and an exit angle of 13°.

In Fig.1 we show the neutral fraction as a function of the azimuthal angle. A considerable variation with azimuthal angles appears in the $[1\bar{1}0]$ direction. For 0.5 keV incident energy, the fraction increases to about 10%, whereas for 2 keV, no variation is observed. In Fig.2 we observe that the neutral fraction on the Ag monolayer is found to be very close to the results obtained on a bulk Ag(111) crystal and is much larger than that for Au(111). The results for Pd(100) and Au(110) were found to be qualiatatively similar to those on Au(111) in magnitude and energy dependence. The more detailed results will be discussed in the conference.

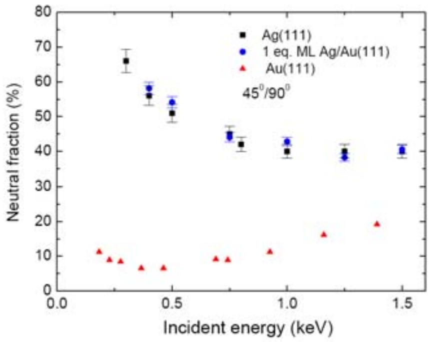

Figure 2: Li^+ neutral fraction as a function of the incident energy for 1 ML Ag coverage on Au(111), at a scattering angle of 135°, and an exit angle of 90°.

In summary, the results for the large work function surfaces (Pd, Au) clearly show some common characteristics: The neutral fraction tends to first decrease with increasing energy and then increase again. The exit angle dependence is also characterized by a similar trend. The case of the Ag layer on Au(111) turns out to be similar to the case of a bulk crystal Ag(111) surface. The theoretical modeling we performed confirms the small distance behavior of the alkali atomic level predicted in previous works and a charge state analysis shows that in all cases adiabatically the charge on the alkali atom tends to unity explaining thus the increase in neutralization at low energies. An accurate description of the full ion trajectory will be necessary to describe the finer characteristics of the azimuthal dependence of the neutralization process.

2. REFERENCES

[1] J. Los and J. J. C. Geerlings, Phys. Rep. **190**, 133 (1990).
[2] E. A. Garc´ıa, M. A. Romero, C. Gonz´alez, and E. C. Goldberg, Surf. Sci. **603**, 597 (2009).
[3] Lin Chen, Jie Shen, Juanjuan Jia, Thirunavukkarasu Kandasamy, Kirill Bobrov, Laurent Guillemot, Javier. D. Fuhr, Maria Luz Martiarena, and Vladimir A. Esaulov, Phys. Rev. A **84**, 052901 (2011).

---

[*] Corresponding author e-mail address: chenlin@lzu.edu.cn

ELECTRONIC STOPPING AT LOW ION VELOCITIES: GOING BEYOND BANDSTRUCTURE EFFECTS

D. Primetzhofer[1,2*], *S. Rund*[2], *D. Roth*[2], *D. Goebl*[2], *and P. Bauer*[2]

[1] Institutionen för Fysik och Astronomi, Uppsala Universitet, Box 516, S-751 20 Uppsala, Sweden
[2] Institut für Experimentalphysik, Johannes Kepler Universität Linz, A-4040 Linz, Austria

1. INTRODUCTION

Electronic interactions of slow light ions in solids are of great relevance in many fields of research like astrophysics, plasma physics and many materials science applications. This of course raises a fundamental interest to understand and quantify the underlying processes. Pioneering work of Fermi et al. [1] predicted the energy loss of slow ions in a free electron gas to be velocity proportional and pointed out the importance of excitation thresholds for target electrons. More quantitative predictions came up [2], and experimental observations of excitation thresholds followed, which could be explained by considering the electronic structure of the solids and screening of the ion in the solid.

In this work we present the observation of a change in velocity dependence of the electronic energy loss for a system (i.e. He in Al), where no excitation thresholds for direct excitation of electrons in the target are expected [3].

2. RESULTS

2.1. Experimental results

Electronic stopping cross sections ε were deduced from experiments using ultrathin Al films deposited on Ta_2O_5 and simulation of the obtained spectra of backscattered ions with Monte-Carlo simulations to account for contributions from multiple scattering and nuclear stopping. Fig. 1 shows the data obtained in this study. Data for H shows perfect velocity scaling and is in practically perfect agreement with DFT predictions for a free electron gas with the appropriate density.

In contrast data for He is velocity proportional only at the lowest energies, and shows a deviation to higher values of e at v > 0.2 i.e. 4 keV. Whereas DFT slightly overestimates the energy loss at low velocities it underestimates the losses at higher velocities.

2.2. Interpretation

We interpret the data by an onset of an additional energy dissipative mechanism. The electronic structure of Al, together with the data for H rules out an origin of the effect similar to the observed excitation thresholds in Au or Cu.

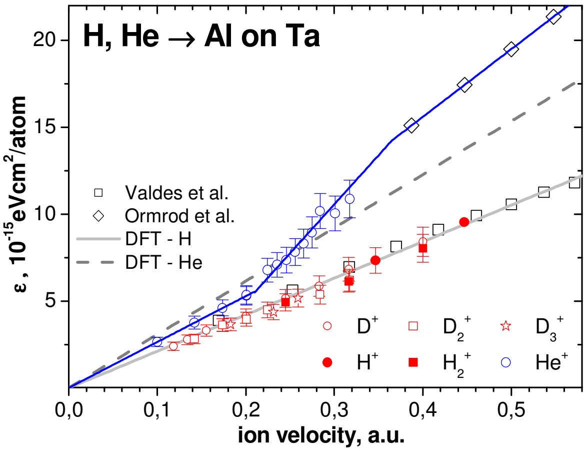

Fig 1: Experimentally obtained stopping cross section ε of H, D and He ions in Al as a function of velocity. Also shown are data from previous experiments. Predictions from DFT for slow H and He are shown as dotted and dashed gray lines respectively.

We trace back the observed effect to charge changing collisions between He and Al atoms. It is known that reionisation of neutral He atoms scattered from Al can occur already at relatively large interaction distances of 0.75 a.u. due to a strong promotion of the He 1s-level [4].

Recurring charge exchange along the trajectory leads to an increase of the observed electronic energy loss by two mechanisms: First, the charge changing collisions consume energy to promote the electron which is subsequently lost by the ion. Second, a He ion interacts stronger with the electronic system of the target than a neutral He atom.

3. ACKNOWLEDGMENTS

The authors would like to thank the Austrian Science Fund FWF for funding of the presented work under Contract No. P19595-N20.

4. REFERENCES

[1] E. Fermi, E. Teller, Phys. Rev. 72 (1947) 399.
[2] I. Nagy, A. Arnau, and P.M. Echenique, Phys. Rev. A 40 (1989) 987.
[3] D. Primetzhofer, S. Rund, D. Roth, D. Goebl, and P. Bauer, Phys. Rev. Lett. 107 (2011) 163201.
[4] S. Wethekam, D. Valdés, R.C. Monreal, and H. Winter, Phys. Rev. B 78 (2008) 075423.

---

[*] Corresponding author e-mail address: daniel.primetzhofer@physics.uu.se

ION SCATTERING INVESTIGATIONS OF THE TEMPERATURE DEPENDENCE OF CHARGE EXCHANGE AND SURFACE COMPOSITION

J. A. Yarmoff,[1] *X. He and A. B. Arjad*

Department of Physics & Astronomy, University of California – Riverside, Riverside, California 92521 USA

1. INTRODUCTION

Surface temperature is an important parameter in ion-surface interactions. For example, the temperature directly affects the probably for charge exchange during scattering, and elevated temperature can induce structural changes in materials that are subsequently investigated by ion scattering. Given the broad scope of ion-surface scattering measurements that are routinely performed, however, there have been relatively few investigations of the effects of surface temperature. We report low energy ion scattering (LEIS) experiments in which temperature influences either the charge exchange probability or the surface composition.

2. EXPERIMENTS

2.1. Correlated Electron Effects

A system of many electrons can display emergent phenomena beyond that predicted from the behavior of individual electrons. Correlated electron behavior has been achieved, for example, by the introduction of a spin impurity into a metal, which causes the free electrons to respond collectively. Here, the unpaired valence electron on singly charged strontium (Sr) ions provides the spin impurity during LEIS from gold (Au). A significant temperature dependence of the neutralization, such as that shown in Fig. 1, is a signature of electron correlations [1].

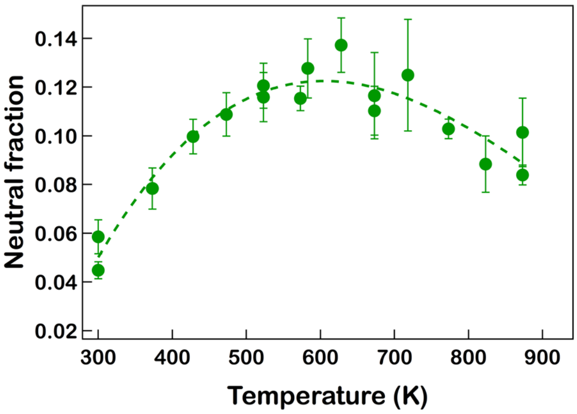

Figure 1: Neutralization probability of 2 keV Sr^+ scattered from Au foil shown as a function of surface temperature [1].

2.2. Surface Termination of Bi_2Se_3

The 3D Topological Insulator, Bismuth Selenide (Bi_2Se_3), is investigated with 3 keV Na^+ ions. Se surface vacancies were believed to be responsible for metallic behavior that has been seen in transport, and LEIS is uniquely sensitive to the outermost atomic layer composition. Bi_2Se_3 is comprised of Se-Bi-Se-Bi-Se quintuple layers (QLs) held together by weak van der Waals bonds, so it was naturally assumed that a Se termination results when cleaved. After cleaving in vacuum at room temperature, however, the LEIS spectra indicate a surface terminated with Bi. The samples display sharp 1x1 LEED and atomic resolution in STM, indicative of an ordered material. It is concluded that Bi_2Se_3 cleaves between the QLs, but that atomic diffusion occurs quickly at room temperature to form an ordered Bi-terminated structure. To test this, the surface was monitored by LEIS after *in situ* cleaving at liquid nitrogen temperature. It was found that the intensity of surface Bi increases over the course of hours, suggesting a slow diffusion of Bi to cover the surface at the lower temperature.

2.3. Buffer Layer Assisted Growth of Au Nanoclusters

Buffer Layer Assisted Growth (BLAG) has been proposed as a novel means for the production of nanoclusters deposited onto a surface. BLAG involves the use of a frozen inert buffer layer at low temperatures to enable the growth of nearly "anything on anything" [2]. The interactions between metal atoms deposited onto the buffer layer are stronger than those with the buffer layer, leading to the formation of 3D clusters rather than a dispersed film. The cluster sizes depend on the diffusion rate of the metal atoms and on the density of atoms deposited. When the sample is warmed to room temperature to desorb the buffer layer, the clusters remain intact and deposit onto the substrate surface. We used neutralization during alkali LEIS [3] to monitor the formation of Au nanoclusters using water as the buffer layer material [4]. An advantage to using LEIS in this manner is the ability to probe the clusters both while they are atop the buffer layer and after the layer has been desorbed.

3. REFERENCES

[1] X. He and J. A. Yarmoff, Phys. Rev. Lett. **105**, 176806 (2010); Nucl. Instrum. Meth. B **269**, 1195 (2011).

[2] J. H. Weaver and V. N. Antonov, Surf. Sci. **557**, 1 (2004).

[3] G. F. Liu, Z. Sroubek, and J. A. Yarmoff, Phys. Rev. Lett. **92**, 216801 (2004).

[4] E. Gross, M. Asscher, M. Lundwall and D. W. Goodman, J. Phys. Chem. C **111**, 16197 (2007).

---

* Corresponding author e-mail address: jory.yarmoff@ucr.edu

CALCULATION OF THE SCATTERING PROBABILITY IN LEIS: EFFECT OF THE SCREENING FUNCTION CHOICE

K. Khalal-Kouache [*] M. Benrekia

USTHB – Faculty of Physics – Algeria.

1. INTRODUCTION

Molecular dynamics simulations and Monte Carlo codes are often used to calculate energy spectra for low energy ion scattering. Due to the large calculation times required by Monte Carlo simulation, an alternative was proposed [1, 2] to calculate angular distribution of the total path length L for the particles inside the solid. Energy spectra are then deduced from these calculated distributions. Comparison between experimental and simulated Time Of Flight (TOF) spectra (or energy spectra) allows the determination of inelastic energy loss if the interaction potential is well known [3]. In the present work, we focus our attention on effect of the potential used to describe projectile-target atom interaction on the computed distributions.

2. RESULTS

This model is based on the solution of the Boltzmann equation in the transport theory frame and is valuable for small scattering angles. The binary collision approximation is assumed with a random homogenous distribution of scattering centers.

At first, energy loss is neglected. ΔP_1 is the probability for a projectile to be scattered at an angle θ (corresponding to the direction $\vec{\Omega}$) and in the solid angle $\Delta\Omega$ with a total path length in the solid comprised between L and $L + \Delta L$ [1, 2].

ΔP_2 is the calculated probability when energy loss is taken into account. Inelastic energy loss values are obtained from SRIM2010 [4]. A screened Coulomb potential is used to describe the interaction between projectile and target atom. In this work, different screening functions are considered. The corresponding results are given and discussed. An example for the scattering of He^+ (4keV) ions from a Si surface is given in figure 1. In this case, ΔP_1 and ΔP_2 are calculated using the Ziegler-Biersack-Littmark (ZBL) [5] potential.

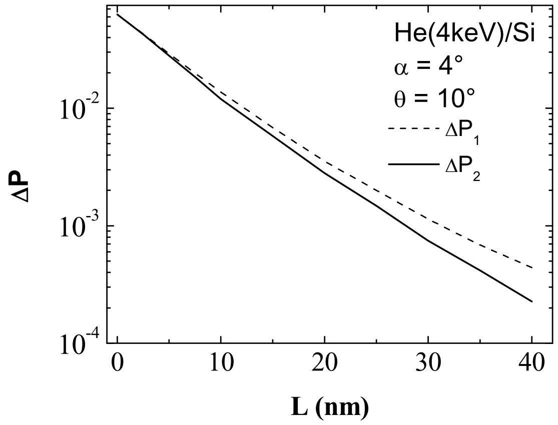

Figure1. ΔP_1 and ΔP_2 variations with the total path length L for He^+(4keV)/Si. Incidence and scattering angles are respectively $\alpha=4°$ and $\theta=10°$.

3. REFERENCES

[1] K. Khalal-Kouache, A.C. Chami, M. Boudjema, P. Benoit-Cattin, C. Benazeth, Y. Boudouma, Nucl. Instrum. Methods Phys. Res. B **183**, 279 (2001).

[2] K. Khalal-Kouache, Thesis, USTHB, Algiers, Algeria, 2002.

[3] S.N. Markin, D. Primetzhofer, M. Spitz, and P. Bauer, Phys. Rev. B **80**, 205105 (2009).

[4] J.F. Ziegler, M.D. Ziegler, J.P. Biersack, Nucl. Instrum. Methods Phys. Res. B **268**, 1818 (2010).

[5] J.F. Ziegler, J.P. Biersack and U. Littmark, *The stopping and Ranges of Ions in Solids* (Pergamon, New York, 1985).

---

[*] Corresponding author e-mail address: kkouache@yahoo.fr

Coherent Acoustic Phonon Spectroscopy of Ion-Implanted Diamond

J. Gregory[1,*], A. Steigerwald,[2] H. Takahashi,[3] A. Hmelo,[2] and N. Tolk[2]

[1] Interdisciplinary Materials Science, Vanderbilt University, Nashville, TN USA
[2] Department of Physics and Astronomy, Vanderbilt University, Nashvill, TN USA
[3] Japan Advanced Institute of Science and Technology, Ishikawa, Japan

1. INTRODUCTION

Ion implantation of single-crystal diamonds has garnered considerable interest in the last few decades due to the potential applications in quantum computing, [1] photonics, [2] and diamond devices. [3] One particularly promising technique [4] involves implantation of diamond crystals with light ions, resulting in a thin layer of buried lattice damage. This is followed by an annealing step, which sharpens the interface between the damage layer and the diamond lattice. Subsequent patterned implants and chemical etching allow for the fabrication of free-standing single-crystal diamond nanostructures.

Clearly, if this technique is to be used for fabrication of photonic and optically-based quantum information devices, a detailed understanding of the effects of ion implantation and annealing on the opto-electronic properties of the diamond lattice is necessary. Coherent Acoustic Phonon (CAP) spectroscopy is an ultrafast optical method well suited to study these phenomena. [5] CAP experiments are an advancement of standard ultrafast optical pump-probe techniques, and provide detailed *depth-dependent* information about the optical and electronic properties of materials in a non-destructive fashion.

2. RESULTS

We will describe a systematic study of the modulation of CAP oscillation patterns in diamond at a variety of He^+ implantation doses, and extract relationships for how the implantation modifies the complex index of refraction of the diamond lattice, as well as its first derivative with strain.

Figure 1 shows the time-resolved optical pump-probe reflectivity signal of a single-crystal diamond specimen implanted with 1-MeV He^+ ions at a dose of 3×10^{15} cm^{-2}. There is a strong modulation of the CAP oscillation pattern beginning near 80 ps. This time delay corresponds to a sample depth of 1.8 μm, which is the expected depth for the greatest concentration of ion implantation damage.

Comparing these results with computer simulations of implantation damage profiles yields a calibration relationship between optical properties and induced damage. These results will aid in the fabrication of photonic and quantum devices based on single-crystal diamonds.

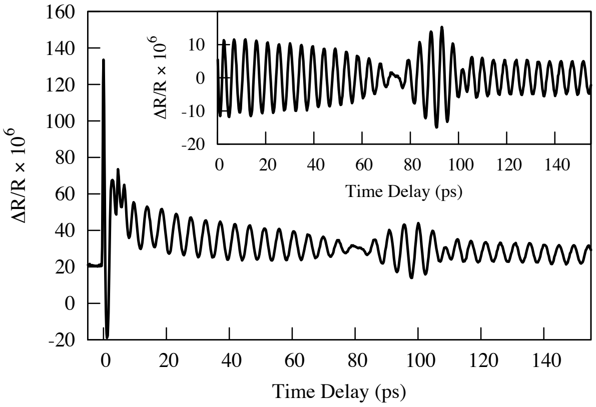

Figure 1: Time-resolved pump-probe reflectivity response from a diamond specimen implanted at 3×10^{15} cm^{-2} 1-MeV He^+ ions. Inset: Isolated CAP signal.

3. REFERENCES

[1] S. Prawer and A. D. Greentree, Science **320**, 1601 (2008).

[2] S. Lagomarsino, P. Olivero, F. Bosia, M. Vannoni, S. Calusi, L. Giuntini, and M. Massi, Phys. Rev. Lett. **105**, 233903 (2010).

[3] P. Olivero, G. Amato, F. Bellotti, O. Budnyk, E. Colombo, M. Jakšić, C. Manfredotti, Ž. Pastuović, F. Picollo, N. Skukan, M. Vannoni, and E. Vittone, Diam. and Rel. Mat. **18**, 870 (2009).

[4] B. Fairchild, P. Olivero, S. Rubanov, A. Greentree, F. Waldermann, R. Taylor, I. Walmsley, J. Smith, S. Huntington, B. Gibson, *et al.*, Adv. Mat. **20**, 4793 (2008).

[5] A. Steigerwald, Y. Xu, J. Qi, J. Gregory, X. Liu, J. K. Furdyna, K. Varga, A. B. Hmelo, G. Lupke, L. C. Feldman, and N. Tolk, Appl. Phys. Lett. **94**, 111910 (2009).

---

[*] Corresponding author e-mail address: justin.m.gregory@vanderbilt.edu

POTENTIAL SPUTTERING FROM F/Si(100) SURFACE WITH EXTRACTION OF THE SURFACE BOND DIRECTION

Norio Okabayashi*

Kanazawa University, School of Mathematics and Physics.

Sputtering by ion irradiation is widely applied technique in a process of surface cleaning and fabrication of nanostructures, where the kinetic energy of ions play essential role (kinetic sputtering). On the other hand, when the highly charged ions (HCIs) are employed, enhancements of sputtering yields with the potential energy take place depending on target materials (potential sputtering). Sputtering yields of adsorbed atoms on solid surfaces such as hydrogen and fluorine are drastically enhanced by the potential energy or charge state of HCI [1,2]. The mechanism of the potential sputtering for the adsorbates is frequently discussed by using analogy to that by electron stimulated desorption (ESD) [3]. As in the case of ESD, in order to interpret the mechanism of potential sputtering, measurements of the emission energy and emission angle are effective. In the present study, we constructed the experimental setup, where we can acquire this information for each sputtered ions [4,5]. .

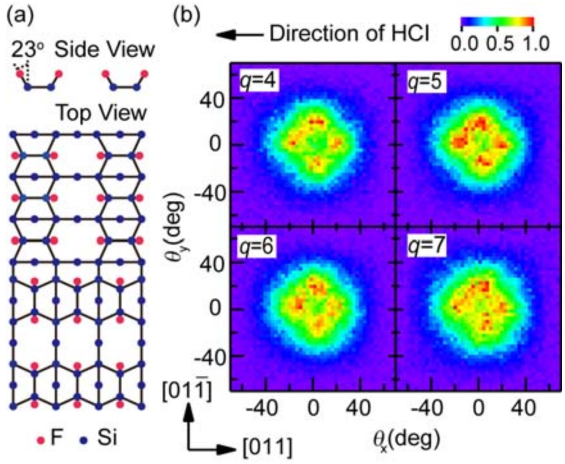

Fig. 1. (a) Schematic diagram of F/Si(100) surface. (b) Angular distributions of F^+ ions emitted by 3.9 keV Ar^{q+} impacts, which reflect the adsorbed state in (a).

In this presentation, we compare results of potential sputtering between for H/Si(100) and F/Si(100) surfaces. In the case of the proton sputtering, the yield is proportional to q^5, where q is the charge state of HCI and the angular distributions of sputtered protons have a single peak along the surface normal [1]. On the other hand, in the case of the F^+ sputtering, its yield is proportional to q^3. Moreover, the emission patterns show four fold symmetry with the peak polar angle of 23° (see Fig. 1(b)) [2]. Those patterns reflect the surface adsorbed state of fluorine atoms on a Si(100) surface, which indicate that potential sputtered F^+ is emitted along the initial bond direction. Similar angular distribution is observed also in the case of ESD, however the kinetic energy of F^+ by HCI impact (2 eV) is smaller than that by ESD (3 eV). This difference of the kinetic energy can be interpreted with the calculation by Ph. Avouris et. Al. [6], if we assume that (1) in the case of the HCI impact, sequential resonant electron transfer of F2p electrons leads to the formation of F^+ state and (2) in the case of ESD, $F^*(2s^12p^6)$ state is formed by the ionization of F2s electron and the emitted F* is converted into F^+ ion by the Coster-Kronig transitions on the way of the desorption.

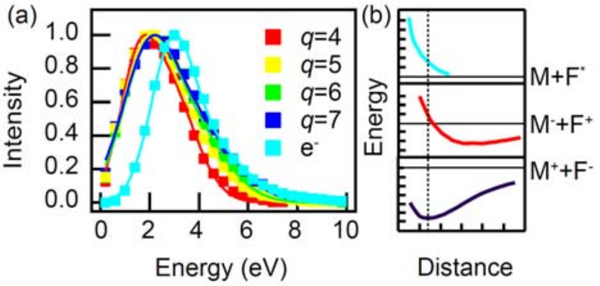

Fig. 2. (a) F^+ emission energy for 3.9 keV Ar^{q+} and 350 eV e^- impacts. For the electron energy studied here, F^+ kinetic energy by ESD is constant. (b) Calculated potential energy surface of F^-, F^*, F^+ on a metal surface calculated by Ph Avouris et. al. [6].

The content of the present talk was performed when I was a graduate student in University of Tokyo with Prof. Yamazaki, Prof. Komaki and Dr. Kuroki. I deeply appreciate the collaboration.

References

[1] K. Kuroki, N. Okabayashi, H. Torii, K. Komaki, and Y. Yamazaki, Appl. Phys. Lett. 81, 3561 (2002).

[2] N. Okabayashi, K. Komaki, and Y. Yamazaki, Phys. Rev. Lett. 107, 113201 (2011).

[3] J. Burgdörfer and Y. Yamazaki, Phys. Rev. A 54, 4140 (1996).

[4] N. Okabayashi, K. Komaki, and Y. Yamazaki, Nucl. Instr. and Meth. B 235, 438 (2005).

[5] N. Okabayashi, K. Komaki, and Y. Yamazaki, Nucl. Instr. and Meth. B 205, 725 (2003).

[6] Ph. Avouris, R. Kawai, N. D. Lang and D. M. Newns, J. Chem. Phys. 89, 2388 (1988).

---

[*] Corresponding author e-mail address: okabayashi@staff.kanazawa-u.ac.jp

LOCAL ELECTRONIC SHORT-TIME EFFECTS DUE TO INTERACTIONS OF FAST HIGHLY CHARGED IONS WITH INSULATORS

G. Schiwietz [1,*], *K. Czerski*[1,2], *M. Roth*[1], *P.L. Grande*[3], *V. Koteski*[4], *F. Staufenbiel*[1]

[1] Helmholtz-Zentrum Berlin f. Materialien u. Energie, Institute G-I2,
Hahn-Meitner-Platz 1, 14109 Berlin, Germany
[2] Presently: Inst. Fizyki, Uni. Szczecinski, ul. Wielkopolska 15, 70-451 Szczecin, Poland
[3] Uni. Federal do Rio Grande do Sul, Av. B. Gonçalves 9500, 91501-970 Porto Alegre, RS, Brazil
[4] VINCA Institute, Dpt. of Physical Chemistry, POB 522, Belgrade 11001, Serbia

1. INTRODUCTION

The interaction of fast ions with solid or liquid matter leads to an excitation of a large phase-space volume regarding the electronic degrees of freedom, suppressing nuclear energy-transfer processes at the same time. Notwithstanding the complexity that arises due to the large variety of ion-solid interaction processes, the primary interaction is extremely well localized in space (typically on an atomic scale) and in time. The time duration of individual energy-transfer processes for fast ions is about 10^{-16} s and less, far below typical electronic or atomic relaxation times.

During recent years, our current knowledge on primary energy-transfer processes has reached a high level of sophistication [1,2]. Thus, fast ions are ideal candidates for short-time investigations specifically of electronic relaxation processes in solids. In this talk, the short-time effects of swift heavy ions interacting with insulators and semiconductors will be discussed. High-resolution Auger spectroscopy is applied to the investigation of rapid electronic and atomic processes in the close vicinity of the surface [3].

2. FAST HEAVY IONS IN METALS

Heavy ions at specific energies of a few MeV/u (at 10% the speed of light) provide extremely high excitation densities, leading to non-linear effects. At volume energy-densities beyond a certain material-dependent limit, plasmons as well as other (quasi-) particle excitations are overlapping. This leads to a coupling of basic excitations and may have a significant influence on energy-dissipation processes. In principle, a breakdown of band-structure-concepts is conceivable, but in most cases indications for a local thermal equilibrium in the electron gas with a Fermi-Dirac distribution at electron temperatures of up to 10^5 K and a rapid neutralization of the ion track have been observed [4,5].

3. INSULATOR AND SEMICONDUCTOR TARGETS

The short-time dynamics of insulators and semiconductor targets displays additional effects in comparison to metals. For Si targets we find Auger-energy reductions that maximize for short decay times and for amorphous samples (in comparison to Si(11 1) crystals with 7x7 reconstruction), reaching 3 eV for very heavy projectile ions [6], consistent with the spectra of [7]. This relatively small effect is assigned to a very slow component of the nuclear-track potential with ($_{\text{track}} > 30$ fs). Very likely, it is due to self-trapped excitons in the amorphous material, resulting in a slightly reduced electron density in the track. For a crystalline Si sample, thermally displaced atoms, specifically those close to the surface, might provide meta-stable self-trapping conditions.

In principle, a nuclear-track potential might also be related to long-lived traps for electrons and for holes near the ion-track center. The corresponding charge separation may lead to an extremely strong positive potential (> 40 V), as determined for 5 MeV/u Ne^{9+} ions in polypropylene [8]. For fast heavy ions penetrating an ionic BeO film, we even observe clear indications for a breakdown of the local electronic band-structure [9] around the Be sites, as will be discussed at the workshop.

4. REFERENCES

[1] P.L. Grande and G. Schiwietz; in “Advances in Quantum Chemistry”, **Vol. 45**, pp.7-46 (book article ed. by J. Sabin, 2004, Elsevier Inc.).

[2] P. Sigmund, Kongelige Danske Vidensk. Selskab: Matematisk-Fysiske Meddel. **Vol. 52**, 557-593 (book article ed. by P. Sigmund, 2006).

[3] G. Schiwietz et al.; NIM-**B226**, 683–704 (2004); ibid., NIM-**B164**, 353-364 (2000).

[4] G. Schiwietz, G. Xiao, P.L. Grande, E. Luderer, R. Pazirandeh, U. Stettner, NIM-**B146**, 131 (1998); ibid. , Europhys. Lett. **47**, 384 (1999)

[5] M. Caron, H. Rothard, M. Beuve, B. Gervais, Physica Scipta **T80**, 331 (1999); ibid. **T92**, 281 (2001).

[6] G. Schiwietz, et al., NIM-**B266**, 1287 (2008).

[7] W. Schmidt, P.Müller, V.Brückner, F.Löffler, Saemann-Ischenko, W. Schubert, Phys.Rev. A24, 2420 (1981).

[8] G. Xiao et al., **Phys. Rev. Lett. 79**, 1821 (1997) and references therein.

[9] G. Schiwietz, K. Czerski, M. Roth, P.L. Grande, V. Koteski, F. Staufenbiel; **Phys.Rev.Lett. 105**, 187603 (2010). ibid; NIM-**B269**, 959 (2011).

---

[*] Corresponding author e-mail address: schiwietz(at)helmholtz-berlin.de

SECONDARY ELECTRON YIELD FROM HCI ON AU AND THIN FILMS OF C_{60}

E. Bodewits[1,*], *K Dobes*[2], *F. Aumayr*[2], *and R. Hoekstra*[1]

[1] KVI - Atomic and Molecular Physics, University of Groningen, Zernikelaan 25, 9747 AA Groningen, The Netherlands
[2] Institute of Applied Physics, TU Wien - Vienna University of Technology, A - 1040 Vienna, Austria

Recently we investigated the influence of C_{60} thin films evaporated on Au(111) on the secondary electron yield of highly charged ions (HCI) [1]. It was found that the relative secondary electron yield from C_{60} follows an exponential growth curve as function of the number of monolayers (ML) and saturates at an increase of 35% for 5 ML of C_{60} on Au as shown in figure 1.

Recently the original over-the-barrier model was extended by Lake et al. [2] by the inclusion of a thin dielectric film on top of a metal surface. They showed that a highly charged ion approaching an Al_2O_3 film may perturb the thin film such that throughout the film the bottom of its conduction band drops below the workfunction of the substrate while the barrier between the HCI and the thin film is still that high that over-the-barrier transitions between the film and the HCI are not yet possible. In this way the insulating aluminium oxide film effectively lowers the substrate workfunction by a few eV. The earlier onset of the neutralization and creation of hollow atoms will give more time in front of the surface for the relaxation processes of the hollow atoms. This would lead to an increase in the secondary electron yields.

There might be another cause for the increase in the secondary electron yield too, namely an increase in the escape length of electrons produced below the surface. The thin films of C_{60} have a very open structure, therefore electrons produced in the C_{60} film may have a higher probability of escaping and being detected as compared to electrons produced below a closer packed Au surface.

Here we discuss further experiments concerning the increase in secondary electron yield. In the new series of experiments we investigated how changing the incidence angle and the kinetic energy of the HCI affects the secondary electron yield. Also, experiments with highly ordered pyrolytic graphite (HOPG) have been done for comparison with the C_{60} layers [3].

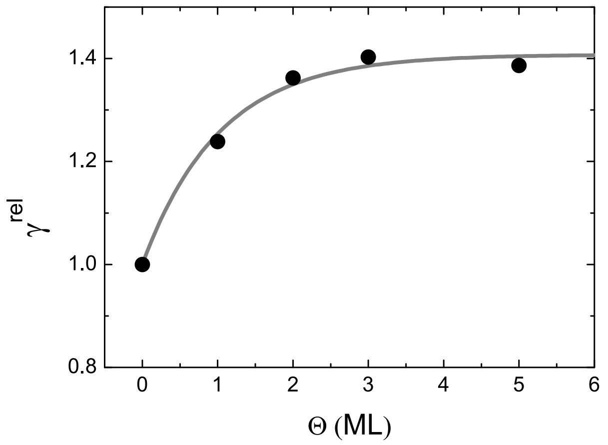

Figure 1: Relative secondary electron yield obtained with 70 keV Xe^{24+} impinging under 40 degree incidence angle as function of C_{60} monolayers compared to clean Au. Also shown is an exponential growth curve.

1. REFERENCES

[1] E. Bodewits, R. Hoekstra, G. Kowarik, K. Dobes, and F. Aumayr, Phys. Rev. A **84** (2011).

[2] R.E. Lake, J.M. Pomeroy and C.E. Sosolik, Nucl. Instr. Meth. B, **169**, 11 (2011)

[3] K. Dobes, E. Bodewits, G. Kowarik, R. Hoekstra and F. Aumayr, this book of abstracts

---

*Corresponding author e-mail address: ebodewits@kvi.nl

VICINAGE EFFECT ON SECONDARY-ELECTRON EMISSION FROM CARBON FOILS PENETRATED BY SWIFT H_2^+ AND C_2^+ IONS

K. Narumi[1, 2, *], Y. Takahashi[2], A. Chiba[1], Y. Saitoh[1], K. Yamada[1], N. Ishikawa[3], H. Sugai[2], and Y. Maeda[2, 4]

[1] Takasaki Advanced Radiation Research Institute, Japan Atomic Energy Agency, Takasaki, Gumma 370-1292, Japan
[2] Advanced Science Research Center, Japan Atomic Energy Agency, Tokai, Ibaraki 319-1195, Japan
[3] Nuclear Science and Engineering Directorate, Japan Atomic Energy Agency, Tokai, Ibaraki 319-1195, Japan
[4] Department of Energy Science and Technology, Kyoto University, Sakyo-ku, Kyoto 606-8501, Japan

1. INTRODUCTION

Secondary-electron (SE) emission from a solid surface bombarded with fast charged particles has been studied extensively for a long time and extended to various kinds of applications. Although it is a very fundamental phenomenon, it is not still understood completely. Vicinage effect on the SE emission induced by swift molecular/cluster ions is one of the unresolved problems. We have investigated the vicinage effect on the SE emission by measuring the SE yield emitted from an amorphous carbon foil bombarded with swift C_2^+ ions. It has been observed for the first time that the vicinage effect on the SE yield in the forward direction induced by 62.5-keV/u C_2^+ ions disappears for thicker foils than 60 μg/cm^2 [1]. This result means that a *transport* or *transmission* process of scattered electrons is very important for the appearance of the vicinage effect. In order to study the previous result further, we have investigated the vicinage effect on the SE emission induced by bombardment with H_2^+ and C_2^+ ions in the same velocity region.

2. EXPERIMENTAL AND RESULTS

62.5-300-keV/u H_2^+ and C_2^+ ions were incident on self-supporting amorphous carbon foils of 2-100 g/cm^2 thickness, which was tilted by 45 to the beam axis. SE's emitted in the forward and backward directions from a carbon foil were detected with two microchannel-plate (MCP) detectors placed at the both sides of the target holder in parallel with the target. Particles transmitted through the foil were detected with a solid-state detector (SSD) placed at the backside of the target on the beam axis, which made it possible to measure the energy and the number of the transmitted particles. The forward and backward SE yields per incident projectile $_{\mathrm{F,B}}$ were determined from the pulse-height distributions of the forward and backward MCP signals, respectively, which were proportional to the number of detected SE's. The vicinage effect was evaluated with the ratios of the forward and backward SE yields $R_{\mathrm{F,B}}$ = $_{\mathrm{F,B}}(2)/2\ _{\mathrm{F,B}}(1)$, where $_{\mathrm{F,B}}(2)$ and $_{\mathrm{F,B}}(1)$ are SE yields induced by bombardment with diatomic and monatomic ions with the same velocity, respectively. The origin of the vicinage effect on the SE yield will be discussed based on the observed foil-thickness and velocity dependence of the vicinage effect.

This work was partially supported by a Grant-in-Aid for Scientific Research (C), a Grant-in-Aid for Young Scientists (Start-up) and a Grant-in-Aid for Young Scientists (B), and also partially supported by the Inter-organizational Atomic Energy Research Program in an academic collaborative agreement between the Japan Atomic Energy Agency and the University of Tokyo.

3. REFERENCES

[1] Y. Takahashi *et al.*, EPL, **88**, 63001 (2009).

---

[*] Corresponding author e-mail address:narumi.kazumasa@jaea.go.jp

DEEP SHELL AUGER RECOMBINATION AFTER HIGHLY CHARGED ION IMPACT: ELECTRONIC EXCITATION AND RELAXATION

M. El Kharrazi[1,*], *O. Osmani*[2], *A. Wucher*[1], *and M. Schleberger*[1]

[1] Fakultät für Physik, Universität Duisburg-Essen, 47048 Duisburg, Germany
[2] Donostia International Physics Center, 20018 Donostia-San Sebastian, Spain

1. INTRODUCTION

After the bombardment of a metal surface by highly charged ions different processes lead to neutralization of the ion. In particular, deep holes in the valence band of the metal are generated by quasi resonant neutralization (QRN)[1]. These energeticly deep holes decay with a material-dependent time constant by recombination with electrons from the conduction band. For low-Z materials radiative transitions can be neglected. Due to the energy released by non-radiative recombination, electrons in the conduction band are excited [2]. Here, we present a model which describes the filling of a hole by electrons from the conduction band. At the same time we consider the electron-electron collisions, which are treated by means of transition rates from different electronic states. These electronic transitions are calculated based on a screened Coulomb potential [3]. Both, recombination and collision processes, are treated in the framework of the Boltzmann equation which discribes the time evolution of the occupation probability. From the distribution of occupied states, we finally calculate the number of electrons, which may overcome the potential barrier into the vacuum.

2. MODEL

Here, we calculate the excitation and relaxation of the free electron gas for aluminum with a Fermi energy of $E_F = 11.2$ eV [2]. As an examplary case we consider the relaxation of an L-shell hole localized at -62 eV, created due to QRN (see figure 1). The characteristic decay time for L-shell holes in aluminum is $\tau_A = 40$ fs [2]. An electron-hole recombination term is constructed assuming that each electron from the conduction band contributes to the recombination with equal probability. Furthermore, we assume that each electron has an equal probability to absorb the released energy under the restriction, that the final state is vacant.

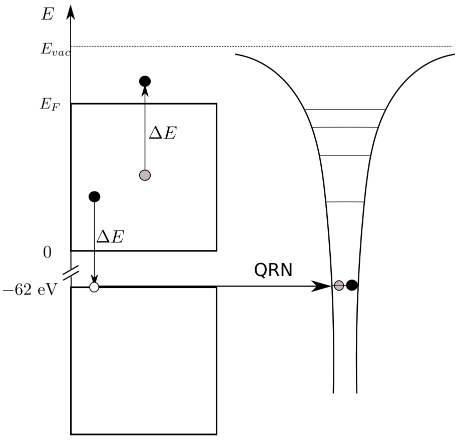

Figure 1: Creation and recombination of a e-h pair due to ion impact.

3. REFERENCES

[1] A. Arnau et al., Surf. Sci. Rep. **27**, 113 (1997).

[2] N. Medvedev, U. Zastrau, E. Förster, D.O. Gericke, and B. Rethfeld, Phys. Rev. Lett. **107**, 165003 (2011).

[3] B. Rethfeld, A. Kaiser, M. Vicanek and G. Simon, Phys. Rev. B **65**, 214303 (2002).

---

[*] mourad.el-kharrazi@uni-due.de

Friday
21 September 2012

Ions at surfaces: An atomistic view of defect and pattern formation

Thomas Michely

II. Physikalisches Institut, Universität zu Köln, Zülpicher Str. 77, 50937 Köln, Germany

Under controlled conditions, scanning tunneling microscopy (STM) in combination with molecular dynamics (MD) simulations are efficient tools to provide detailed insight into damage production by keV ions and details of the ion-surface interaction.

Examples for such insights are: the discovery and precise measurement of adatom production by ions incident on metals [1]; the precise determination of sputtering yields as a function of the surface morphology [2]; the effect of adsorbates on the sputtering yield under grazing incidence ion exposure [3]; the determination of interstitial diffusion parameters based on in situ observations of their annealing to surfaces [4]; and understanding of thermal spike induced swelling near metal surfaces [5].

Here the focus will be on the interaction of keV noble gas ions with low index crystal surfaces when impinging under grazing incidence. Depending on the conditions chosen, surface channeling (the particle is reflected), subsurface channeling (the particle enters at a step edge and moves along a crystal axis in the layer underneath the surface), interface channeling (the particle moves along the interface of two materials) and thermal spike formation (the particle hits a surface defect, e.g. a step edge) take place.

In the limit of low ion fluence, at a low temperature that prevents damage annealing, and on clean surfaces the signature of the interaction of grazing incidence ions can be observed on the surface. It turns out that for the cases of subsurface and interface channeling the damage patterns of single ions visualizes the trajectory of the ion when in contact with the sample in atomic precision.

Two examples will be discussed in detail. The damage trails of keV Ar^+ and Xe^+ left behind upon subsurface channeling of Pt(111) [6,7] and upon interface channeling between graphene and Ir(111).

Besides providing insight into the interaction of single ions with surfaces, scanning tunneling microscopy is also an ideal tool to observe and investigate ion beam induced pattern formation. Pattern formation depends largely on the details of temperature dependent surface diffusion processes and the materials chemistry. However, occasionally also the details of the ion surface interaction may have a strong effect on pattern formation. Upon variation of the ion incidence angle it is demonstrated that the onset of subsurface channeling and the correlated damage production along the projection of the ion beam direction on the surface greatly enhances the regularity of ripple patterns [8].

Finally, ion induced defect production may also be viewed as a tool to create defects that otherwise could neither be generated nor studied. An example is the formation of single vacancy defects in supported graphene through low energy ion impacts.

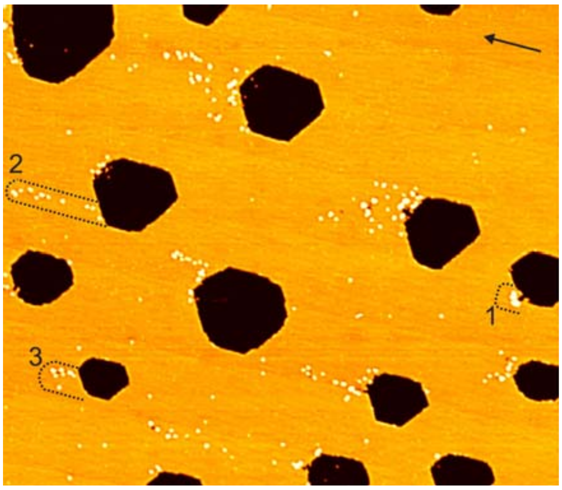

Figure 1: STM topograph of Pt(111) after an exposure to 6×10^{16} ions m^{-2} of 2.5 keV Ar^+ at 62 K. The ion beam direction is indicated by the arrow. The angle of incidence of the ion beam is 86° with respect to the surface normal. The labeled impact patterns represent (1) a damage resulting from a collisional spike at a step edge and (2),(3) ion trails resulting from subsurface channeling events. Image width is 1280 Å.

REFERENCES

[1] T. Michely and G. Comsa, Phys. Rev. B **44**, 8411 (1991). T. Michely and C. Teichert, Phys. Rev. B **50** 11156 (1994).

[2] H. Hansen, C. Polop, T. Michely, A. Friedrich, H. Urbassek, Phys. Rev. Lett. **92**, 246106 (2004).

[3] A. Redinger, Y. Rosandi, H.M. Urbassek, T. Michely, New J. Phys. **11**, 063011 (2009).

[4] M. Morgenstern, T. Michely, G. Comsa, Phys. Rev. Lett. **79**, 1305 (1997).

[5] C. Busse, H. Hansen, U. Linke, T. Michely, Phys. Rev. Lett. **85**, 326 (2000).

[6] A. Redinger, S. Standop, Y. Rosandi, H.M. Urbassek, and T. Michely, New J. Phys. **13**, 013002 (2011).

[7] A. Redinger, S. Standop, T. Michely, Y. Rosandi, and H.M. Urbassek Phys. Rev. Lett. **105**, 075501 (2010).

[8] A. Redinger, H. Hansen, U. Linke, Y. Rosandi, H.M. Urbassek, T. Michely, Phys. Rev. Lett. **96**, 106103 (2006).

---

[*] Corresponding author e-mail address: michely@ph2.uni-koeln.de

SELF-ASSEMBLED NANOSCALE PATTERNS PRODUCED BY ION BOMBARDMENT OF TWO-COMPONENT MATERIALS

R. Mark Bradley[1,*], *Patrick D. Shipman*[2], *and Francis C. Motta*[2]

[1] Department of Physics, Colorado State University, Fort Collins, CO 80523, USA
[2] Department of Mathematics, Colorado State University, Fort Collins, CO 80523, USA

A review will be given of our recent work that demonstrates that a surface layer of altered composition can have a crucial effect on pattern formation induced by ion bombardment of a solid surface. First, we will discuss a theory that explains the genesis of the strikingly regular hexagonal arrays of nanodots that can form when the binary material GaSb is bombarded at normal incidence [1 – 3]. In our theory, the coupling between a surface layer of altered stoichiometry and the topography of the surface is the key to the observed pattern formation. For a certain range of the parameters, we find that nanodot arrays with strong short range hexagonal order emerge spontaneously. Our theory also predicts that remarkably defect-free ripples can be produced by oblique-incidence bombardment of a binary material if the ion species, energy and angle of incidence are appropriately chosen [4]. This high degree of order cannot be achieved by bombarding an elemental material.

A related theory yields insight into pattern formation induced by ion bombardment of an elemental material with concurrent deposition of impurities [5,6]. We show that if the impurities are deposited obliquely during normal- or near-normal-incidence ion bombardment, a novel instability can yield surface ripples. This instability can set in even if the curvature dependence of the sputter yields is negligible and the two atomic species are completely miscible.

REFERENCES

[1] R. M. Bradley and P. D. Shipman, Phys. Rev. Lett. **105**, 145501 (2010).
[2] P. D. Shipman and R. M. Bradley, Phys. Rev. B **84**, 085420 (2011).
[3] R. M. Bradley and P. D. Shipman, Appl. Surf. Sci. **258**, 4161 (2012).
[4] F. C. Motta, P. D. Shipman, and R. M. Bradley, J. Phys. D (Fast Track Communications) **45**, 122001 (2012).
[5] R. M. Bradley, Phys. Rev. B **83**, 195410 (2011).
[6] R. M. Bradley, Phys. Rev. B **85**, 115419 (2012).

---

[*] Corresponding author e-mail address: bradley@lamar.colostate.edu

PERIODIC NANOSCALE PATTERNS INDUCED BY ION IRRADIATION: RIPPLES, DOTS, AND HOLES

S. Facsko

Institute of Ion Beam Physics and Materials Research, Helmholtz-Zentrum Dresden-Rossendorf,
Bautzner Landstr. 400, 01328 Dresden, Germany

1. INTRODUCTION

The morphology of surfaces after irradiation with low energy ions ($E < 50$ keV) exhibits a variety of characteristics depending on the ion beam parameters and the material properties. Surfaces exposed to the ion beam can turn atomically smooth, stochastically or self-affine rough, or can evolve towards regular self-organised patterns. The structure size of these patterns is in the range of 10 to 100 nm and occasionally a high degree of ordering is achieved. Therefore, they have attracted interest recently as templates for nanostructured thin films or for structuring films by an erosive process [1].

On materials which turn amorphous during ion irradiation the formation of periodic patterns relies on at least two interplaying processes: surface roughening due to local variation of erosion rate and smoothing via diffusional processes. In addition, atomic relocations on the surface and in the bulk resulting from the collision cascade have been identified as equally important. Therefore, the surface morphology depends on the details of the energy deposition by the incoming ion beam and on the details of surface and bulk diffusion. At the atomic level sputtering, the creation of surface and bulk defects, and the influence of the ion beam on surface diffusion processes play a decisive role for the morphology evolution.

2. SELF-ORGANIZED PERIODIC PATERNS

2.1. Ripple Patterns

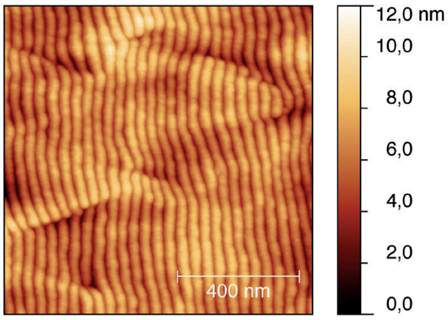

Figure 1: Atomic force microscope image of ripple pattern on Si induced by ion irradiation with 500 eV Ar$^+$ at 67°.

On elemental materials, like Si and Ge, ion irradiation at off-normal angle of incidence between 50° and 70° to the surface normal and at room temperature produces ripple patterns oriented perpendicular to the ion beam direction. Higher incidence angles can lead to ripple patterns oriented parallel to the ion beam direction. Normally, coarsening of the ripple pattern with ion fluence is observed. In addition, the order increases with fluence up to 1×10^{18} cm^{-2} .

2.2. Dot and hole patterns

At normal incidence or for incidence angles smaller than 50° smoothing dominates on elemental materials. However, additional surface instabilities can exist due to the presence of a second atomic species on the surface. Hexagonally ordered dot or hole patterns are thus observed at normal ion incidence on compound materials, like III-V semiconductors, or on Si and Ge surfaces with concurrent deposition or implantation of foreign atoms [2, 3].

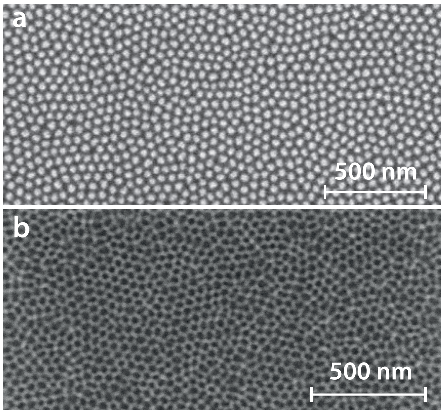

Figure 2: Scanning electron microscope image of a) dot pattern on GaSb induced by ion irradiation with 500 eV Ar$^+$ and b) hole pattern induced by 5 keV Ga$^+$ at 0°.

3. REFERENCES

[1] A. Keller, L. Peverini, J. Grenzer, G.J. Kovacs, A. Mücklich, and S. Facsko, Phys. Rev. B **84**, 035423 (2011).

[2] J. Zhou, S. Facsko, M. Lu, and W. Möller, J. Appl. Phys. **109**, 104315 (2011).

[3] M. Fritzsche, A. Muecklich, and S. Facsko, Appl. Phys. Lett. **100**, 223108 (2012).

---

*Corresponding author e-mail address: s.facsko@hzdr.de

SURFACE PATTERNING OF Ge AND Si BY HEAVY ION AND CLUSTER IMPACTS: EXPERIMENTS, ATOMISTIC SIMULATIONS AND THEORY

K.-H. Heinig[1,*], *R. Böttger*[1], *B. Liedke*[1], *L. Bischoff*[1], *C. Anders*[2] *and H. Urbassek*[2]

[1] Helmholtz-Zentrum Dresden-Rossendorf, Institute of Ion Beam Physics and Materials Research, Dresden
[2] Fachbereich Physik und Forschungszentrum OPTIMAS, Universität Kaiserslautern

1. INTRODUCTION

The driving forces for pattern formation on surfaces by ion irradiation have been under discussion for many years. Bradley and Harper published a straightforward derivation of a partial differential equation based on the surface curvature dependent sputtering

$$\partial_t h = \left(A\nabla^2 + D\nabla^4\right)h,$$

which describes some features. Later on, ion impact induced viscous flow and a mass drift in the amorphous surfaces layer caused by the impinging ions where discussed. Only a few years ago it became obvious that on semiconductor surfaces the formation of many of the beautiful patterns are dominated by contaminations with metals. Thus, a discussion started, whether the pattern formation is induced by preferential sputtering of one of the components or by driving forces like phase separation. Additionally, the kinetics of the collision-induced defects in a sub-surfaces layer can produce instabilities resulting in surface pattern.

In order to identify the dominating driving forces at least for Ge and Si surface patterning by heavy ion (Bi) and cluster (Bi_3) impacts of a few to a few tens of keV, experimental Focussed Ion Beam (FIB) and broad-beam studies were combined with computer experiments (MD and kinetic Monte Carlo simulations) and theoretical studies, e.g. of the damped Kuramoto-Sivashinsky equation

$$\partial_t h = -\left(\alpha + \nu\nabla^2 + D\nabla^4\right)h - \lambda\left(\nabla h\right)^2$$

A detailed comparison between experiments, simulations and PDE solutions of the surfaces evolution of specific morphologies is a powerful approach for a deeper understanding of this kind of self-organization of structures.

1.1. Examples

In this abstract for each approach, experiment, simulation and theory, an example is presented. Experiments cover a wide range of ion energies and fluences, Fig. 1 shows typical patterns. The atomistic simulations study the influence of the ion collision cascades on the pattern formation via defect kinetics (Fig. 2). And finally, relations of this defect kinetics to parameters of the damped Kuramoto-Sivashinsky equation are studied (Fig. 3).

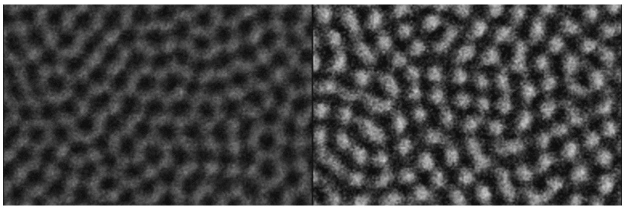

Figure 1: SEM images of Ge surface pattern after irradiation with $1x10^{17}$ $Bi^{+}cm^{-2}$ of 6 keV (left) and 10 keV (right). The morphology changes from hole-like (left) to dot-like (right).

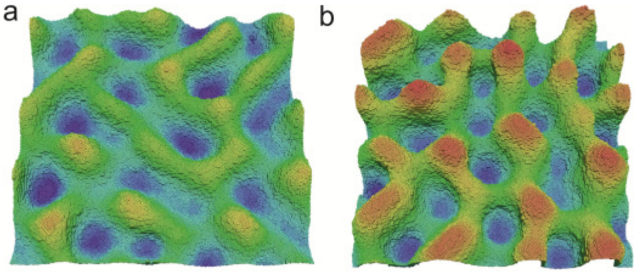

Figure 2: Combined 3D TRIM/kMC simulation of Bi atom impacts taking into account the full collision cascade and subsequent vacancy and interstitial kinetics. Low ion energies causes hole pattern (a), whereas dot patter are found for higher energies.

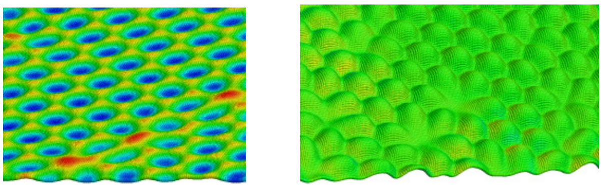

Figure 3: Hole-like (left) and dot-like pattern (right) as predicted by the damped Kuramoto-Sivashinsky equation with α=0.225, ν=1, D=1, and λ= -1 (left) and λ = +1 (right).

1.2. Acknowledgement

The authors thanks the DFG for funding projects of a German-wide researcher group.

2. REFERENCES

[1] R.M. Bradley, and J.M.E. Harper, J. Vac. Sci. Technol. A6, 2390 (1988).

---

[*] Corresponding author e-mail address: k.h.heinig@hzdr.de

SILICIDE INDUCED ION BEAM PATTERNING OF SILICON(001)

M. Engler[1,*], *S. Müller*[1], *F. Frost*[2], *R. Feder*[2], *D. Spemann*[3] *and T. Michely*[1]

[1] II. Physikalisches Institut, Universität zu Köln, Cologne, Germany
[2] Leibniz-Institut für Oberflächenmodifizierung e.V., Leipzig, Germany
[3] Universität Leipzig, Leipzig, Germany

Low energy ion beam erosion of silicon surfaces is a simple and versatile method for producing regular nano-scale patterns. Recent experiments showed that metal deposition during ion beam erosion causes the pattern formation at low incidence angles [1, 2, 3, 4].

We performed 2 keV Kr^+ ion beam erosion of Si(001) experiments using a scanned fine focus ion source with simultaneous deposition of metal atoms. After ion beam erosion we analyzed our samples in-situ with scanning tunneling microscopy (STM) and ex-situ with atomic force microscopy (AFM). The metal concentration on the Si surface was analyzed ex-situ with Rutherford backscattering spectrometry (RBS).

To distinguish the effects of collision kinetics versus chemical interaction in metal co-deposition induced pattern formation on Si(001) we conducted Ag and Pd sputter co-deposition from a target mounted on the Si sample. This setup results in a flux and concentration gradient of the co-deposited metals on the Si sample. While for Pd a concentration dependent ripple pattern is observed, no pattern evolves for Ag co-deposition under ultra high vaccum conditions. Since Ag and Pd possess nearly the same nuclear charge and atomic mass, their different ability to form a pattern must be attributed to their different ability to form silicides. While Pd forms a variety of silicides, Ag forms none. Silicide formation of the co-deposited metal appears thus to be a necessary condition to induce a pattern on Si during ion exposure.

We note that in-situ sample characterization is of great relevance for the proper data interpretation. For the case of Ag co-deposition we observed after exposure to air spontaneous pattern formation through Ag cluster precipation at the surface. We propose the cluster formation to be a consequence of SiO_2 formation.

Spinodal decomposition can trigger metal induced ion beam pattern formation. Spinodal decomposition occours when the free energy G as function of concentration c is negatively curved $\partial^2 G/\partial c^2 < 0$, e.g. between two stable compositions. The system is then unstable and concentration fluctuations lead to the decomposition into regions with high and low concentration with a preferred wavelength [5]. As the erosion rate depends on the composition, the concentration modulation leads to a height modulation. Steel co-evaporation experiments provide evidence for spinodal decomposition by tuning the Fe to Kr^+ flux ratio. Without Fe co-deposition the surface remains flat. With increasing Fe concentration on the surface dot and ripple patterns develop. But with further increased Fe concentration the surface remains flat again.

The pattern formation can be enhanced by the geometry of the ion and metal beams. Opposing ion and metal beams produce a modulation of local flux ratios in phase with the pattern amplifying the composition modulation. Ion and metal beams incident from the same direction do not produce a modulation in local flux ratio.

The key ingredients for metal induced ion beam patterning are silicide formation leading to the dependence of the erosion rate on the chemical composition and phase separation by spinodal decomposition leading to a spacial modulation of the chemical composition. The composition dependence of the erosion rate transforms a composition modulation into a pattern in morphology. The growth of the pattern can be enhanced by the geometry of the ion and metal beams.

1. REFERENCES

[1] G. Ozaydin, A. S. Ozcan, Y. Wang, K. F. Ludwig, H. Zhou, R. L. Headrick and D. P. Siddons, Appl. Phys. Lett. **87**, 163104 (2005).

[2] S. Macko, F. Frost, B. Ziberi, D. F. Förster, and T. Michely, Nanotechnology **10**, 085301 (2010).

[3] S. Macko, F. Frost and M. Engler, D. Hirsch, T. Höche, J. Grenzer and T. Michely, New. J. Phys. **13**, 073017 (2011).

[4] K. Zhang, M. Brötzmann, and H. Hofsäss, New. J. Phys. **13**, 013033 (2011).

[5] J. W. Cahn, Acta Metallurgica **9**, 795 (1961).

---

*Corresponding author e-mail address: engler@ph2.uni-koeln.de

Determining the Structure of Dye Layers Adsorbed on Nanoporous Titania Substrates

G. Andersson[1,*], *L. Ellis-Gibbings*[1], *V. Johansson*[2], *R. Walsh*[3], *L. Kloo*[2], *J. Quinton*[1]

[1] Flinders Centre for NanoScale Science and Technology, Flinders University, PO Box 2100, Adelaide SA 5001, Australia
[2] Applied Physical Chemistry, KTH Royal Institute of Technology, S-10044 Stockholm, Sweden
[3] Department of Applied Mathematics, Research School of Physics and Engineering, The Australian National University, Canberra ACT 0200 Australia

1. INTRODUCTION

The structure of the dye layer adsorbed on the nanoporous titania substrate in a dye-sensitized solar cell (DSC) is of fundamental importance for the function of this type of solar cell, since it strongly influences the injection of photoelectrons from the excited dye molecules into the titania substrate. The adsorption isotherms of the N719 ruthenium-based dye were both determined with a direct method using the depth profiling technique Neutral Impact Collision Ion Scattering Spectroscopy (NICISS) and with the standard indirect solution depletion method. It is widely assumed that the dye molecules adsorb in monolayers but an experimental proof is missing. It is assumed that the structure of the adsorbed dye layer has influence on the function of DSCs.

2. EXPERIMENTAL WORK

Determining the adsorption on a corrugated surface such as that of a nanoporous titania substrate is a challenging task as the curvature of the surface has to be taken into account as well as the straggling of the stopping power. In order to determine the adsorption and the structure of the layer, the NICISS data have been deconvoluted both for the influence of straggling of the stopping power as well as the curvature of the substrate. The latter is illustrated in Figure 1.

It is found that the dye layer adsorbed on the titania surface is laterally inhomogeneous in thickness and growth already from low coverage levels involving a combination of monolayers and multilayers. It is also found that the amount of N719 adsorbed on the substrate depends on the titania structure, i.e. is different for titania nanoparticles and atomic layer deposited titania. The present results show that dye molecules in dye-sensitized solar cells are not, as presumed, necessarily adsorbed as self-assembled monolayer on the substrate as illustrated in Figure 2.

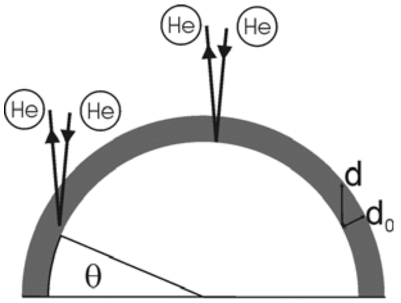

Figure 1: Schematic illustrating the relation between the length of the trajectory and the depth for a single titania nanoparticle. The image represents a view from the side. The correlation between the length of the trajectory d and the depth d_0 is illustrated.

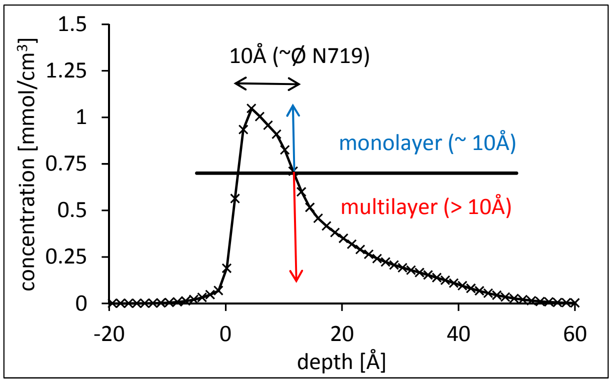

Figure 2: The figure shows the concentration depth profile of the sample immersed into the 0.3 mM N719 dye solution. The measured profile is deconvoluted and corrected for the spherical nature of the substrate. The profile shows that a fraction of the surface is covered with a monolayer of the dye (region with a thickness < 10 Å, fraction indicated with the upper arrow) and a region with multilayers (region with a thickness > 10 Å, fraction indicated with the lower arrow). The choice of 10 Å for separating mono- and multilayer is to some degree arbitrary.

3. REFERENCES

[1] M. Grätzel, M., J. Photochem. Photobio. C: Photochemistry Reviews 4, 145 (2003).
[2] L. Ellis-Gibbings, V. Johansson, R. B Walsh, L. Kloo, J. S Quinton, G. G Andersson, submitted to Langmuir.

---

[*] Corresponding author e-mail address: gunther.andersson@flinders.edu.au

Train and Boat Schedules

Chiemsee Boat Service

Sommerfahrplan 2012

Chiemsee-Bahn und Schifffahrt
Gültig vom 26. Mai mit 23. September

Zeichenerklärung:
a = werktags außer Samstag
d = nur an Samstagen
w = nur an Werktagen
● = zum/vom Nordsteg
○ = Große Rundfahrt

Explanation of codes:
a = on weekdays except Saturday
d = only on Saturday
w = runs on weekdays only
● = to/from Nordsteg
○ = roundtrip

Fahrten Nr 1		1	2	3	4	5	6	7	8	9	10	11	12	13	14	15	16	17	18	19	20	21	22	23	24
Chiemsee-Bahn						Bus		Bus	= ab Busbahnhof																
Prien/Bhf	ab					a 8.35		a 9.30	10.10	......	11.10	12.10	......	13.00	......	......	14.15	15.05	......	15.55	......	16.45	17.35	18.15	
Prien/Stock Hafen	an					a 8.42		a 9.37	10.18	......	11.18	12.18	......	13.08	......	......	14.23	15.13	......	16.03	......	16.53	17.43	18.23	
Schiff					Große Rundfahrt	Insel Rundfahrt		Große Rundfahrt	Insel Rundfahrt	Insel Rundfahrt	Insel Rundfahrt	Insel Rundfahrt	Große Rundfahrt	Insel Rundfahrt	Insel Rundfahrt	Insel Rundfahrt	Insel Rundfahrt	Große Rundfahrt	Insel Rundfahrt	Insel Rundfahrt		Große Rundfahrt	Insel Rundfahrt		
Prien/Stock Hafen	ab		6.40w	7.15	8.15	9.00	9.25	9.50	10.30	11.00	11.40	12.20	12.40	13.15	13.55	14.15	14.55	15.20	15.45	16.25		16.55	18.00	19.30	
Herreninsel	ab		6.55w	7.30	8.30	9.15	9.40 an	10.10	10.50	11.20	12.00	12.40	13.00	13.35	14.15	14.35	15.10	15.35	16.00	16.40		17.15	18.15	19.45	
Gstadt	ab		↓	↓	↓	↓		↓	↓	↓	↓	↓	↓	↓	↓	↓	↓	↓	↓	↓		↓	↓	19.55	
Fraueninsel	an		7.04w●	7.39●	8.39	9.25		10.20	11.00	11.30	12.10	12.50	13.10	13.45	14.25	14.45	15.20	15.45	16.10	16.50		17.25	18.25	20.04●	
Fraueninsel	ab	6.05w●	7.05●	7.40●	8.40	9.30		10.25	11.05	11.35	12.20	13.05	13.15	13.55	14.40	15.00	15.35	15.50	16.25	17.05		17.35	18.30	20.05●	20.05d●
Seebruck	ab	↓	↓	↓	9.10	↓		10.55	↓	↓	↓	↓	13.45	↓	↓	↓	↓	16.20	↓	↓		18.05	↓	↓	↓
Chieming	ab	↓	↓	↓	9.40	↓		11.30	↓	↓	↓	↓	14.15	↓	↓	↓	↓	16.50	↓	↓		18.30	↓	↓	↓
Gstadt	ab	6.15w	7.20	8.05	Fraueninsel 10.10	9.40		↓	11.20	11.45	12.30	13.20	↓	14.05	14.55	15.15	15.45	↓	16.35	17.15		↓	18.40	20.15 an	20.15d
Fraueninsel	ab	↓	7.30	8.15	Gstadt 10.20	↓		12.00	↓	↓	↓	↓	14.45	↓	↓	↓	↓	17.25	↓	↓		19.00	↓		↓
Herreninsel	ab	6.25w	7.40	8.25	10.30	9.50		12.15	11.30	12.00	12.45	13.30	14.55	14.20	15.10	15.25	16.00	17.35	16.50	17.30	18.10	19.10	18.50		20.25d
Prien/Stock Hafen	an	6.39w	7.55	8.40	10.45	10.05		12.30	11.45	12.15	13.00	13.45	15.10	14.35	15.25	15.40	16.15	17.50	17.05	17.45	18.25	19.25	19.05		20.40d
Chiemsee-Bahn			Bus																		Bus				
Prien/Stock Hafen	ab	......	a 8.49	9.30	.....	10.30	11.30	12.35	......	12.35	......	13.55	15.35	14.45	15.35	......	16.25	17.56*	17.15	17.56*	a18.44				
Prien/Bhf	an	......	a 8.55	9.38	......	10.38	11.38	12.43	......	12.43	......	14.03	15.43	14.53	15.43	.....	16.33	18.04	17.23	18.02	a18.50				

Taxistand Prien
Tel. 0 80 51 - 44 04

*Anschluss zur DB kann nicht garantiert werden

Zusätzliche Fahrten Gstadt - Fraueninsel

Gstadt	ab	8.50	9.20	9.50	10.20	10.50	11.20	weiter alle 30 Minuten every 30 minutes	18.20	18.50	19.20 d	19.55	21.00	21.50 d	22.50 d
Fraueninsel	an	8.59	9.29	9.59	10.29●	10.59	11.29		18.29●	18.59	19.29 d●	20.04●	21.09●	21.59 d	22.59 d
Fraueninsel	ab	9.00	9.30	10.00	10.30●	11.00	11.30●		18.30●	19.00	19.30 d●	20.05●	21.15●	22.00 d	23.00 d
Gstadt	an	9.10	9.40	10.10	10.40	11.10	11.40		18.40	19.10	19.40 d	20.15	21.25	22.10 d	23.10 d

Auf den Strecken Fraueninsel-Gstadt und Herreninsel-Gstadt verkehrt nach der letzten fahrplanmäßigen Kursfahrt ein Nachttaxidienst, direkt erreichbar unter: Telefon: 01 70-205 35 42

Bernau/ Felden - Herreninsel

Bernau- Felden	ab	10.15	11.30	13.00	14.00	15.00	16.00	
Herreninsel	an	10.38	11.53	13.25	14.25	15.25	16.25	
Herreninsel	ab	10.40	11.55	13.30	14.30	15.30	16.30	17.55
Bernau- Felden	an	11.05	12.20	13.55	14.55	15.55	16.55	18.20

Übersee/Feldwies - Fraueninsel - Herreninsel

* = umsteigen auf der Fraueninsel

10.00	11.55	14.15	16.00	ab	↓	**Feldwies**	↑	an	9.50	11.54	14.10	15.50	17.50
10.20	12.15*	14.35	16.20	an	↓	**Fraueninsel**	↑	ab	9.30	11.35	13.50	15.30	17.30
10.30	12.45	14.45	-	an	↓	**Herreninsel**	↑	ab	9.15*	11.20*	13.35*	15.10*	17.15*

Sommerfahrplan 2012
Abfahrtszeitenplan

Chiemsee-Bahn und Schifffahrt
Gültig vom 26. Mai mit 23. September

Zeichenerklärung:
a = werktags außer Samstag
d = nur an Samstagen
w = nur an Werktagen
● = zum/vom Nordsteg
○ = Große Rundfahrt

Explanation of codes:
a = on weekdays except Saturday
d = only on Saturday
w = runs on weekdays only
● = to/from Nordsteg
○ = roundtrip

Prien/Stock
▸ Herreninsel ▸ Fraueninsel ▸ Gstadt (Inselrundfahrt)
▸ Herreninsel ▸ Fraueninsel ▸ Seebruck ▸ Chieming
(○ = Große Rundfahrt)

6:40w | 7:15 | 8:15 ○ | 9:00 | 9:25② | 9:50 ○ | 10:30 | 11:00
11:40 | 12:20 | 12:40 ○ | 13:15 | 13: 55 | 14:15 | 14:55 | 15:20 ○
15:45 | 16:25 | 16:55 ○ | 18:00 | 19:30 ② = nur Herreninsel

Herreninsel ▸ Prien/Stock
6:25w | 7:40 | 8:25 | 9:50 |10:30 | 11:30 | 12:00 | 12:15
12:45 | 13:30 | 14:20 | 14:55 | 15.10 | 15.25 | 16:00
16:50 | 17:30 | 17:35 | 18:10 | 18:50 | 19:10 | 20:25d

Herreninsel
▸ Fraueninsel ▸ Gstadt

6:55w | 7:30 | 8:30③ | 9:15 | 10:10③ | 10:50
11:20 | 12:00 | 12:40 | 13:00③ | 13:35 | 14:15
14:35 | 15:10 | 15:35③ | 16:00| 16:40 | 17:15③
18:15 | 19:45 | ③ = nicht nach Gstadt

Herreninsel
▸ Fraueninsel ▸ Seebruck ▸ Chieming

8:30 | 10:10 | 13:00 | 15:35 | 17:15
Übersee/Feldwies siehe Fraueninsel

Herreninsel ▸ Bernau/Felden
10:40 | 11:55 | 13:30 | 14:30 | 15:30 | 16:30 | 17:55

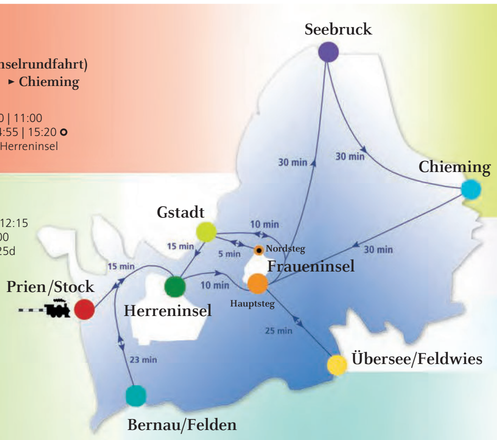

Gstadt ▸ Fraueninsel
7:20 | 8:05 | 8:50 | 9:20 | 9:50 | 10:20 ● | 10:50 | 11:20
11:50 | 12:20 ● | 12:50 | 13:20 | 13:50 | 14:20 ● | 14:50
15:20 ● | 15:50 | 16:20 ● | 16:50 | 17:20 ● | 17:50 | 18:20 ●
18:50 | 19:20 ●d | 19:55 ● | 21:00 ● | 21:50d | 22:50d

Gstadt ▸ Herreninsel ▸ Prien/Stock
6:15w | 7:20 | 8:05 | 9:40 | 10:20 | 11:20 | 11:45 | 12:30
13:20 | 14:05 | 14:55 | 15:15 | 15:45 | 16:35 | 17:15
18:40 | 20:15d

Seebruck
▸ Chieming ▸ Fraueninsel ▸ Herreninsel ▸ Prien/Stock

9:10 | 10:55 | 13:45 | 16:20 | 18:05

Chieming
▸ Fraueninsel ▸ Herreninsel ▸ Prien/Stock

9:40 | 11:30 | 14:15 | 16:50 | 18:30

Übersee/Feldwies
▸ Fraueninsel ▸ Herreninsel

10:00 | 11:55 umsteigen auf der Fraueninsel | 14:15 |
16:00 nur bis Fraueninsel

Bernau/Felden ▸ Herreninsel
10:15 | 11:30 | 13:00 | 14:00 | 15:00 | 16:00

Chiemseebahn

Prien Bhf ▸ Prien/Stock Hafen
(Fahrdauer 8 min, Strecke 1,8 km)

8:35 Bus ① | 9:30 Bus ① | 10:10 | 11:10 | 12:10 | 13:00 | 14:15
15:05 | 15:55 | 16:45 | 17:35 | 18:15

Prien/Stock Hafen ▸
Prien Bahnhof (Fahrdauer 8 min, Strecke 1,8 km)

8:49 Bus | 9:30 | 10:30 | 11:30 | 12:35 | 13:55 | 14:45
15:35 | 16:25 | 17:15 | 17:56* | 18:44 Bus

① = ab Busbahnhof | * = Anschluss zur DB kann nicht garantiert werden

Fraueninsel ▸ Herreninsel ▸ Prien/Stock
6:05w ● | 7:30 | 8:15 | 9:30 | 10:10 | 11:05 | 11:35 | 12:00
12:20 | 13:05 | 13:55 | 14:40 | 14:45 | 15:00 | 15:35 | 16:25
17:05 | 17:25 | 18:30 | 19:00 | 20:05d ●

Fraueninsel ▸ Seebruck ▸ Chieming
8:40 | 10:25 | 13:15 | 15:50 | 17:35

Fraueninsel ▸ Übersee/Feldwies
9:30 | 11:35 | 13:50 | 15:30 | 17:30
von Herreninsel nach Übersee auf Fraueninsel umsteigen Abfahrt Herreninsel: 9:15 | 11:20 | 13:35 | 15:10 | 17:15

Fraueninsel ▸ Gstadt
6:05w ● | 7:05 ● | 7:40 ● | 9:00 | 9:30 | 10:00 | 10:10
10:30 ● | 11:00 | 11:05 | 11:30 ● | 11:35 | 12:00 | 12:20
12:30 ● | 13:00 | 13:05 | 13:30 ● | 13:55 | 14:00 | 14:30 ●
14:40 | 15:00 | 15:30 ● | 15.35 | 16:00 | 16:25 | 16:30 ●
17:00 | 17:05 | 17:30 ● | 18:00 | 18:30 | 18:30 ● | 19:00
19:30 ● d | 20:05 ● | 21:15 ● | 22:00d | 23:00d

Auf den Strecken Fraueninsel-Gstadt und Herreninsel-Gstadt verkehrt nach der letzten fahrplanmäßigen Kursfahrt ein Nachttaxidienst, direkt erreichbar unter:
Telefon: 01 70-205 35 42

Trains from Prien Station to Munich Airport

Prien (am Chiemsee)
und
München, Flughafen

Abfahrt Freitag, 21.09.2012 um 10:00 Uhr

		Linie	Zeit	Linie	Zeit	Linie	Zeit	Linie	Zeit	Linie	Zeit	Linie	Zeit	Linie	Zeit	Linie	Zeit	Linie	Zeit
Verkehrshinweis		**V101**		**V102**		**V103**		**V104**		**V105**		**V106**		**V107**		**V108**		**V109**	
Prien am Chiemsee	ab	**RE**	09:08	**RE**	10:08	**IC**	10:25	**EC**	10:34	**RE**	11:08	**RE**	12:08	**EC**	12:34	**RE**	13:08	**RE**	14:08
Ostbahnhof München	an		10:07		11:01		11:15		11:22		12:07		13:07		13:22		14:07		15:01
Ostbahnhof München	ab	S8	10:24	S8	11:04	S8	11:24	S8	11:44	S8	12:24	S8	13:24	S8	13:44	S8	14:24	S8	15:04
Flughafen München	an		10:55		11:35		11:55		12:15		12:55		13:55		14:15		14:55		15:35
Zeitbedarf (Stunden:Minuten)			**01:47**		**01:27**		**01:30**		**01:41**		**01:47**		**01:47**		**01:41**		**01:47**		**01:27**
Umsteigen (Anzahl)			**1**		**1**		**1**		**1**		**1**		**1**		**1**		**1**		**1**

		Linie	Zeit	Linie	Zeit	Linie	Zeit	Linie	Zeit	Linie	Zeit	Linie	Zeit	Linie	Zeit
Verkehrshinweis		**V110**		**V111**		**V112**		**V113**		**V114**		**V115**		**V116**	
Prien am Chiemsee	ab	**EC**	14:34	**RE**	15:08	**RE**	16:08	**EC**	16:34	**RE**	17:08	**RE**	18:08	**RE**	19:08
Ostbahnhof München	an		15:22		16:07		17:07		17:22		18:07		19:01		20:07
Ostbahnhof München	ab	S8	15:44	S8	16:24	S8	17:24	S8	17:44	S8	18:24	S8	19:04	S8	20:24
Flughafen München	an		16:15		16:55		17:55		18:15		18:55		19:35		20:55
Zeitbedarf (Stunden:Minuten)			**01:41**		**01:47**		**01:47**		**01:41**		**01:47**		**01:27**		**01:47**
Umsteigen (Anzahl)			**1**		**1**		**1**		**1**		**1**		**1**		**1**

Author Index

Author Index

A
Abad 69
Ahsan Zeb 28
Anders 109
Andersson 111
Andrade 86
Andrzejczuk 92
Antonenko 64
Arjad 95
Armon 66
Arnau 28
Artacho 28
ASDEX Upgrade team 72
Atkinson 47
Aumayr 25, 50, 53, 59, 75, 83, 100
Ayyad 65

B
Ban-d'Etat 74
Baryshev 38
Bauer 22, 33, 56, 67, 69, 73, 94
Becker 85
Bekkerman 66
Benrekia 96
Benyagoub 74
Bereczky 25
Bernshtein 66
Betz 41
Beyer 50
Bhattacharyya 62
Bielesch 85
Bischoff 109
Bobrov 93
Bocan 58
Bodewits 53, 100
Boduch 86
Bordalo 86
Borisov 29, 45
Böttger 109
Bradley 107
Brezinsek 72
Briner 82
Brinkmann 51
Bundesmann 55
Burgdörfer 25, 34
Busch 46

C
Chakraborty 35
Chen 52, 93
Cheng 77
Cherkov 64
Cherkova 64
Chiba 70, 101
Ciupiński 92
Cohen 66
Czerski 99

D
Dartois 86
da Silveira 86
Dassanayake 65
de Barros 86
Debiossac 47
De Temmerman 91
Díez Muino 29
Dobes 53, 83, 100
Domaracka 86

E
Eddrief 27
Eddrieff 47
El Kharrazi 61, 102
Ellis-Gibbings 111
El–Said 54
Engler 110
Esaulov 93

Author Index

Etgens 27, 47

F

Facsko 50, 54, 108
Feder 55, 110
Frost 55, 110
Fuhr 93

G

Gafton 27
Garrison 82
Göbl 22, 33, 56, 69, 94
Gölzhäuser 50
Gräfe 34
Grande 99
Gravielle 32, 57, 58
Gregory 97
Gruber 25, 59
Guillemot 93
Gunacker 25
Guo 52
Gutierrez 63

H

Hakola 72
Harnisch 84
He 95
Heinig 109
Hensen 91
Herman 84
Heuser 60
Hippler 62
Hischenhuber 59
Hishita 26
Hmelo 97
Hoekstra 53, 100
Hojou 42
Hopster 61

I

Ishikawa 42, 101
Isoda 42

J

Jakšić 43
JET EFDA contributors 90
Jia 93
Johansson 111
John 62
Jouin 63
Juaristi 28

K

Kachurin 64
Kamaev 64
Kandasamy 93
Karlušić 43, 61
Keerthisinghe 65
Keim 84
Khalal-Kouache 96
Khemliche 47
Kimura 23, 42
King 38
Kleyn 80
Kloo 111
Koch 51
Kohanoff 28
Kolodney 66, 81
Koshikawa 67
Koteski 99
Koval 29
Kowarik 25, 53
Kozubek 61
Krämer 61
Krantzman 82
Krieger 90
Kurzydłowski 92

Author Index

L
Ladinig 25
Lake 30, 31
Lamour 27
Lebius 74
Lei 77
Lemell 25, 41
Li 77
Liedke 109
Likonen 72
Linsmeier 51, 85
Luo 27
Lv 86

M
Maeda 70, 101
Mai 68
Maier 85
Marangolo 27
Marin 64
Marpe 68
Martiarena 93
Mayer 72, 92
Medvedev 71
Meissl 75
Meyer 46
Michely 106, 110
Miraglia 32, 57
Miyashita 23
Momeni 47
Monreal 69
Moore 38
Morgan 91
Morita 42
Motta 107
Mücklich 50
Müller 110

N
Nakajima 23, 42
Nakanishi 67
Naramoto 70
Narumi 42, 70, 101
Neumann 55

O
Oberkofler 85
Ogorodnikova 92
Okabayashi 98
Oshima 23
Osmani 61, 71, 102

P
Palumbo 86
Patidar 76
Petersson 72
Pilling 86
Płociński 92
Pomeroy 30, 31
Possnert 72
Prigent 27
Primetzhofer 22, 33, 56, 69, 73, 94
Pruneda 28
Purohit 76
Pyszkowski 83

Q
Quinton 111

R
Rasiński 92
Rauschenbach 55
Ren 77
Rethfeld 71
Reuschl 27
Ríos Rubiano 58
Ritter 50
Roessler 73

Author Index

Rogalla 85
Rohde 72
Roncin 47
Roth 22, 33, 56, 94, 99
Rothard 86
Rozet 27
Rubel 72
Rund 22, 94

S
Saitoh 42, 70, 101
Salou 74
Sánchez-Portal 28, 29
Schäfer 83
Scheier 84
Schiwietz 99
Schleberger 61, 71, 102
Schrempf 25, 75
Schüller 44, 57
Seifert 44, 46
Seperuelo-Duarte 86
Shen 93
Shipman 107
Simon 59
Singh 76
Skuratov 64
Sosolik 30
Spemann 110
Spitz 22
Staufenbiel 99
Steigerwald 97
Steydli 27
Stöger-Pollach 50
Stolterfoht 24, 65
Strazzulla 86
Sugai 101
Sun 77
Suzuki 23, 26, 42, 67

T
Taglauer 22
Takahashi 97, 101
Takeda 67
Tanis 65
Tiwald 34
Tőkési 25, 41
Tolk 97
Trassinelli 27
Tripa 38
Tsujimoto 42

U
Urbassek 109

V
Vernhet 27
Veryovkin 38
Volodin 64

W
Wachter 41
Walsh 111
Wampl 59
Wang 77
Werner 50
Wickramarachchi 65
Wilhelm 50, 54
Winter 44, 46, 57
Wirtz 34
Wittmaack 40
Wucher 39, 60, 68, 102

X
Xiao 77
Xu 91

Y
Yamada 70, 101
Yamauchi 26
Yarmoff 95

Author Index

Yasue 67
Yu 77

Z
Zhao 77
Zhou 52, 77
Zielinski 91
Zinovev 38
Zugarramurdi 45

IISC-19

Frauenchiemsee 2012 Germany

List of Participants

List of Participants

Andersson, Gunther G.	Australia	gunther.andersson@flinders.edu.au
Artacho, Emilio	Spain	e.artacho@nanogune.eu
Aumayr, Friedrich	Austria	aumayr@iap.tuwien.ac.at
Bauer, Peter	Austria	peter.bauer@jku.at
Bielesch, Stefan	Germany	stefan.bielesch@ipp.mpg.de
Bodewits, Erwin	The Netherlands	ebodewits@kvi.nl
Bradley, R. Mark	USA	bradley@lamar.colostate.edu
Brinkmann, Jens	Germany	jens.brinkmann@ipp.mpg.de
Chakraborty, Purushottam	India	purushottam.chakraborty@saha.ac.in
Chen, Lin	China	chenlin@lzu.edu.cn
Ciupinski, Lukasz	Poland	lukas@inmat.pw.edu.pl
De Temmerman, Gregory	The Netherlands	g.c.detemmerman@differ.nl
Debiossac, Maxime	France	maxime.debiossac@u-psud.fr
Dobes, Katharina	Austria	dobes@iap.tuwien.ac.at
Douglas, Petra	Germany	petra.douglas@ipp.mpg.de
El Kharrazi, Mourad	Germany	mourad.el-kharrazi@uni-due.de
El-Said, Ayman S.	Saudi Arabia	elsaid@kfupm.edu.sa
Engler, Martin	Germany	engler@ph2.uni-koeln.de
Facsko, Stefan	Germany	s.facsko@hzdr.de
Feder, René	Germany	rene.feder@iom-leipzig.de
Göbl, Dominik	Austria	dominik.goebl@jku.at
Gravielle, Maria S.	Argentina	msilvia@iafe.uba.ar
Gregory, Justin	USA	justin.m.gregory@vanderbilt.edu
Gruber, Elisabeth	Austria	egruber@iap.tuwien.ac.at
Gutierrez, Fernando A.	Chile	fgutierr@udec.cl
Heinig, Karl-Heinz	Germany	k.h.heinig@hzdr.de
Heuser, Christian	Germany	Christian.Heuser@uni-due.de
Hoekstra, Ronnie	The Netherlands	hoekstra@kvi.nl
Hopster, Johannes	Germany	johannes.hopster@uni-due.de
John, Angelin E.	Germany	ebanezarja@uni-greifswald.de
Jouin, Hervé	France	jouin@celia.u-bordeaux1.fr
Juaristi, Joseba I.	Spain	josebainaki.juaristi@ehu.es

List of Participants

Kachurin, Gregory A.	Russia	kachurin@isp.nsc.ru
Karlušic, Marko	Croatia	marko.karlusic@irb.hr
Keim, Alan	Austria	alan.keim@uibk.ac.at
Khalal-Kouache, Karima	Algeria	kkouache@yahoo.fr
Kimura, Kenji	Japan	kimura@kues.kyoto-u.ac.jp
King, Bruce	Australia	bruce.king@newcastle.edu.au
Kleyn, Aart W.	The Netherlands	a.w.kleijn@uva.nl
Kolodney, Eli	Israel	eliko@tx.technion.ac.il
Koshikawa, Takanori	Japan	kosikawa@isc.osakac.ac.jp
Koval, Natalia E.	Spain	natalia_koval@ehu.es
Krantzman, Kristin D.	USA	krantzmank@cofc.edu
Krieger, Karl W.	Germany	krieger@ipp.mpg.de
Lake, Russell E.	Finland	rlake@g.clemson.edu
Linsmeier, Christian	Germany	linsmeier@ipp.mpg.de
Marpe, Mario	Germany	mario.marpe@uni-due.de
Michely, Thomas W.	Germany	michely@ph2.uni-koeln.de
Miraglia, Jorge Esteban	Argentina	miraglia@iafe.uba.ar
Nakajima, Kaoru	Japan	nakajima.kaoru.4a@kyoto-u.ac.jp
Narumi, Kazumasa	Japan	narumi.kazumasa@jaea.go.jp
Neitzert, Elmar	Germany	elmar.neitzert@ipp.mpg.de
Oberkofler, Martin	Germany	martin.oberkofler@ipp.mpg.de
Okabayashi, Norio	Japan	okabayashi@staff.kanazawa-u.ac.jp
Osmani, Orkhan	Spain	orkhan_osmani@ehu.es
Petersson, Per	Sweden	Per.Petersson@ee.kth.se
Piechoczek, Rainer	Germany	rainer.piechoczek@ipp.mpg.de
Pomeroy, Joshua	USA	joshua.pomeroy@nist.gov
Primetzhofer, Daniel	Sweden	daniel.primetzhofer@physics.uu.se
Rößler, Wolfgang	Austria	wolfgang.roessler@jku.at
Roth, Dietmar	Austria	dietmar.roth@jku.at
Rothard, Hermann	France	rothard@ganil.fr
Saha, Biswajit	India	biswajit25@gmail.com
Salou, Pierre	France	salou@ganil.fr

List of Participants

Schiwietz, Gregor	Germany	schiwietz@helmholtz-berlin.de
Schrempf, Dominik	Austria	schrempf@iap.tuwien.ac.at
Schwarz-Selinger, Thomas	Germany	thomas.schwarz-selinger@ipp.mpg.de
Seifert, Jan	Germany	jan.seifert@physik.hu-berlin.de
SINGH, PRITHVI	India	prithvipurohit@gmail.com
Stolterfoht, Nikolaus	Germany	nico@stolterfoht.com
Suzuki, Taku	Japan	suzuki.taku@nims.go.jp
Tanis, John A.	USA	john.tanis@wmich.edu
Tiwald, Franz Paul	Austria	paul@dollywood.itp.tuwien.ac.at
Trassinelli, Martino	France	martino.trassinelli@insp.jussieu.fr
Wachter, Georg	Austria	georgwachter@gmail.com
Wang, Yu Yu	China	wangyuyu@impcas.ac.cn
Winter, Helmut	Germany	winter@physik.hu-berlin.de
Wittmaack, Klaus	Germany	wittmaack@helmholtz-muenchen.de
Wucher, Andreas	Germany	andreas.wucher@uni-due.de
Yarmoff, Jory A.	USA	yarmoff@ucr.edu
Zugarramurdi, Asier	France	asier.zugarramurdi@u-psud.fr

System **INA-X**

SECONDARY NEUTRAL MASS SPECTROMETRY

KEY FEATURES & APPLICATIONS

- High Depth Resolution ≤ 1nm
- Detection Limit down to 1ppm
- Simple Quantification
- Quantitative Analysis
- Impurity Analysis

SPECS™

+49 30 46 78 24-0 | sales@specs.com | www.specs.com

19th International Workshop on Inelastic Ion-Surface Collisions (IISC-19)

Frauenchiemsee, Germany

Organized by Max-Planck-Institut für Plasmaphysik
Christian Linsmeier (chair)

Sunday 16 September 2012

15:00		**Registration**
18:00		*Dinner*

Monday 17 September 2012

09:00		***Opening***
09:10	P	**Bauer**
09:55	R	**Nakajima**
10:25		*Coffee break*
10:40	R	**Stolterfoht**
11:10	O	**Gruber**
11:30	R	**Suzuki**
12:00		*Lunch*
13:30	O	**Trassinelli**
13:50	R	**Artacho**
14:20	O	**Koval**
14:40	R	**Lake**
15:10		*Coffee break*
15:30	O	**Pomeroy**
15:50	O	**Miraglia**
16:10	O	**Roth**
16:30	O	**Tiwald**
16:50	O	**Chakraborty**
18:00		*Dinner*

Tuesday 18 September 2012

09:00	P	**King**
09:45	O	**Wucher**
10:05	O	**Wittmaack**
10:25		*Coffee break*
10:40	R	**Wachter**
11:10	O	**Kimura**
11:30	R	**Karlusic**
12:00		*Lunch*
13:30	R	**Seifert**
14:00	O	**Zugarramurdi**
14:20	O	**Winter**
14:40	O	**Debiossac**
15:00		**Poster Intro**
		Poster session *Coffee break*
18:00		*Dinner*
		Committee Meeting

Wednesday 19 September 2012

09:00	P	**Kleyn**
09:45	O	**Kolodney**
10:05	O	**Krantzman**
10:25		*Coffee break*
10:40	R	**Dobes**
11:10	O	**Keim**
11:30	O	**Bielesch**
11:50	R	**Rothard**
12:20		*Lunch (boxes)*
		Conference Excursion to Kampenwand
18:30		*Dinner*

Thursday 20 September 2012

09:00	P	**Krieger**
09:45	R	**de Temmerman**
10:15	O	**Ciupinski**
10:35		*Coffee break*
10:55	R	**Chen**
11:25	R	**Primetzhofer**
12:00		*Lunch*
13:30	R	**Yarmoff**
14:00	O	**Khalal-Kouache**
14:20	O	**Gregory**
14:40	R	**Okabayashi**
15:10		*Coffee break*
15:30	R	**Schiwietz**
16:00	O	**Bodewits**
16:20	O	**Narumi**
16:40	O	**El Kharrazi**
18:00		***Conference Dinner***

Friday 21 September 2012

09:00	P	**Michely**
09:45	R	**Bradley**
10:15	R	**Facsko**
10:45		*Coffee break*
11:00	O	**Heinig**
11:20	O	**Engler**
11:40	O	**Andersson**
		Closing
12:30		*Lunch*

P Plenary Talk (40+5 min)
R Progress Report (25+5 min)
O Oral Contribution (15+5 min)